



# A 3D fault seal analysis study conducted in the Ibhubesi Gas Field Offshore the West Coast of South Africa

**By**

**Nondumiso Ntombela**

**NTMNOK003**

**SUBMITTED TO THE UNIVERSITY OF CAPE TOWN**

**In fulfilment of the requirements for the degree**

**MSc Geology**

**Faculty of Sciences**

**UNIVERSITY OF CAPE TOWN**

**Supervisor: Dr. Beth Kahle**

# Abstract

A three dimensional fault seal analysis study of the AK fault situated offshore of the West Coast of South Africa is presented. This study is aimed at informing the development plan of the Ibhubesi gas field with regards to the compartmentalization of the reservoirs, by understanding whether a key fault, the AK fault facilitates hydrocarbon migration to the Ibhubesi field reservoirs or whether it provides a seal.

In order to address this research aim, a seismic interpretation of the area was carried out and combined with an interpretation of well data to construct a 3D structural model from which the fault seal analysis was carried out. Juxtaposition analysis was used to determine the lithologies that had been juxtaposed across the fault. Fault clay was determined using the Shale Gouge Ratio (SGR) algorithm and permeability and threshold pressure were also used to quantify the fault seal capacity.

The results from the SGR were correlated to the across fault pressure difference and plotted on a reference diagram which is a comparison of sealing faults vs. leaking faults. This diagram indicates that faults with an SGR greater than 25% and threshold pressures greater than 8bars, have a high potential to seal. The AK fault SGR results range between 25 and 55 % with a threshold pressure of up to 20bars. These results indicate that the AK fault is likely to be a sealing fault.

# DECLARATION

**I, Nondumiso Ntombela, hereby declare that the work on which this dissertation/thesis is based is my original work (except where acknowledgements indicate otherwise) and that neither the whole work nor any part of it has been, is being, or is to be submitted for another degree in this or any other university.**

**I empower the university to reproduce for the purpose of research either the whole or any portion of the contents in any manner whatsoever.**

Signed by candidate

Signature Removed

**Signature: ……**

**Date:** August 2017……

# Acknowledgements

My sincere gratitude goes to my supervisor, Dr. Beth Kahle, for her continuous support, patience and guidance.

To PetroSA, thank you for giving me the opportunity to study and for providing financial support. To my managers: Varsha Singh; Answa de Lange and Sumesh Naidoo. I appreciate the confidence that you have in me, for your mentorship, for pushing my limit and for believing in me.

A special thanks to my family, especially my husband, Mr. B. M Msezane for his support, his confidence in me and for being the biggest critic of my work.

# List of Figures

# List of Tables

# CONTENTS

# 1. INTRODUCTION

## 1.1 General Background

In the petroleum industry, risk is associated with uncertainties in petroleum elements, which include the source, migration of fluids, trap and the seal. This study focuses on the seal element, particularly the membrane or fault seal. Fault seals are found where a petroleum reservoir is dependent on a fault for trapping the hydrocarbons and preventing further migration.

The aim of the study is to understand the role or behavior of the AK fault (Fig. 1), whether it is a migration pathway or whether it acts as a hydrocarbon barrier to the Ibhubesi gas reservoirs. It is important that this behavior is understood because the Ibhubesi gas field is currently in the development phase and understanding whether it acts as a seal or a migration pathway, will determine the development plan (compartmentalized reservoirs) of the Ibhubesi gas field (Fig. 1).

Five wells have been drilled in the Ibhubesi gas field. The drilling of these wells was motivated by high amplitude seismic response, thought to be related to a good-quality sand reservoir.

Four of these wells were drilled next to the AK fault (100m to 1km from the fault), three wells (A-K1, A-K2 and A-V1) on the footwall side of the fault and one (A-Y1) on the hanging wall side of the fault (Fig.1). These wells intersected good quality reservoirs and they were gas bearing. However, one well was drilled further away from the AK fault (3km) (Fig.1). This well also intersected good reservoir sand but it was water bearing. The one possible reason to the difference of the results from these wells is the distance of the AK fault to these wells.

It is therefore important to understand the role of the AK fault in these reservoirs: Is it acting as a migration pathway and the water bearing well that was far from the fault was not charged; or it is acting as a fault seal and there was no trap for the hydrocarbons, which would have been trapped in the water bearing well.

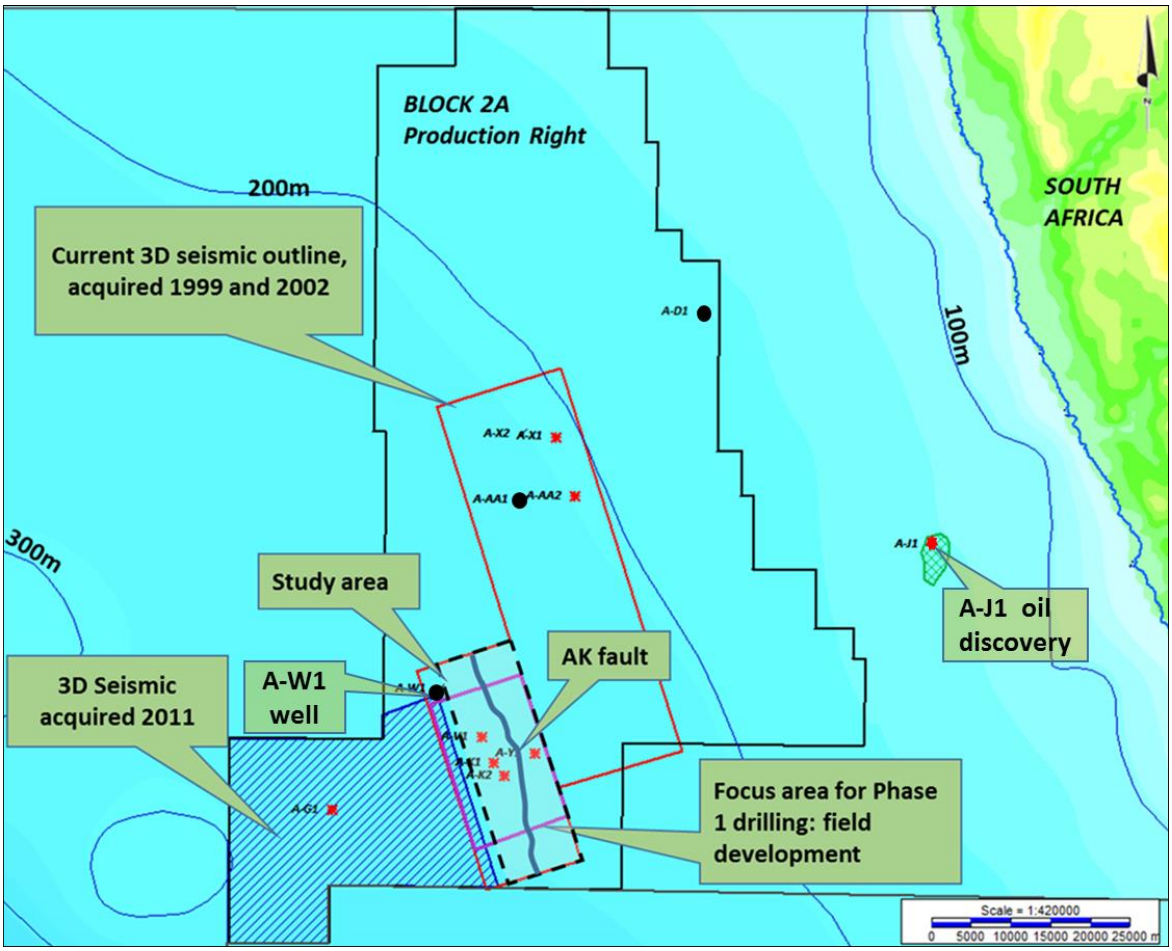


*Figure 1: Map showing showing the study area, located offshore of the west coast of South Africa. The large black box shows the extent of Block 2A. My study area is outlined in a black dashed line, with the AK fault shown as a solid blue line. 3D seismic surveys of different vintages are shown in red (1999 and 2002) and blue striped (2011) boxes. Wells shown in red are discoveries and in black are dry wells. The purple box shows the focus area for Phase 1 drilling.*

## 1.2 Scope of work and General Research Criteria

The fault seal analysis study has been conducted in the Ibhubesi gas field in Block 2A, offshore the West Coast of South Africa (Fig. 1). The Ibhubesi gas field is situated in the Orange Basin. The study area covers about 64 square kilometers ($km^2$). 11 wells have been drilled in Block 2A, of which 4 are within the study area. Numerous vintages of three dimensional (3D) seismic data have been acquired over Block 2A, from the period between 1999 and 2011. The AKAM06 survey was used as part of the research criteria in this study.

The 3D fault seal analysis is an integrated study which includes the seismic mapping and well data interpretation. The results from the interpretation of these data are integrated into a 3D structural model. The 3D structural model is populated with the well data through a process of property modelling and the results are 3D properties. These 3D properties (permeability; facies

and volume of clay (Vclay)) are then mapped to the fault to determine: across fault juxtaposition; fault rock properties (fault clay (SGR), fault permeability and fault rock thickness) and fault sealing capacity in terms of the threshold pressure of the fault that can withstand the hydrocarbon buoyancy pressure. The fault rock properties are also required as inputs in the determination of the fault transmissibility. This summarised workflow is presented in Figure 2.

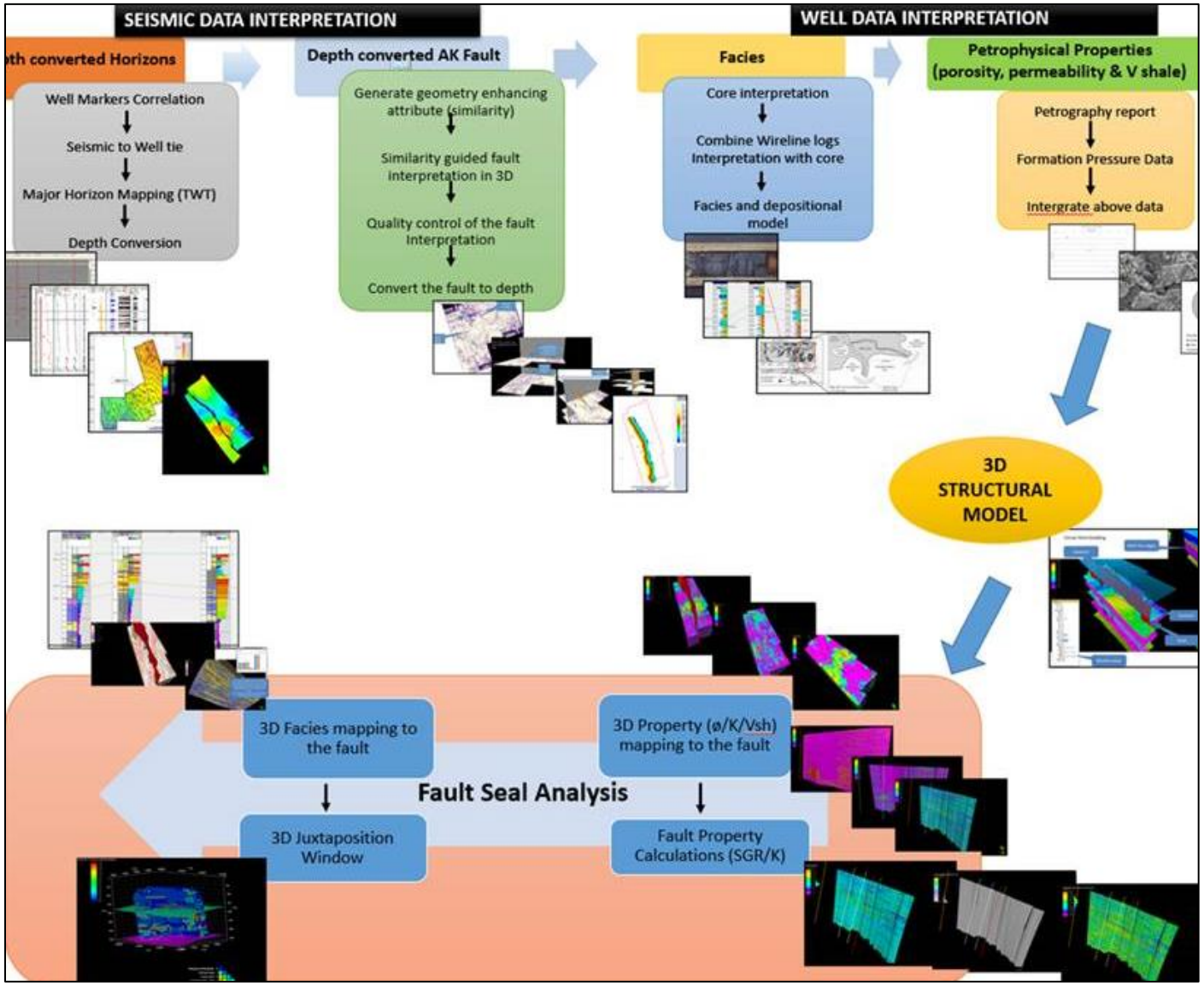


*Figure 2: Fault Seal Analysis Study Work Flow in Ibhubesi Gas Field*

## 1.3 Study Area

The study area is situated in the Ibhubesi gas field, in the petroleum licence Block 2A, offshore the west coast of South Africa. The study area covers about 64 km2. 11 wells have been drilled in Block 2A, of which 4 are within the study area. Numerous vintages of three dimensional (3D) seismic data has been acquired over Block 2A, from the period between 1999 and 2011 (Fig. 1).

### 1.3.1 Geological Background

The study area is situated in the Orange Basin. The Orange Basin is located offshore the South-Western margin of Africa and straddles the border between Namibia and South Africa. To the north, it is bounded by the Walvis Ridge in Namibia and to the South by the Columbine Arch in South Africa, having an aerial extent of about 130 000 km2 (Gerrard and Smith, 1982) (Fig. 3). The Orange Basin owes its character to three major geological processes: tectonic evolution; drainage and sedimentation changes and changes in climate. Special attention will be focused on the tectonic evolution as it is most relevant to this study.

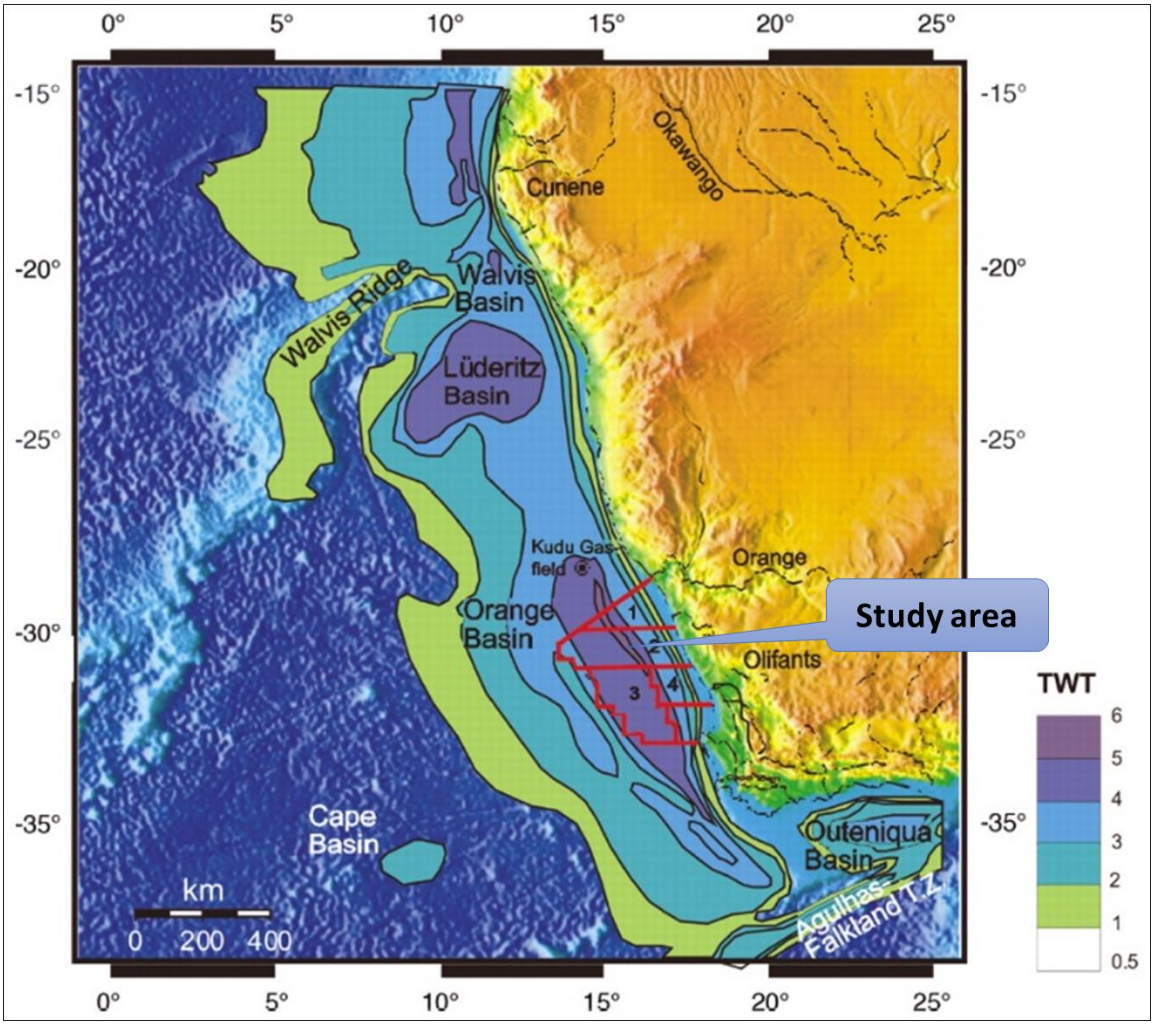


*Figure 3: Depocenters of the Orange Basin located in the offshore Southwest coast of Africa (modified after Paton et al., 2007)*

#### *1.3.1.1 Tectonic Evolution*

The sediments of the Orange Basin provide a record of the tectonic evolution of the Basin. This record is captured from the rift phase during the break-up of Gondwana to the full onset of the drift phase. The different tectonic phases are discussed below:

##### 1.3.1.1.1 Rifting

The onset of rifting is dated at approximately 130 Ma (Macdonald et al., 2003). Rifting occurred in response to extensional stress due to the separation of the Falkland Plateau and Mozambique Ridge (Gerrard and Smith, 1982). The rift phase is characterised by the grabens and half grabens,

which trend north-northwest parallel to the present Western South African coastline (Gerrard and Smith, 1982; Muntingh, 1993; Broad et al., 2006) (Fig. 3).

Numerous wells have been drilled to the rift sequence in the Orange Basin. These wells were drilled to target the sediments that were deposited in the half grabens and grabens that formed during rifting. These a variety of sediments including those deposited in lacustrine, terrigenous and volcanic environments. The source rock in this phase is oil prone and is predominantly lacustrine shales. This source rock has been proven by the A-J1 well, which was drilled in Block 2B, east of Block 2A (Fig.1).

The rifting phase continued until the Hauterivian age (117.5Ma) (Muntingh, 1993; Gerrard and Smith, 1982). The end of the rifting phase and onset of drift phase is marked by the Barremian unconformity 6At1 (Fig.4).

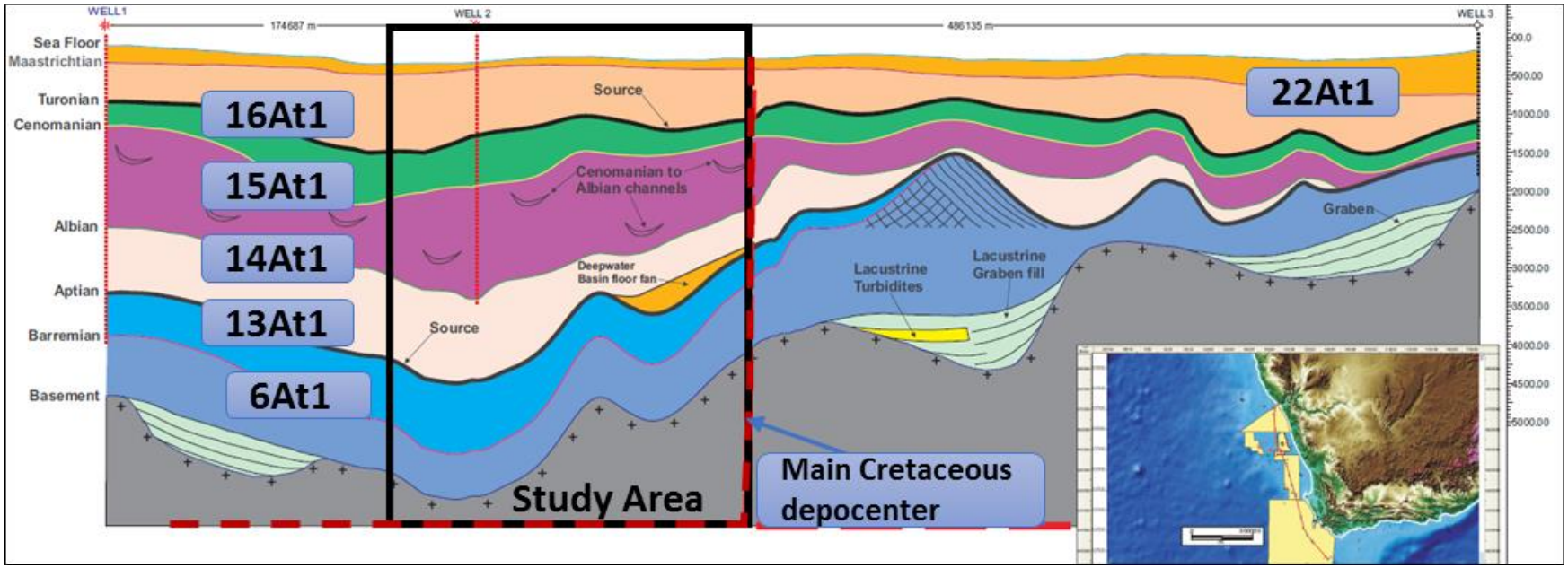


*Figure 4: Longitudinal section taken from the North (Block 1 petroleum licence) to the South (Block 5/6 petroleum licence) of the Orange Basin, illustrating the depocenter of the Orange Basin and the location of the study area relative to that.*

#### 1.3.1.1.2 Drift

Muntingh, (1993) and Gerrard and Smith (1982), estimated the ages of the geological events that occurred during the drift phase. They estimated the beginning of the drift phase in the Hauterivian age (117.5Ma) and to have continued until the Albian age (112Ma). From this age (112Ma), full drift took place. The early drift is marked by the initiation of anoxic and restricted shallow sea in which the transitional source rock sequence was deposited (McMillan, 2003). The Aptian source rock has been proven in the Orange Basin, through well intersections DSDP 361 and A-C1.

The wells that penetrated the early drift sequence intersected fluvial to transitional sediments interbedded with red beds. The full drift continued from 112Ma (Muntingh, 1993; Gerrard and Smith, 1982). This was marked by uplift and erosion along the margin of the Orange Basin. This was followed by open marine conditions and the formation of a passive margin environment (McMillan, 2003; Muntingh, 1993; Paton et al., 2008).

The other geological events which occurred during the drift phase consist of the thermal subsidence and gravity slides. The subsidence created accommodation space for the sediments which later formed the sedimentary wedge (McMillan, 2003; Muntingh, 1993; Paton et al., 2008). The thick sedimentary wedge is characteristic of the Orange Basin depocenter (Fig. 4).

Towards the end of Cretaceous era, there was a north – west ward shift in the location of the Orange Basin depocenter and extensive faulting due to gravity slides at the slope break-(Brown et al., 1994)(Fig. 3b). This was followed by the uplift and erosion at the basin margins which marked the end of the Cretaceous era.

In the Cenozoic era, deposition occurred towards the Basin. The recorded sedimentary sequence that was deposited throughout the Cenozoic era, ranges between 50 to 250m on the shelf (Dingle et al., 1992; Light et al., 1993; McMillan, 2003)

#### *1.3.1.2 Stratigraphy*

The stratigraphy of the Orange Basin is largely attributed to the tectonic events that occurred, which gave rise to the Orange Basin. The syn-rift and the drift stratigraphy is discussed below.

#### 1.3.1.2.1 Syn-rift stratigraphy

The syn-rift sediments consist of sandstone, conglomerate, shale, siltstone with basaltic volcanic extrusive rocks (Muntingh & Brown, 1993). These were deposited in the syn-rift half and full grabens, as observed from well intersections. The source rock that is associated with this sequence stratigraphy, is mid to Late Hauterivian lacustrine source rock, which is the regional source rock in the Orange Basin, proven by the A-J1 well. In the chronostratigraphy (Fig. 5), the syn-rift sequence is documented as the sequence that occurs pre-6At1 unconformity.

#### 1.3.1.2.2 Drift Stratigraphy

The drift stratigraphy has been divided by Muntingh & Brown (1993) into Super-sequences. These consist of Super-sequences: 6; 12; 13; 14; 15 and 16 and are presented in the chrono-stratigraphy of the Orange Basin (Fig. 5).

Super-sequence 6 to 12

This Super-sequence was deposited in the early drift phase from 117Ma to 112.5Ma (Fig.3d). The wells which intersected this sequence indicate that it consists of red beds, aeolian sands, fluvial channel sandstone and associated overbank claystones sediments. The basaltic extrusives are also present in some locations, e.g. Ba-A1 well location. In the 6 to 12 Super-sequence, there are four regional unconformities. These are namely: 6At1 (117Ma); 7At1 (116Ma); 9At1 (114Ma) and 11At1 (113.5Ma).

Super-sequence 13

This sequence marks the beginning of the main drift phase (Muntingh and Brown, 1993). This sequence is bounded to the top by the mid Albian unconformity, 14At1 (103Ma) and to the base by the late Aptian unconformity, 13At1 (112Ma) (Fig. 3d). The sediments in this sequence were deposited following the regional erosion event which occurred at 112Ma (Muntingh & Brown, 1993). This regional unconformity marks the Late Aptian/Early Albian and is referred to as 13At1. The sequence displays prograding stacking pattern of sediments deposited in a shelf environment.

Super-sequence 14

This sequence was deposited following a minor uplift and relative fall in sea level around 103Ma (Munting & Brown, 1993). It consists of cyclic prograding and aggrading sequences. The sediments of this sequence were deposited in the fluvial to deltaic environment, consisting of stacked

channel sandstone, siltstone, and shale. The reservoirs in the study area, Ibhubesi gas field, were deposited during this Super-sequence (Fig. 5b).

Super-sequence 15 to 16

This sequence consists of the Cenomanian sequence and the Turonian sequence. The Cenomanian sequence is bounded to the top by 15At1 sequence boundary – which marks the minor uplift and relative fall in sea level around 93Ma and to the base by the 14At1 sequence boundary (103Ma) (Munting & Brown, 1993). The Turonian sequence is bounded to the top by the 16At1 sequence boundary (90Ma) and to the base by the Cenomanian boundary – 15At1 (93Ma), (Munting & Brown, 1993).

The sediments in this Super-sequence consist of coarsening upward sequences of marine shales, siltstones with distal and channel sand deposits. The sequence boundaries (14At1, 15At1, 16At1) and the regional unconformities (13At1) will be used in this study as an age reference for the specific Super-sequence.

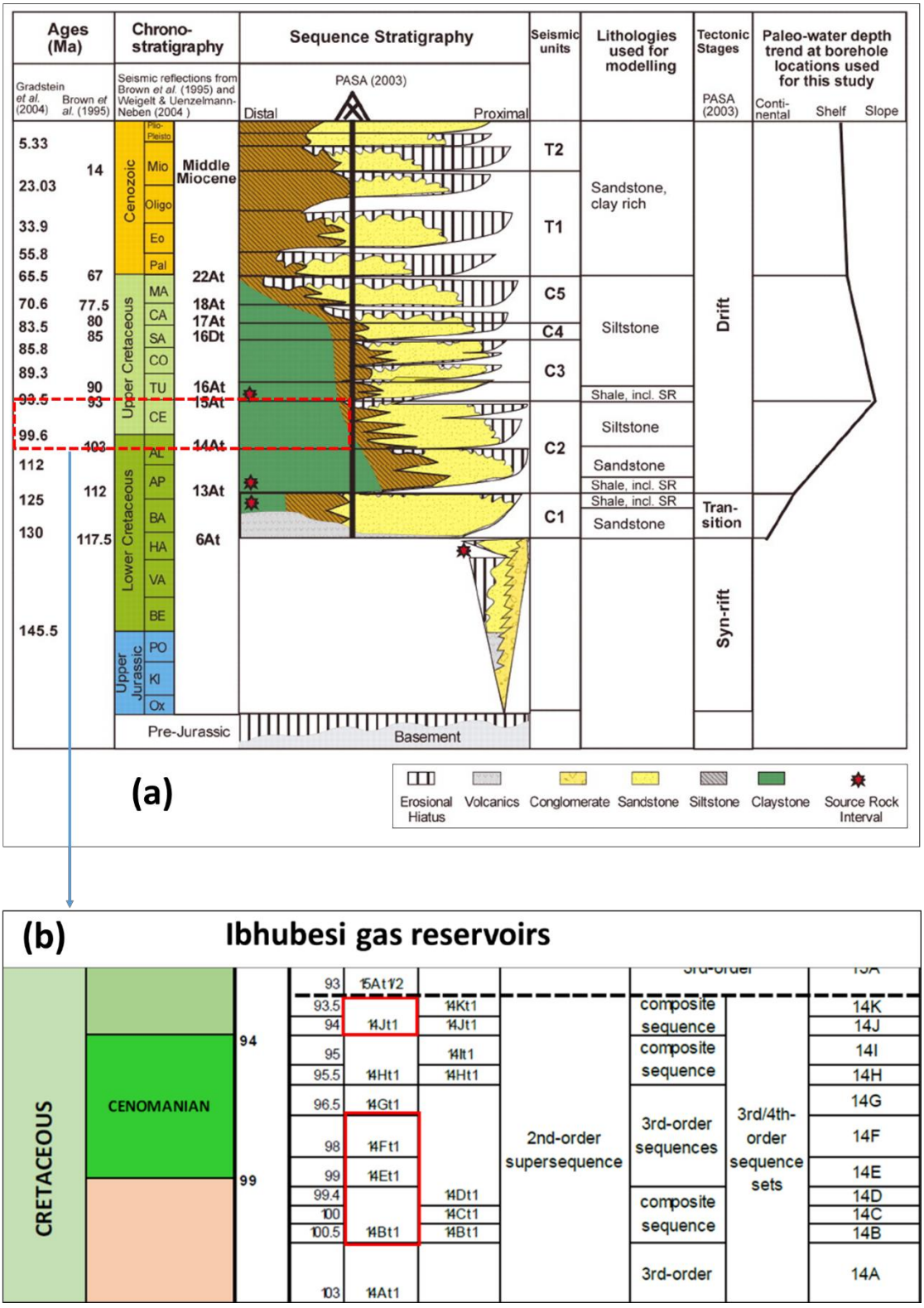


*Figure 5: Chronostratigraphy of the Orange Basin (modified after Brown et al, 1995). (b) A presention of a focused section showing the Albian to Cenomanian sequence. The reservoir s of the Ibhubesi gas field are stratigraphically stacked, with the 14Jt1 as the youngest and 14Bt1 as the oldest.*

## 1.4. Fault seal analysis background

Fault seal analysis is the main aim of this study, which is to determine the behaviour of the AK Fault. The ultimate goal is to understand whether the fault provides migration pathway to the reservoirs of the Ibhubesi gas field or whether it acts as a barrier and prevents further hydrocarbon migration.

Fault seals may develop in different ways depending on the style of deformation, the petrophysical composition (clay smears result from clay rich zones and cataclasites from quartz rich zones) of the faulted stratigraphy and post depositional processes, i.e., diagenesis, (Knipe et al., 1997; Fisher et al., 1998). These methods are briefly outlined below:

### 1.4.1 Juxtaposition seals

Juxtaposition seals occur when lithologies with different permeabilities are juxtaposed against each other across the fault. In this way, the capillary entry pressure of the sealing rock is higher than that of the juxtaposed lithology with hydrocarbons (Watts et al., 1987). The fault rock is then regarded as a seal. This fault rock sealing mechanism is presented in Figure 6. Juxtaposition analysis can be evaluated using well data and seismic data (Davies, et al., 2003). The results from the seismic interpretation provide the hanging wall and foot wall horizons intersection with the fault plane. The stratigraphy from the well data, is projected into the fault plane where reservoir overlaps can be evaluated.

Where the low permeability rock is juxtaposed against a high permeability rock, the fault seal will result (Davies et al., 2003). Davies et al., (2003), explains how the capacity of the fault to seal a certain hydrocarbon column height is a function of the threshold pressure. The threshold pressure is the pressure required to withstand the buoyance pressure of the hydrocarbons and thus providing a seal (Davies et al., 2003). The threshold pressure is described in detail in the fault seal analysis section of this study.

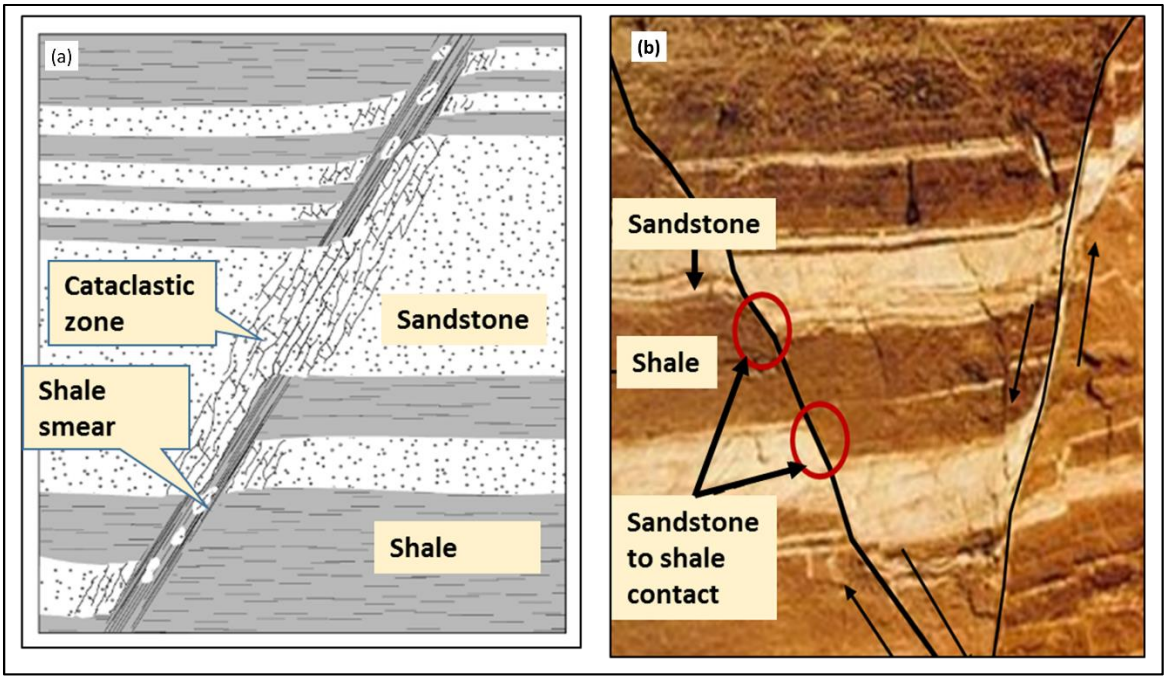


*Figure 6: Illustration of the different fault sealing mechanism. (a) cataclastic zone and shale smear (modified after Gibson, 1994), (b) Juxtaposition between shale and sandstone with vary fault throw, indicating areas of shale to sand contact (seal) and sand to sand contact (leak) (modified after Coohan et al.,(n.d)*

### 1.4.2 Clay (Shale) smears

Shale smears form in clay rich rocks, with the volume of clay in the framework of these rocks greater than 40% (Fisher and Knipe et al, 1998). During deformation, a continuous clay rich smear is entrained parallel to the fault. In this way, the fault rock will have a higher entry pressure causing it to seal. The clay smears on the fault plane is dependent on the thickness of the shale source bed and the distance from the shale source bed. The clay smear becomes thinner with increased distance from the source bed (Weber et al., 1978).

There are three algorithms that have been used in the process of predicting the fault zone properties. These algorithms are namely: Shale Smear Factor (SSF), published by Lindsay et al., (1993); Clay Smear Potential (CSP), published by Bouvier et al., (1989) and the Shale Gouge Ratio (SGR), published by Yielding et al., (1997).

All three of these algorithms show that the probability of the development of a continuous clay membrane increases as the throw to clay ratio decreases (Sperrevik et al., 2000).

#### *1.4.2.1 Clay Smear Potential (CSP)*

Bouvier et al., (1989), described the CSP algorithm as a measure of the probability of the development of a continuous clay membrane along the fault plane where lithologies with similar permeabilities, i.e. sandstone against a sandstone are juxtaposed against each other.

The CSP is dependent on the following factors: (a) the CSP increases with shale source bed thickness; (b) it will also increase if numerous source beds are displaced past a particular point along the fault plane and (c) the CSP will decrease with increased fault throw. A higher CSP indicates a higher probability of a continuous clays smear to occur. This relationship is displayed in equation (1.1) and Figure 7 (a).

$$CSP = \sum \frac{(thickness)^2}{dis\tan ce} \qquad (1.1)$$

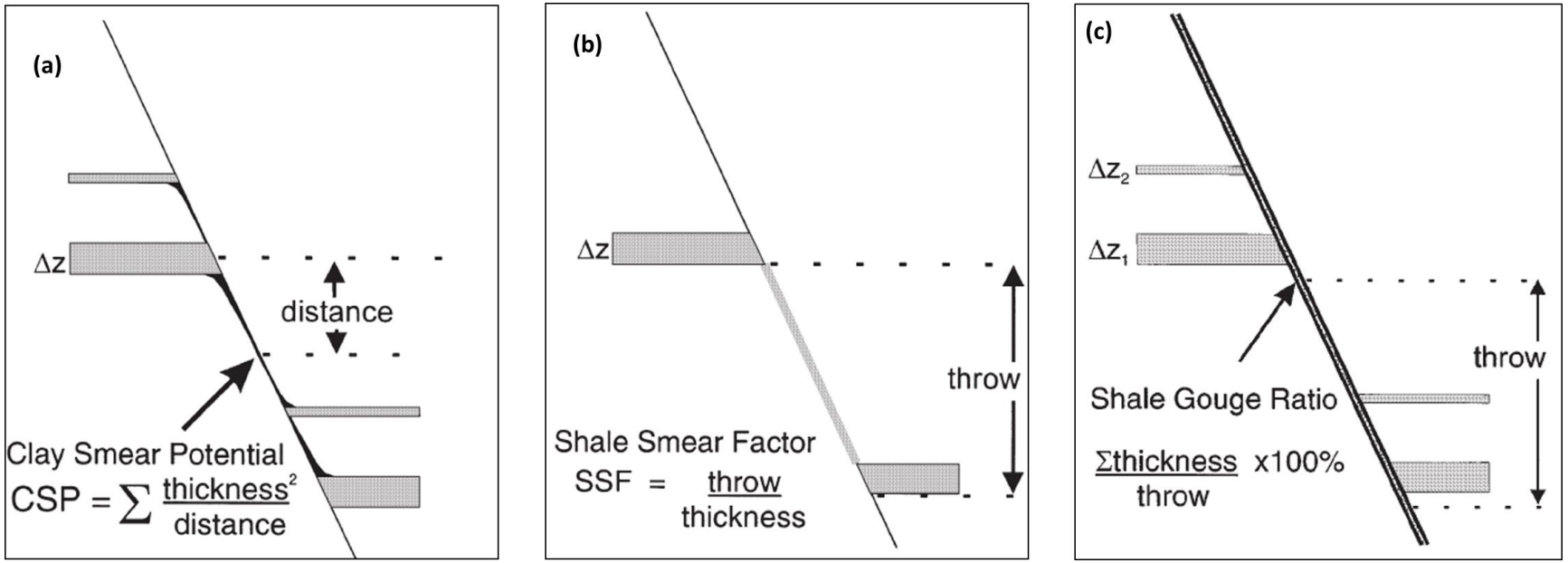


*Figure 7: The three algorithms that can be used to predict the shale smears in the fault zone. (a) Clay smear potential after Bouvier et al., 1989.The CSP algorithm measures the probability of the formation of the clay smear membrane along the fault plane (b) Shale smear factor (Lindsay et al., (1993), provides the limit of the continuity of the clay smear along the fault plane and (c) Shale gouge ratio algorithm for estimating the probability of the formation of clay smear membrane in the fault zone. The Shale gouge ratio can be used to estimate the fault seal capacity.*

#### *1.4.2.2 Shale Smear Factor (SSF)*

Lindsay et al., (1993), identified three types of shale smears: Shear, abrasion and injection smears. The shear smears develop where an impermeable lithology (shale) is juxtaposed against a permeable lithology (sandstone). The sheared sandstone does not form a continuous gouge when compared to the shale, however the apices of the sand beds point to the direction of movement (Fig, 7). The thickness of the smear decreases with distance from the source bed.

The abrasion smears also occur when a shale is juxtaposed against a sand. In this instance, the fault displacement is less than the sandstone thickness. In this instance, a thin layer is formed when the sandstone scrapes past a shale bed. Lindsay et al., (1993) explains the relationship of the source bed thickness and the fault throw in the development of the abrasion smears. If the source bed is thicker and fault throw is small then the abrasion smear is the thickest and vice versa.

Lindsay et al., (1993), defined the SSF as "the ratio of the throw to the shale bed thickness for a single offset shale bed". Lindsay et al., further proposed that this factor would be used to define the limit of the probability of the continuity of the shale smears. Faerseth (2006), cited in Yielding et al., (2010), proposed a critical SSF of </= 4. If the SSF is small (<4 -5), there is a higher probability of a continuous smear along the fault plane (Yielding et al., 2010). This continuous shale smear will form a layer that is sealing and conversely when the SSF is large (>7), the smears become discontinuous and the likelihood of leaking is high (Lindsay et al., 1993). This is presented in Figure 7(b) and equation (1.2)

$$SSF = \sum \frac{Fault\ Throw}{shale\ bed\ thickness} \tag{1.2}$$

#### *1.4.2.3 Shale Gouge Ratio (SGR)*

The fault gouge consist of a variety of the host rock lithologies that are combined together during the process of deformation. It is assumed that these lithologies are combined in a uniform manner during deformation (Yielding et al., 2010). This assumption implies that, the bulk composition found in the fault rock will have the same composition as the host rock composition of the lithologies that were faulted (Yielding et al., 2010).

In the fault sealing potential studies, the clay content of the fault rock is the most important. This is because the clays/shale have small grains with small pore throats and therefore higher capillary threshold pressure.

The SGR algorithm is used in the process of estimating fault sealing capacity by taking the summation of the product of the individual shale beds and the change in shale bed thickness across a throw (Yielding et al., (1997), cited in Rivenaes & Dart (2002). The SGR is expressed as a percentage. Yielding et al., (1997), further observed a relationship between the throw of the fault and the preservation of the clay smear, if the throw is large, then it erodes the shale smear. This relationship is expressed in Equation 1.3 and Figure 7c

$$SGR = \frac{\sum (Vcl.\Delta z)}{throw} \times 100 \qquad (1.3)$$

Where Vcl = individual clay bed and Δz represent the change in bed thickness across the throw. A compilation of SGR data by Yielding et al., (2002) from various fault dependent reservoirs in the North Sea Fields show that SGR values of approximately 15 -20% are the cut-off for sealing versus non-sealing faults. If the SGR is less than this cut-off, (15-20%), there is a high probability that the fault rock is not sealing and where the SGR is greater than this cut-off, it is assumed that the fault rock will be sealing.

In this way, this cut-off can be used as an analog to other fault bounded reservoirs. This SGR data is presented in Figure 8.

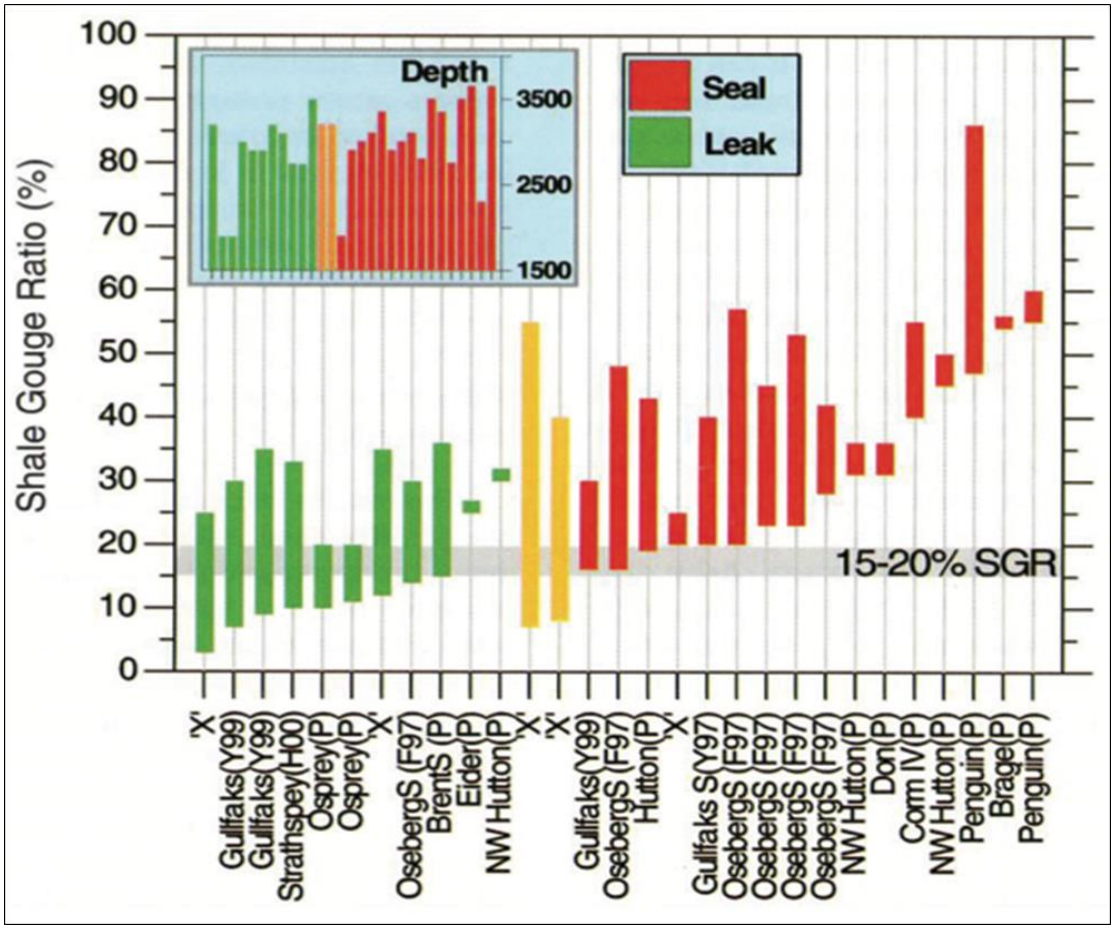


*Figure 8: A graphical illustration of the SGR for fault bounded reservoirs. The SGR of 15 – 20% has been observed as a cut-off, where fault rocks with SGR greater than 20% for seals and those with SGR less than 20% will result in leakages.This data was compiled by Yielding et al., 2002, using fault dependent reservoir in the North Sea fields.*

### 1.4.3 Cataclasites

In contrast to the clay smears which form in clay rich rocks, cataclasites form in porous sandstones with low clay content, about less than 15%, within the rock framework (Milliken and Reed et al., 2002). During deformation, there is mechanical compaction where the grains come to contact, this leads to grains being crushed, rotated and sliding). In this process, porosity is reduced by change in grain geometry, sliding and the resulting crushed material fills in the pore spaces and thus reduces permeability.

Cataclasites can be weakly lithified, partially lithified or lithified, based on the degree of compaction and cementation process (Knipe, 1992). Knipe, (1992) quantifies the degree of lithification by the amount of change in grain size reduction, pressure solution, quartz cementation and the conditions of deformation (pressure and temperature). This fault sealing mechanism is displayed in Figure 6a.

### 1.4.4 Phyllosilicate fault rock

This fault rock forms in impure rocks with clay or phyllosilicate content between 15% and 40% (Fisher, 1998). The fault rock seal mechanism is developed by the mixing of the clays, chemical alteration of the clays, e.g. swelling of the clays and in the process, the pore throat size is reduced and consequently the permeability is reduced (Fisher, 1998; Knipe, 1992).

# 2. DATA

To successfully complete a fault seal analysis study, it is important that the fault rock properties are well understood and can be quantified. This can be achieved by evaluating the distribution of stratigraphy against the fault, using the well data and the fault throw as a basis. In this study, this was achieved by the integration of four aspects: (1) seismic interpretation; (2) well data interpretation; (3) 3D structural modelling and 3D fault seal analysis (Fig. 2). In this section the database is discussed.

## 2.1 Database

The database consists of 3D seismic data and well data from the four wells that are within the study area. The 3D seismic data was used for the structural and fault interpretation. It is in SEGY format and in the time domain (Table 1). The well data that was used consist of whole core data (A-K1 well only available); cuttings or sidewall core (A-K2, A-Y1 and A-V1 wells) (Table 2).

There is a full suite of logs for all the four wells and they are in a LAS format (Table 1). The formation pressure data for the four wells was also used and is presented in Table 3. The A-K1, A-K2 and A-Y1 were drill stem tested (DST). The DST at the A-V1 well site was not successful due to mechanical failure of the DST tool.

*Table 1: Available and used data in this study*

| **WELL DATA** | | | | |
|---|---|---|---|---|
| **Parameter** | **A-K1** | **A-K2** | **A-V1** | **A-Y1** |
| Year drilled | 1986 | 2000 | 2003 | 2001 |
| Type of well | Exploration | Appraisal | Appraisal | Appraisal |
| Core data | Yes | No | No | No |
| Well results | Gas/ condensate discovery | Gas/ condensate discovery | Gas/ condensate discovery | Gas/ condensate discovery |
| Well status | Plugged and abandoned | Temporarily abandoned | Temporarily abandoned | Temporarily abandoned |
| Wireline logs | Full suite | Full suite | Full suite | Full suite |
| Formation pressure data | Available | Available | Not available | Available |
| **SEISMIC DATA** | | | | |
| Survey Name | AKAM06 | | | |
| Date Acquired | Merged and reprocessed AK99 and AM02 survey in 2006 | | | |
| Survey Size | 1125 $km^2$ | | | |

*Table 2: Core and cuttings depth intervals with associated reservoir depths*

| Well Name | Reservoir Sand | Top Depth m (MD) | Base Depth m (MD) | Whole Core data | Side wall core / cuttings |
|---|---|---|---|---|---|
| A-K1 | 14Bt1 | 3353.867 | 3370.936 | | Whole interval |
| A-K1 | 14Et1 | 3274.314 | 3286.963 | 3283 -3297 | Whole interval |
| A-K1 | 14Jt1 | 3217.621 | 3239.567 | 3236 - 3245 | Whole interval |
| AK-2 | 14Et1 | 3237.281 | 3259.226 | Not available | Whole interval |
| A-Y1 | 14Et1 | 3197.809 | 3228.137 | Not available | Whole interval |
| A-Y1 | 14Dt1 | 3330.245 | 3339.541 | Not available | Whole interval |
| A-V1 | 14Bt1 | 3419.856 | 3436.01 | Not available | Whole interval |
| A-V1 | 14Ft1 | 3320.644 | 3329.178 | Not available | Whole interval |

*Table 3: Formation Pressure Data survey, associated reservoirs and reservoir depths*

| Well Name | A-K1 | | | A-K2 | | A-Y1 | | |
|---|---|---|---|---|---|---|---|---|
| DST Number | 2A | 3 | 4 | 1 | 2* | 1 | 2 | 3 |
| Interval (mbKb) | 3354 - 3371 | 3275 - 3287 | 3231 - 3241 | 3239 - 3251 | 2699 - 2708 | 3338 - 3340 | 3215 - 3220 | 3199 -3211 |
| Net Interval | 17 | 12 | 10 | 11 | 9 | 2 | 5 | 12 |
| Pinitial (psia) | 4961 | 4847 | 4723 | 4180 | 3876 | 4764 | 4648 | 4627 |
| Pfinal (psia) | 4908 | 4848 | 4723 | | 3876 | 4814 | 4532 | 4539 |
| CGR | 6.1 | 10.6 | 16.1 | 2.4 | | 10 | 22.4 | 23.2 |
| Distance to barrier | 189.6 | | | 167.6 | | 365.8 | 15.2 | 45.7 |

# 3. METHODOLOGY

The 3D fault seal analysis was conducted using the following workflow. Each of these processes will be outlined further below.

- Seismic interpretation
  - Horizon and fault mapping
  - Depth conversion
- Well data Interpretation:
  - Facies definition from the well data (core, cuttings, wireline logs)

- Petrophysics
  - porosity, permeability and Volume of clay (Vcl)

- Pressure data
  - To calibrate the permeability,
  - determine gas water contacts and
  - assess hydraulic communication between the wells on the foot wall vs. hanging wall well
  -
- Structural modelling
  - fault modelling,
  - pillar gridding;
  - horizon modelling;
  - Make zones and layering

- Facies modelling
  - Upscale logs and make facies property model

- Petrophysical modelling
  - upscale logs and make property models of Vcl and permeability

- Fault seal analysis:
  - Juxtaposition analysis (1D well juxtaposition analysis and 3D facies juxtaposition)
  - Calculate fault rock properties
  - Column height prediction
  - Fault transmissibility

## 3.1 Seismic interpretation

Four steps that were carried out towards seismic interpretation. These are: well marker correlation; seismic to well tie; major horizon mapping (structural interpretation); fault mapping, in two way time (TWT) and depth conversion of the horizons and fault interpretation (Fig. 2).

### 3.1.1 Well marker correlation

The aim of doing well marker correlation was to determine the stratigraphic position of the different age makers between different well locations and to determine the thickness trends of the intervals of interest. This was done so that these well markers can be used as reference points to tying the stratigraphic interval of interest that will be mapped on seismic data. The trends in the thickness changes will be used as a reference to assist with seismic interpretation, for example, intervals that pinch-out between wells.

The horizons of interest in this study include the major regional unconformities: Cenomanian (15At1), Albian – Upper Peak horizon (14At1) and Aptian (13At1). These horizons were mapped to understand the structure of the study area and to build the structural model. The wireline logging began at the Cenomanian interval.

The reservoir markers of interest in this study are stratigraphically stacked and are located between the Cenomanian unconformity (15At1) and the Albian unconformity (14At1). These reservoir markers are namely: 14Jt1, which is the shallowest reservoir and is the closest to the Cenomanian boundary (15At1); it is followed by the intermediate 14Et1 reservoir, 14Ft1 and the deepest reservoir marker is at the 14Bt1 level, which is stratigraphically closest to 14At1 horizon.

The source of the data that was used for well marker correlation includes: paleontological studies, end of well reports and wireline logs. This well data was integrated and the final well markers were compared to the reflection on the seismic data.

The markers were then loaded into the IHS Kingdom software. The well correlations were done for regional markers and the reservoirs using the four wells within the study area. The final markers that were used are presented in Table 4.

*Table 4: Final well markers for the regional horizons and reservoirs*

| | Regional Horizons markers (m) | | | | Reservoir Markers (m) | | | |
|---|---|---|---|---|---|---|---|---|
| **Well Name** | **Sea Floor** | **16At1** | **15At1** | **14At1** | **14Jt1** | **14Et1** | **14Ft1** | **14Bt1** |
| ***A-K1*** | *270* | *1256* | *1826.63* | *3458* | *3205* | *3248* | *3284* | *3330* |
| ***A-K2*** | *260* | *1250* | *1800* | *3332* | *N/A* | *3212* | *N/A* | *N/A* |
| ***A-V1*** | *245* | *1275* | *1831.34* | *3600* | *N/A* | *3293* | *3337* | *3394* |
| ***AY-1*** | *294* | *1235* | *1795* | *3437* | *N/A* | *3170* | *N/A* | *N/A* |

### 3.1.2 Seismic to well tie

The aim of a seismic to well tie process is to match the seismic data that is acquired in two way time, to the well logs that are measured in depth. This process is important in this study because it makes it possible to relate and compare between the well logs that are in depth units and seismic data that is measured in time units.

The seismic to well tie was done on the IHS Kingdom software. The workflow is outlined below and in Figure 9. In Synpak, which is a module in IHS Kingdom software, the seismic to well tie is done in three steps: The initial step is to select input parameters needed to generate a synthetic trace; generate a wavelet to convolve with the reflection co-efficient log and display synthetic seismogram in Synpak.

In order to generate a synthetic trace, the required input parameters are: the well of interest; time depth chart; velocity data; density data and a reference log. In this study, the source of the velocity data that was used was the well of interest sonic log, the source of the density data was the well of interest RHOB log and the reference log was the well of interest Gamma Ray log.

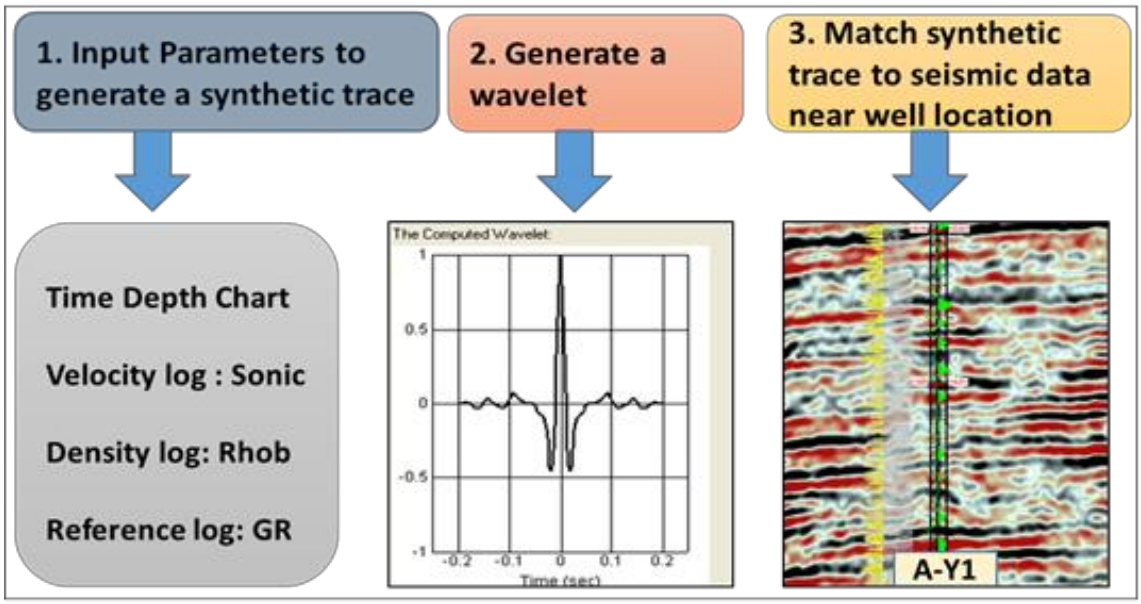


*Figure 9: Seismic to well tie workflow*

### *3.1.2.2 Generate a wavelet*

The second process was to generate a wavelet that will be convolved with the reflection coefficient. There are two methods that can be used to generate a wavelet. These are: to compute a wavelet from a theoretical wavelet and the second one is to extract a wavelet from seismic traces by matching it to frequency. In this study, the wavelet was extracted from seismic traces (Frequency Matching). The traces and time range to use is then selected. In this study the traces were selected within a set distance from a wellbore.

All the data that has been loaded into the Synpak is then updated and next process will be to display the data in Synpak and quality control and display on the seismic data while editing.

### *3.1.2.3 Match generated synthetic trace to seismic data*

A synthetic trace is then generated, which shows the tie between the well data and the seismic data. The synthetic is compared to the real seismic data that is collected near the well location. The synthetic trace is then shifted to tie the reference point (selected well marker) until a good character match is achieved. The good character match should be achieved with the least time shift so that the time to depth curve is not altered. The final step is to quality control the whole process.

### 3.1.3 Structure (Horizon) mapping

The aim of mapping the regional horizons in this study was to understand the structure of the study area and to use these regional horizons to build the 3D structural model. The sea floor and the regional horizons from the correlated markers (Cenomanian, Albian and Aptian) above, were used for the structural mapping.

Structural mapping was done on the IHS Kingdom software, using the AKM06 3D seismic data. This 3D seismic data is in the time domain and therefore all horizons mapped were in time domain. The results from the seismic to well tie indicated that the unconformity marker correlates with the peak of the seismic data reflection and as a result, all regional horizons were mapped on the peak.

The interval between the seismic lines used to map the different horizons depend on the structural variability of the different horizons. The horizons that show a high degree of structural variation were mapped in detail to capture the structural variation. The sea floor for example was not mapped in detail, since the structure of the sea floor does not vary significantly and it can easily be auto-tracked in the study area.

The increment that was used to map the sea floor is every 500 m for the inlines and 250 m for the cross lines. The other horizons; Turonian, Cenomanian, Albian and Aptian were mapped at every 250m interval for the inlines and 125m for the crosslines. Reservoir mapping had already been done by means of seismic amplitude extractions. Reservoir mapping is therefore not part of this study.

### 3.1.4. Fault mapping

The aim of fault mapping in this study is to determine the spatial location of the AK fault; to determine what type of fault it is; to get the fault surface from which the fault seal analysis study will be carried out and the fault displacement that will be used as an input in the calculation of the fault thickness, fault clay prediction (SGR/SSF) and juxtaposition analysis in the fault seal analysis study.

In juxtaposition analysis, the resulting juxtaposition is the function of the fault displacement (Cerveny et al., 2004). In this way, the amount of the offset in the faulted stratigraphy has an impact in the fault zone properties that result after deformation. There are two instances in which the fault seal can result which could be attributable to the throw of the fault:

(1) In a sequence, where a reservoir is deposited on top of a shale. In this case, if the fault displacement is larger than the reservoir thickness, then the reservoir will be juxtaposed against the shale, with lower permeability, causing the fault to seal.

(2) If the fault displacement is smaller than the reservoir thickness, then the reservoirs will be juxtaposed against each other. The fault seal can still result because the rock within the fault zone, may have lower permeability as compared to the host rock permeability.

In fault clay prediction process, the fault displacement is a required input. In this methodology, the fault displacement, which is derived from the horizon intersections with the fault, is combined with the stratigraphy thickness and clay content from the host rock. These are then contoured on to the fault surface. Furthermore, there is a relationship between the clay smear and the fault throw (equation 1.1). If the throw of the fault is large, it will erode the shale smear.

The objective of the fault analysis study is to understand the behavior of the AK fault and as a consequence, the AK fault is the only mapped fault.

Fault interpretation can be done on well data (wireline logs and core), provided that the well was drilled through the fault of interest, and on seismic data. In the study area, there are currently no wells that have been drilled through the AK fault. The distance from the AK fault to the wells ranges between 200m in the A-K2 well location and 3 km at the A-Y1 well location. The AKMO6 3D seismic data is the only available data that could be used for the AK fault mapping.

The workflow that was used for fault mapping is shown in Figure 10 and has been described by Marfurt, (2007). This workflow follows four steps. These steps are namely: Generate a geometry enhancing seismic attribute (similarity/variance); generate time slices; 3D visualization mapping guided by coherency attribute and Quality control the interpretation.

#### *3.1.4.1 Generate Coherency Attribute*

The first step is to generate a coherency type seismic attribute. Two coherency type seismic attributes that were created, similarity and variance attributes. A vertical seismic profile of the coherency attribute is presented in Figure 10a. This type of attribute is useful for highlighting edges and geometry on the seismic data (Marfurt, 2007). This can be achieved by studying the similarity of the local waveforms of the inline and crosslines. The coherent traces that show similar waveforms indicates lateral continuity. The incoherent traces have different waveforms, indicating possible breaks in seismic, which may be associated with fractures or faults (Marfurt, 2007).

In this study, two coherency (geometric) attributes were used: variance and similarity attributes. The two were used to compare which attribute would best delineate the geometry of the AK fault.

#### *3.1.4.2 Generate seismic time slices*

The time slices were generated at an increment that will accommodate the nature of the fault, meaning a bigger increment used for a fault with a small throw will not capture the fault adequately. It is important then to scroll through the time slices and observe the trend of the fault from the different levels. The increment is varied until desired observations are reached. The sea floor time slice was taken at time 0s, and then successively at times: 0.504s, just below the Sea floor marker; at the Cenomanian Sequence at time 1.68s and at the Albian sequence at 2.480s (Fig. 10b).

#### *3.1.4.3 3D Visualization: Mapping guided by coherency attribute*

3D visualization allows for fault mapping while having guided control from the time slice generated above and the vertical seismic line. The fault is then mapped through successive vertical seismic lines and its successive time slices of the similarity attribute (Fig. 10c). In this way the fault mapping is guided by the similarity attributes.

#### *3.1.4.4 Quality Control the interpretation*

After the fault interpretation was completed in the study area, the whole fault interpretation was checked to evaluate the quality of the interpretation. This was also done in the 3D Vu Pak module of the IHS Kingdom software. In this way, the fault that was interpreted through the various successive time slices and vertical seismic lines should appear vertically through the profile, tying the mapped seismic line and the corresponding time-slice as shown in Figure 10d.

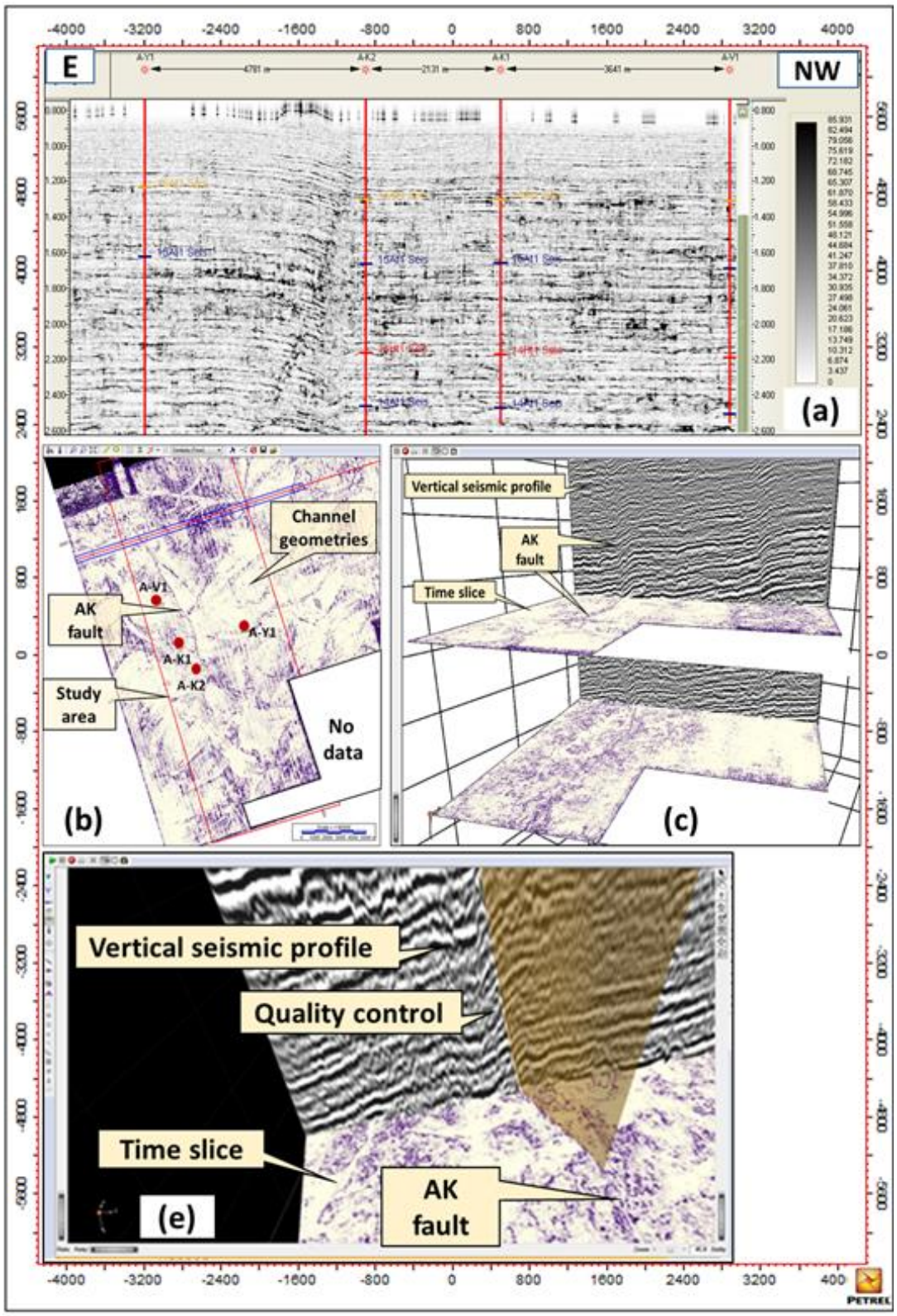


*Figure 10: An illustration of the coherency guided workflow that was used for fault mapping. (a) A vertical seismic profile of the generated coherency seismic attribute; (b) The generated coherency time slices, which highlight the geometry of the AK fault and the channels. The study area presented is outlined in red; (c) 3D visualisation*

## 3.2 Depth conversion

Depth conversion is a geophysical process whereby the seismic data which is acquired in the time domain is converted in to the depth domain. Depth conversion is also done on interpretation that has been done on seismic data in the time domain. In this study, there are three reasons for doing depth conversion:

- To convert the AK fault that was mapped in two way time to be able to create a fault model;
- To convert the horizon maps from time into depth, which will be used to create the 3D structural model and
- To get the displacement of the AK fault in depth.

The data that was used for the depth conversion includes: formation tops that correspond to the horizons to be used; travel time from seismic horizon and fault interpretation and velocity data. The workflow that was used for converting the time surfaces and AK fault will be discussed below.

The workflow begins with quality controlling the formation tops and seismic horizons that will be used. The interval velocities were determined between 2 zones: Zone 1 (Sea floor to 15At1) and Zone 2 (15At1 to 14At1). The interval velocity map was then generated for these two zones, using velocity control points representing the interval velocity at well locations. This was done between two boundaries, using two time surfaces H1 (Sea floor) and H2 (15At1), for zone1.

The time surfaces that were used were in a grid format and the two corresponding formation tops F1 (Sea floor) and F2 (15At1), for zone 1. The calculated interval velocity can be expressed using the equation 3.1

$$V_{\text{int}} = \frac{2[D2 - D1]}{[T2 - T1]} \qquad (3.1)$$

Where, D1 is the formation top at the top of the interval (corresponding to horizon 1), D2 is the formation top below (corresponding to horizon 2), T2 is the two way time to the second reflector (horizon 2) and T1 = two way time to the first reflector (horizon 1).

The interval velocity maps for the Sea Floor to 15At1 and 15At1 to 14At1 were created. The layered depth conversion method was used and the different layers were depth converted subsequently.

The next step was to define the 3D velocity model. The IHS Kingdom software was used to define the 3D velocity model. The inputs to the model are: time surfaces, interval velocity maps and formation tops. The results were quality controlled by checking the depth at formation tops and the depth at the depth converted surface (depth error).

## 3.3 Well data interpretation

The well data interpretation was carried out using core, wireline logs, petrography and formation pressure data. The interpretations from these datasets were integrated to determine the petrophysical composition; facies and depositional model. These in turn were used to populate the 3D structural model, from which fault seal analysis would be conducted. The data from four wells, which are within the study area was used.

### 3.3.1 Petrophysical Interpretation

The objective of doing the petrophysical study was to obtain the volume of clay, porosity and permeability logs. This study focuses on the calculation of the logs and quality control of the calculated logs by matching it to the core, cuttings and pressure data where relevant. These three parameters were selected because of their relevance to the fault seal analysis study.

#### *3.3.1.1 Volume of clay*

The shale or clay volume (Vsh) refers to the percentage of the rock, which is made up by the shale volume. The volume of shale can be expressed as a percentage or a ratio. There are various methods of calculating the volume of shale, these methods are: Calculating from the GR log; calculating from the electromagnetic propagation attenuation, calculating from the resistivity logs and spontaneous potential logs.

For this study the volume of shale was calculated from the GR log. The GR log was chosen over the SP log because of the limitation of the SP log. In hydrocarbon bearing intervals the SP log overestimates the volume of shale (Alberty, 1992). The reservoirs in the study area are all gas bearing and this would have an effect on the volume of shale calculated from the SP log.

The GR log measures the radioactivity of the formation (Alger, 1980) in this way it can be used as a lithology indicator. Shales have high concentrations of radioactive material. The shales will give high GR values as a consequence, while sandstones and carbonates have low concentrations of radioactive material and therefore give low GR values. It is therefore

possible to use the GR log to estimate the volume of shale in the sampled formation, by using equation 3.2. This is assuming that clean sandstones and pure shales exist in the well.

$$Vsh = \frac{GR\log - GR\min}{GR\max - GR\min} \quad (3.2)$$

Where, *Vsh* is the volume of shale, *GR log* is the Gamma Ray Log (API units), *GR max* is the Gamma Ray Maximum (measuring the shale response) and *GR min* is the Gamma Ray Minimum (measuring the sand response).

#### *3.3.1.2 Porosity*

Porosity was estimated from the density wireline logs of the four wells within the study. The bulk density of the rock is composed of fluid density, which is present between the pore spaces and the density of the minerals that form the rock. The porosity can be estimated from the bulk density of the rock, using equation 3.3.

$$Porosity = \frac{\rho matrix - \rho bulk}{\rho matrix - \rho fluids} \quad (3.3)$$

The porosity logs for the four wells were calculated using the IHS Kingdom petrophysical evaluation module. The equation above was used to calculate the porosity. The logs that were used as input parameters include the density logs (Rhob) and the Gamma Ray (GR) log was used as a reference log. The reservoir cut-off value was set at 10%.

#### *3.3.1.3 Permeability*

The permeability is reliably measured from core data (Timur, 1968). In the study area, there is only one well that had core cut, the A-K1 well. In the absence of core data, the permeability can be estimated from empirical equations. These equations are based on the factors that control permeability, which are: pore throat; pore throat geometry and porosity. This relationship is mathematically presented in Equation 3.4 is expressed as follows.

$$\log_{10^k} = C\log_{y10^\phi} + D \quad (3.4)$$

Where, C and D are constants equal to about 7, k is permeability and ø is the porosity. Permeability can also be correlated with wireline logs that have been logged in the cored well. The porosity to permeability correlation is the most commonly used and comes with its inherited errors. The neutron log has proved to correlate with the least statistical scatter

(Timur, 1968). Based on this, the wire logs that were used as input are: the reference log (GR) and an acoustic log, the neutron log was used.

To quality control the permeability logs, the core data from the A-K1 well as well as permeability determined from pressure data of the four wells within the study area was compared.

### 3.3.2 Sedimentology

The aim of this section is to determine the depositional environment of the reservoirs in the study area. This depositional environment will be used as a basis for facies modelling and petrophysical modelling. The data that was used for this study consist of core and cuttings data, the extracted sand bodies and the log data.

#### *3.3.2.1 Sand bodies*

The extracted sand bodies were used to determine the channel geometries. The channel geometries were used in conjunction with the well data to determine the depositional environment. Fluvial channels can be meandering or braided. The sinuosity ratio of the extracted sand bodies was used to determine the geometry of the channel. Sinuosity ratio refers to the distance between two points measured along the curve of the stream or a distance of the straight line between two points.

Sinuosity values range from 1 to about 4 (GIS 4 Geomorphology). A straight channel will have a sinuosity of 1 and channels with ratios from 1.5 are considered to be sinuous. Channels with higher ratios of sinuosity are considered to be meandering (Leopold, Wolman and Miller, 1964).

#### *3.3.2.2 Core and cuttings data*

The A-K1 well is the only borehole that has cored data within the study area. This is not enough to represent the whole study area. The cuttings reports were used in conjunction with the core data. The core and cuttings reports were used to identify the depositional features and based on these features classify the different facies. Table 2, shows the depths of the cored interval and the sampled cuttings interval.

#### *3.3.2.3 Wireline logs*

The wireline logs were used to determine facies using the log response. This was conducted by studying changes in well log response's baseline, trends or shapes, abrupt breaks and anomalies. The facies were defined by intervals with similar log response.

## 3.4 3D Structural Model

The workflow for building the 3D structural model is presented in Figure 9 and outlined below:

- Create a Petrel project – import seismic interpretation done in IHS kingdom software into

  Petrel and well data (wells, well logs, well markers)
- Fault modelling
- Build a 3D structural grid – corner point gridding
- Scaling up well logs
- Facies and petrophysical modelling

Points, number 2 to 5 will be discussed below:

### 3.4.1 Fault Modelling

The purpose of fault modelling is to define the faults that will be incorporated into the structural grid. In this way, the faults that were interpreted, in this case the AK fault was converted into a fault model which can be used in the structural model. This is an important step in the process of building a structural model because the faults act as foundation for building the structural grid.

There is only one fault that was used in this model, the AK fault. The orientation of the fault is NNW to SSE. The fault propagates from the Tertiary sequence to the Aptian sequence, where the offset can be observed. The fault was modelled as a plane.

### 3.4.2 Structural Grid

The structural grid defines the upper and lower most limits of the area to be modelled. The extent of the structural grid is limited by the grid boundary. The structure of the grid is determined by the input data, horizons and faults. In the study area, the Ibhubesi grid uppermost limit is defined by the Cenomanian horizon (15At1) and the lower most limits were defined by the Albian near (14At1) Horizon. The grid boundary was constrained by the boundary of the study area and as a consequence, all the wells in the study area are included in the grid. These wells are sitting on different cells of the structural grid. The cell trends were set to follow the depositional trend and the AK Fault.

There are two other steps which form part of creating structural grid, these are horizon modelling and layering.

#### *3.4.2.1 Horizon modelling*

The input data that was used for horizon modelling includes the 3 horizons: Cenomanian Horizon (15At1), Upper Peak and Base of the model. The respective horizon was used with its corresponding well marker as an input in the horizon modelling process. The well marker is important for tying the horizon to the well. The results from this horizon modelling process created two zones: Zone 1 = Cenomanian (15At1) to Upper peak (UP); Zone 2 = Upper peak (UP) to base of the model (BM).

#### *3.4.2.2 Layering*

The two zones that have been created above are then subdivided into layers during the process of layering. This process adds the fine scale grid cells, which describe the spatial variation in the reservoir properties within each zone. In order to capture this variation, it is important that the grid cells must be smaller than the geological features being modelled. In this study, the geological features that were considered while doing the layering process are the facies and the AK fault.

In the case of the facies, it was considered that the thickness of the grid cells should be small enough to capture the thinnest facies that were defined in the study area. In the case of the throw, the cell thickness should capture the smallest throw from the AK fault that was observed. This is presented in Table 5.

*Table 5: Thickness of the facies observed in the study area and the throw that was used to guide the cell thickness in the layering process.*

| **Facies thickness (m)** | | | | **AK Fault throw (m)** |
|---|---|---|---|---|
| **Zone** | **Porous sandstone** | **Tight sandstone** | **Shale** | |
| 15At1 to Upper Peak | 3 - 22 | 3 -10 | 3m - 16 | 7 - 54 |
| Upper Peak to base of model | 10 - 30 | 2 - 7 | 2m - 40 | 10 - 120 |

The layering scheme that was used in the different zones is presented in Table 6. In the 15At1 to Upper Peak, the layering scheme that was used is the Parallel layering. In this scheme, the cell layering is parallel to the base. In Petrel Software, this is referred to as “follow the base. The cell thickness that was used in this interval was based on the minimum thickness of the different facies defined in the study area and 1m was used.

The cell thickness of 1m that was used based on the facies thickness also accommodates the throw in this interval. The minimum throw in this interval is 7m and a cell with 1m thickness should capture the variation in the throw adequately.

In the Upper Peak to the base of the model, Parallel layering was also used. The minimum cell thickness used in this interval was 2m based on the facies thickness and it also accommodates the throw variation as the minimum throw in this interval is 10m. Table 6 below, illustrates the parameters that were used in the layering process. The next phase would be to define the properties of the model.

*Table 6: Parameters that were used in the layering process*

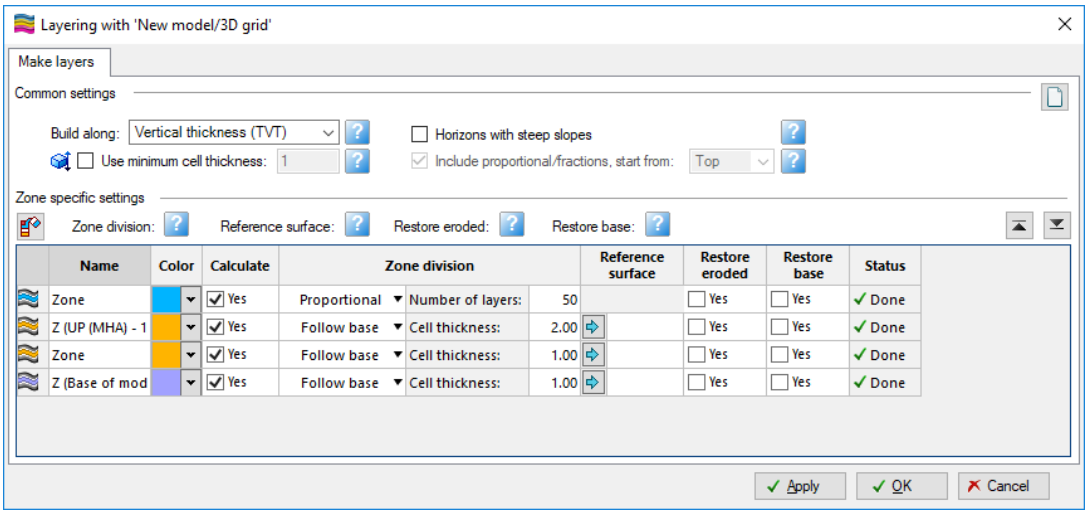


## 3.4.3. Property modelling

There are two processes that define the model properties: facies modelling and petrophysical modelling. Prior to property modelling the well properties need to be scaled up to accommodate the difference in the scale of the sampling density between the well logs and the 3D grid.

### *3.4.3.1 Scaling up well properties*

In the process of scaling up well properties, the Petrel software requires the input data to be in the form of: well logs; well tops or points attributes. In this study all the well properties that were used as input data were in the form of well logs. The discrete (facies) well properties were up scaled first followed by the continuous (petrophysical) well properties. The discrete well properties were scaled up first so that the petrophysical properties could be scaled up based on the facies type. To be able to do this, the software requires an up scaled facies log.

The “most of” method was chosen as the averaging method in the scaling up of the facies logs. This method selects a value which is most represented in the input facies log for each particular cell and assign it to the cell. The results of the facies log up scaling were displayed on the well cross section for quality control.

A similar process was conducted when scaling up the continuous (petrophysical) data. As alluded before the calculation method was set to be based on the facies type. In this process, the software assigns the up scaled petrophysical property value to a cell so that the assigned value of the petrophysical property correspond to the type of facies. For example, if a cell has a flood plain shale facies, the results of the upscaling should have a cell with petrophysical properties that are representative of a flood plain shale facies, not that of a channel sand facies.

The averaging method that was used for the different petrophysical properties is different. The porosity upscaling was calculated using the arithmetic mean averaging method, the permeability by harmonic mean and Volume of clay by arithmetic mean. These averaging methods were chosen based on the petrophysical properties results which best fit the facies during the quality control process.

#### *3.4.3.2 Facies Modeling*

The up scaled facies logs were used to populate the grid using the Sequential indicator simulation method. The modelling was based on the interpreted depositional model as a result the zones were modelled separately because they do not indicate the same depositional model. The Sequential indicator simulation method was chosen because it is most appropriate to use where the shape of the facies bodies in uncertain. The relative acoustic impedance attribute which was used to extract the sand bodies in the Ibhubesi gas field was used to control the probability of the occurrence of the facies.

#### *3.4.3.3 Petrophysical Modelling*

The up scaled petrophysical properties: porosity, permeability and Vcl were populated to the grid using Sequential Gaussian Simulation algorithm and biased to the facies as explained in the petrophysical upscaling process. The log derived porosity in this study was mainly used to determine a relationship with permeability. This relationship was used as a basis for modelling permeability in the study.

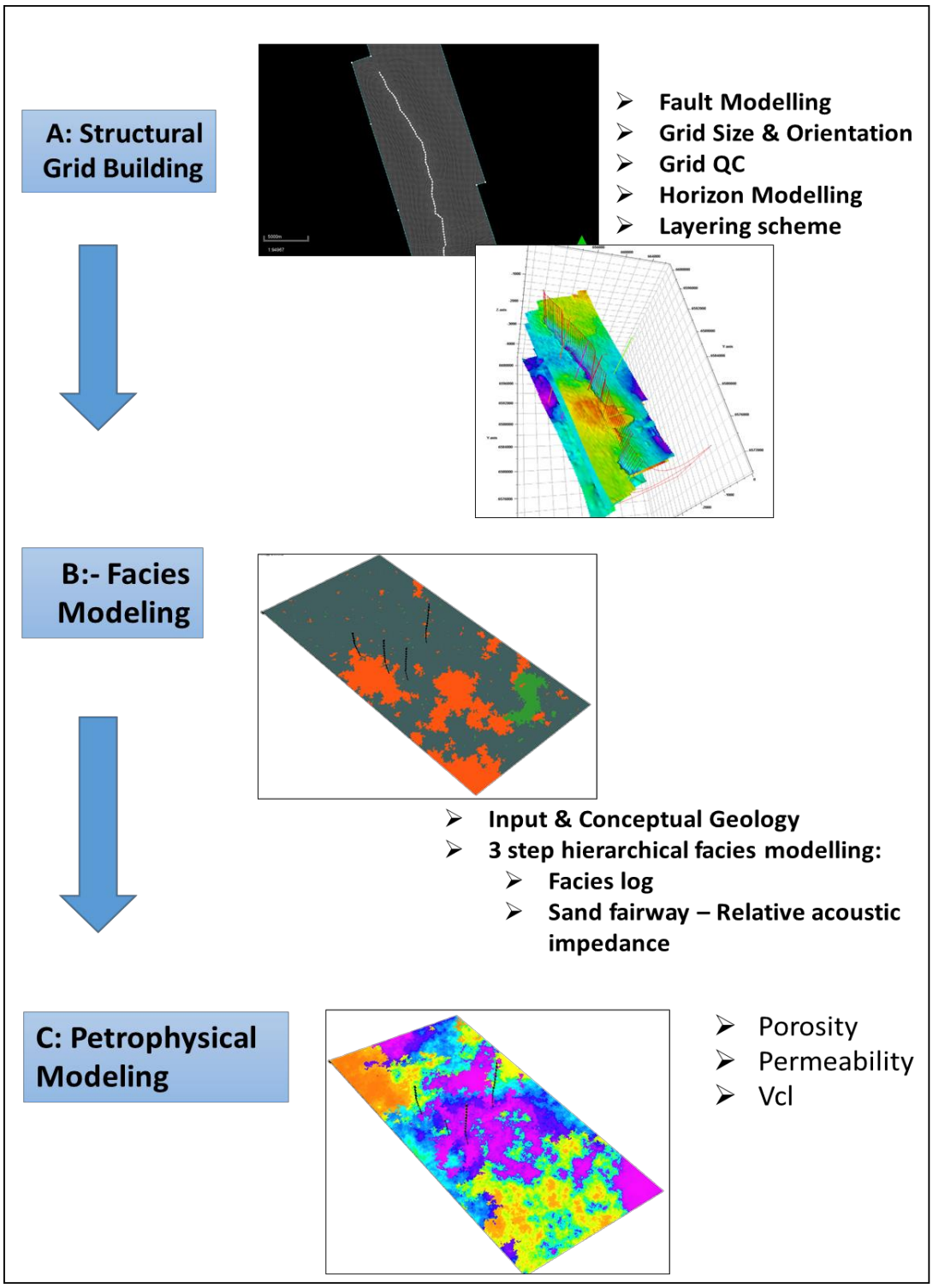


*Figure 11: Modeling workflow in the study area. A illustrates the beginning of the modelling workflow, which is the structural grid building process. In the figure, the AK fault model and horizons are shown. B illustrates the second part of the modelling phase. `In the figure, the facies property is shown. The last part of the modelling process is the petrophysical modelling presented by C. In the figure the porosity property is shown. The porosity, permeability and Vcl were used for petrophysical modelling.*

## 3.5 Fault Seal Analysis

The fault seal analysis process begins with the Juxtaposition analysis. Juxtaposition analysis is a quick analysis which focuses on the lithology of the juxtaposed stratigraphy on the hanging wall and that on the footwall. The second part is the evaluation of the fault rock properties. This is a more detailed study, integrating the seismic and the well data. The results from the fault rock properties evaluation give more confidence as compared to juxtaposition analysis on its own. These fault rock properties are then integrated into a flow model to estimate the transmissibility of the fault.

### 3.5.1 Juxtaposition analysis

Juxtaposition analysis is the initial look at the possibility of the formation of fault seals. There are two methods that were used in this study to do this analysis: 1D well juxtaposition (triangle diagram) and the 3D facies juxtaposition analysis.

In the 1D well juxtaposition analysis, the fault seal potential is determined from the juxtaposed stratigraphy with varying fault displacement at different stratigraphic intervals by using the triangle diagram. The input data that is required for this study is the well data, in form of: GR log, which is used as the lithology reference log; Vsh log, which is used to estimate the shale content with the change in the throw (hence SGR) and the defined facies. The SSF can also be determined using the triangle diagram. In this way, the critical throw can be determined using the triangle diagram, where leaks or seals will form.

In the 3D facies juxtaposition analysis, the fault seal potential is determined using the defined facies. These facies are namely, shale, porous sand and tight sand. The defined are mapped into the AK fault model. The operation uses the facies and the fault throw to determine all the different juxtaposition types that can occur.

### 3.5.2 Fault rock properties

The second part of this process is to evaluate the properties of the fault rock. These properties are namely: fault rock clay; fault rock permeability; fault rock thickness and the column height. The first three properties are also used in the flow model which determine the transmissibility of the fault.

#### *3.5.2.1 Fault rock clay prediction*

The fault rock clay property is an estimation of the percentage of the clay from the host lithology mixed within the fault rock (Childs et al., 2007). The fault rock clay property is used to estimate the probability of the fault to seal by using it to infer the fault permeabilities and transmissibility. Studies show that faults with higher shale content generally have a significant

reduction in permeability compared to the host rock permeability. Jolley et al., 2007, used a clay to transform function to indicate that faults with clay content of up to 50%, will have a permeability reduction of two orders of magnitude when compared to the host rock permeability.

There are different algorithms that can be used to determine the fault rock clay property. These include the Shale Smear Factor (SSF), Effective Shale Gouge Ratio (ESGR), Clay Smear Potential (CSP) and Shale Gouge Ratio (SGR).

In this study the SGR algorithm was used. This algorithm calculates the net clay within the host lithology that has passed a point along the fault plane. This is mathematically presented by Equation 1. In the Petrel software, this calculation is derived using the grid property Vcl, and the throw of the AK fault. The Vcl estimates are modelled across the fault surface with a calculated throw distribution from the AK fault model.

#### *3.5.2.2 Fault rock permeability predictor*

The fault rock permeability is the measure of the ability of the fluids to move through the pore throats within the fault rock. The method that was used to predict the fault rock permeability is the SGR method. This is based on studies that have been conducted by Manzocchi et al., (1999), Childs et al., (2007), and Sperrevik et al., (2002). These studies show a negative correlation between the phyllosilicate percentage and the permeability within the fault rock. The phyllosilicate percentage is equated to the SGR. This relationship was used as a basis to derive the fault permeability.

In this study, the fault clay to permeability transform was used to convert the fault clay content to fault permeability, using the Sperrevik (2002) defined transform. In addition to the fault clay content, this transform also requires the depth of the fault rock, the depth at timing of the fault and the maximum depth of the fault rock. The addition of the depth of the fault rock is based on the work that Sperrevik (2002) conducted where both authors Manzocchi (1999) and Sperrevik (2002) concluded that the permeability of the fault rock from deeper levels is lower than the permeability from the shallower levels (Fig. 10a).

It is based on this study that the Sperrevik (2002) transform was used as compared to the Manzocchi (1999) equation, which does not take account of the fault rock depth. Even though the Sperrevik (2002) transform was calibrated by the core measurements from North Sea reservoirs. This was used as there is no available data of cored faults measurements from the Orange Basin. The fault rock permeability can be expressed mathematically using equation 3.5.

$$K_f = a\exp[-\{bCCR + cZ_{\max} + (dZ_{f-e})(1-CCR)^7\}] \quad (3.5)$$

Where, is the fault rock permeability, Zmax is the maximum subsurface depth of target fault rock, Zf is the depth at the timing of the fault, CCR is the clay content in the fault rock, Constants: a = 80 000; b = 19.4; c = 0.00403; d = 0.0055 and e = 12.5.

Sperrevik et al., (2002) used the diagenetic history from the cored samples in the fault zone to estimate the timing of faulting that was used in the Equation (3.5) for variables Zf and Zmax. In the study there are no samples from the fault zone and as a result the seismic data was used to estimate the timing of the faulting. The depths 750m and 3.5 km for the Zf and Zmax were used respectively.

In the study area, The AK fault can be observed in the seismic data from the Aptian through to the younger sequences in the Tertiary (Fig. 10). The first appearance of the fault can be seen at 0.5s on the time slice. When the 0.5 is converted to depth, it is 750m. This is the depth that was used for the equation input Zf. Munting and Brown (1993), reported a minor uplift in the Orange Basin during the Albian times. This minor uplift was interpreted to have not had significant influence in the AK fault in the study area. This is because, there was no inversion observed in the throw direction of the AK fault.

It is interpreted that as the AK fault is young and progresses to the younger sequences, it is post depositional and therefore the present burial depth of 3.5km is the maximum burial depth. This depth was used as the input for the Zm.

#### *3.5.2.3 Fault rock thickness*

The fault rock thickness has been defined by Childs et al., (2007) as the total thickness of the deformed rock, measured on a perpendicular traverse across a fault zone (Fig. 10b). The fault rock is made up of smaller fault fragments that are separated by relay zones. These relay zones break during deformation to form a thicker fault rock with increased displacement, (Manzochhi et al., 1999). There is therefore a positive correlation between the average fault thickness and the throw of the fault (Walsh, 1998 and Hull, 1988). This relationship can be graphically presented in Figure 12 and by the equations 3.6 (Walsh, 1998) and equation 3.7(Hull, 1988) below:

$$t_f = \frac{D}{66} \text{ and } t_f = \frac{D}{170} \quad \text{(3.6) ; (3.7)}$$

Where, D is the fault displacement. In this study, the Petrel software (RDR) uses the fault displacement to fault thickness ratio in order to calculate the fault rock thickness. The fault rock thickness that will be produced should be directly proportional to the displacement of the AK fault at that particular point along the fault plane. The software assumes that the fault displacement to fault thickness ratio is constant. In this way, for a fault with 1:100 fault displacement to thickness ratio, the software will produce a 1m thick fault for 100 m displacement. This relationship may be unfavorable to faults with small displacements. This is because it may underestimate the thickness of the fault rock.

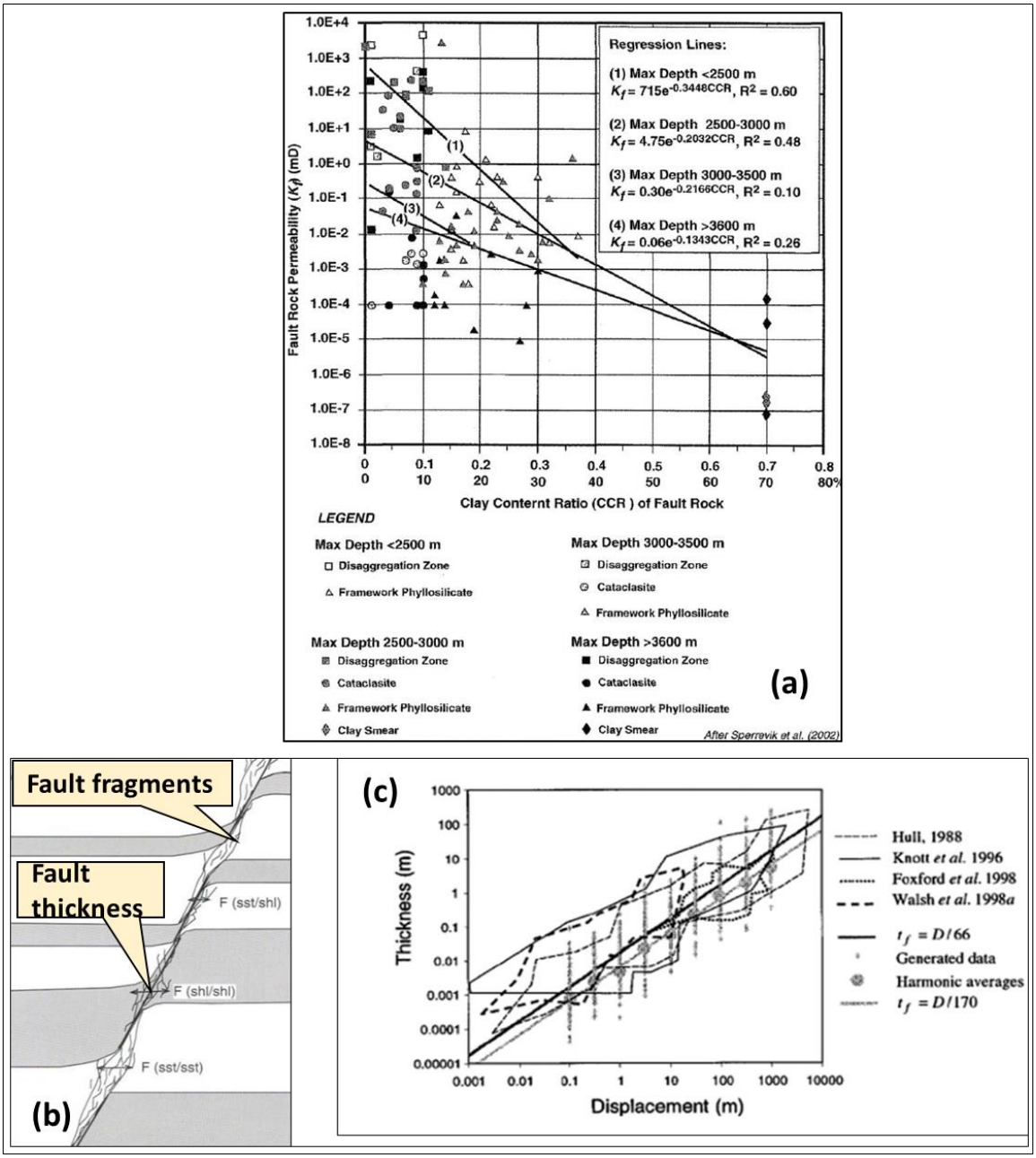


*Figure 12: Fault rock properties, (a) Fault rock permeability versus clay content relationship indicating the fault permeability change with depth (Sperrevik et al., 2002); (b) Illustration of the fault rock thickness and associated fault fragments and relay zones (modified after Knott et al., 1996) and (c) graphical plot showing the relationship between fault thickness and fault displacement (Hull, 1988 Knott et al, 1996; Foxford et al. 1998 and Walsh et al. 1998a;*

### *3.5.2.4 Across fault pressure difference (AFPD)*

The across fault pressure difference refers to the difference between the in situ pressure on the hanging wall reservoirs and the footwall reservoir. This across fault pressure difference can be determined from well pressure data. This study was conducted so that the SGR values can be calibrated in order to determine the strength of the fault seal and hence column height.

In the study area, the 14Et1 reservoir was used for this study. There are two reasons why the 14Et1 reservoir was selected: 1) the reservoir is present in the wells located on the foot wall (A-K1, A-K2) and the well on the hanging wall (A-Y1); 2) there is well pressure data available to successfully conduct this study.

A depth pressure plot was created for the 14Et1 reservoir for the A-K2 and the A-Y1 wells, using data pressure data points from the Repeat Formation Testing (RFT) (Fig. 13). The A-K1 well was not included in this evaluation because the RFT points were insufficient to calculate a fluid gradient (Fig. 13a). The fluid gradients and gas water contacts were determined from this plot. The fluid gradients from the footwall and the hanging wall were compared to determine the AFPD. The results of this AFPD will be plotted on the calibration plot of SGR from a variety of worldwide fault data sets based on a study conducted by Yielding et al.,2002 and Bretan et al., 2003 (Fig. 13d).

### *3.5.2.5 Column height on AK fault rock*

Cerveny et al., (2004) relate the threshold pressure (Pt), to the sealing capacity of the fault. The fault threshold pressure is the measure of the strength of the fault seal that can support a certain hydrocarbon column height. The hydrocarbons will be supported at a certain threshold pressure for as long as the capillary pressure of a fault (threshold pressure) is greater than the buoyancy pressure of the hydrocarbons (Cerveny et al., 2004). In this way the effective permeability to the hydrocarbons is zero. Where the hydrocarbons buoyancy pressure is greater than the threshold pressure, then the seal is breached. The measure of the sealing capacity can be mathematically expressed as:

$$H = \frac{dP}{g(\rho w - \rho h)} \qquad (3.8)$$

Where, d*P* is the buoyancy pressure, ρw is the density of water, ρh is the density of hydrocarbons and g is the acceleration due to gravity. In this study, the column height on the AK fault was determined using the empirical relationship between the fault zone composition

(SGR) and the capillary entry of the fault zone (AFPD). This methodology is based on Childs et al., (2002). The potential hydrocarbon column height on the fault is calculated in two parts:

Firstly, the SGR of the fault is calibrated to estimate the maximum pressure that can be supported by the AK fault, using equations that relate the SGR to the threshold pressure. This maximum pressure is taken to be equivalent to capillary entry pressure along the fault plane (Brentan et al., 2003). The software allows the calculation method to either use a function that displays the relationship between the SGR and the threshold pressure or the use of global equations. In this study, the latter method was selected. This is because there is no core calibrated data in the study area that can be used as input into defining a core calibrated function.

Secondly, the properties of the fluids at reservoir conditions are incorporated to translate the pressure difference (derived from the SGR) into the potential hydrocarbon column height. According to the reservoir fluids analysis in the study area, the density of the gas is about 0.2 g/cc and that of the water is 1.115 g/cc.

### 3.5.3 Fault transmissibility

The fault transmissibility prediction is the final step in fault seal analysis process in this study. In this step, the fault properties are integrated into the flow model to determine whether the fault has the ability to transmit fluids. The transmissibility can be expressed mathematically by equation 3.9.

$$Tm = [(1 + \frac{tf}{Lg}) \times ((\frac{Kg}{Kf}) - 1)]^{-1} \quad (3.9)$$

Where, *tf* is the fault thickness, *K* is the permeability and *Lg* = length of the block.

*The measure of transmissibility is between 0 and 1, where:*

- The fault is sealing, the transmissibility multiplier is zero
- The fault is open, the transmissibility multiplier is 1
- The fault is partially sealing and partially open, the transmissibility multiplier is between 0 and 1

In the Petrel software, the process that is followed to predict the fault transmissibility is outlined below:

- Calculate a transmissibility multiplier

- Insert the 3D grid permeability
- Chose a sealing scenario
- Chose the fault that will be analysed
- Fault properties ( Vsh, fault permeability, fault thickness)
- Run the simulation

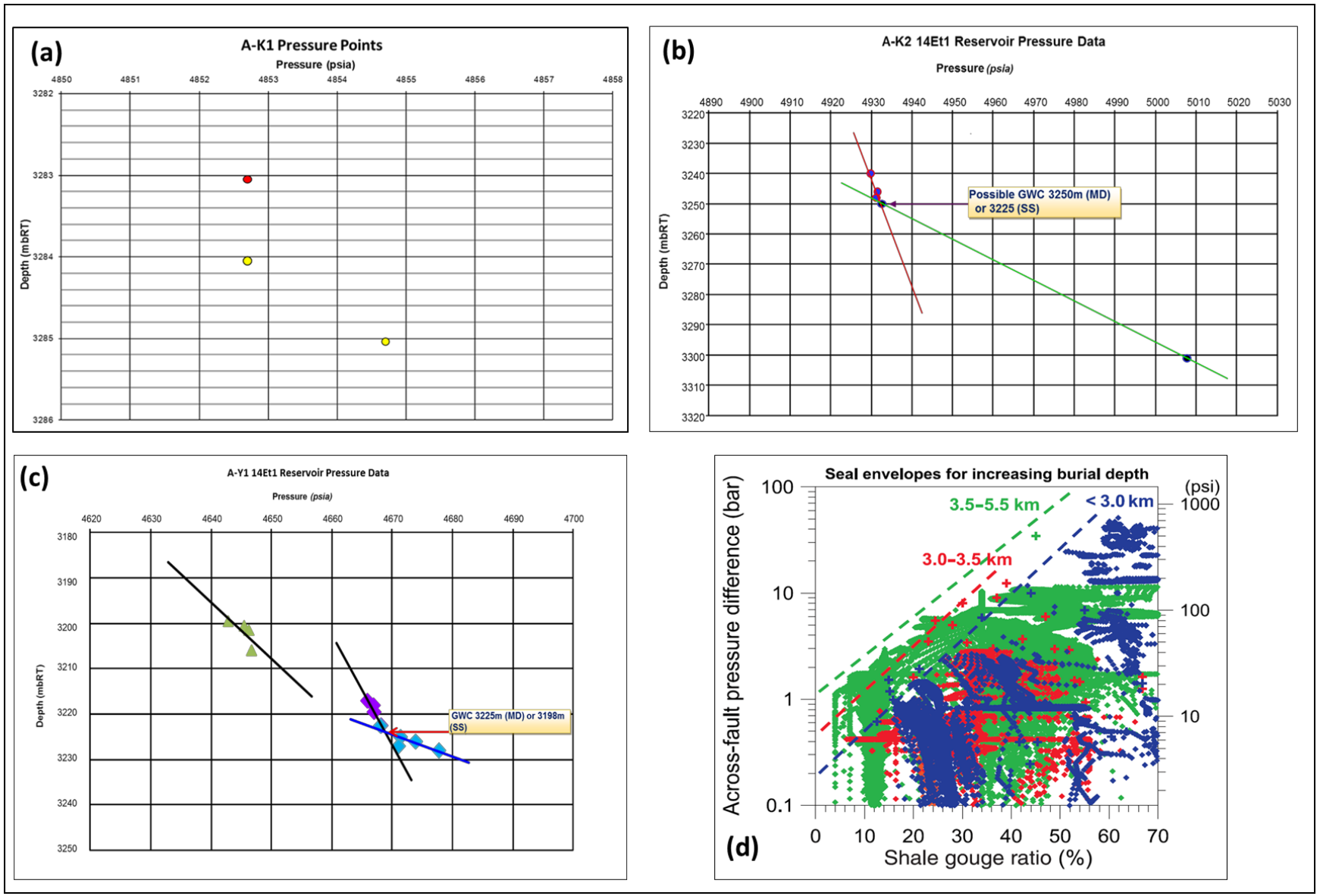


*Figure 13: Pressure versus depth plot of the three wells within the study area. (a) The A-K1 well only had three valid pressure points and these were insufficient to calculate a fluid gradient and (d) the seal envelopes for increasing burial depths ranging between 3.0 km to 5.5 km, indicating the relationship between the across fault pressure difference and shale gouge ratio (Yielding et al., 2002 and Brentan et al., 1993)*

# 4. RESULTS

## 4.1 Seismic interpretation

This section consists of the results of the well correlation, seismic to well tie and how this feeds in to the structural interpretation.

### 4.1.1 Well marker correlation

The well correlation of the regional horizon markers was only possible at the Albian to Cenomanian interval. This is because the wireline logs that could be correlated were only available within this interval in all four wells within the study area. The well correlation of the regional horizon markers show that there is a thick sedimentary wedge at the Albian to the Cenomanian interval. This is part of the main depocenter of the Orange Basin.

The study area is too localized to show the regional extent of this interval. Regional horizons (Fig. 14) and literature (Fig. 15) show however that this sequence becomes thinner as you approaching the present day coastline towards the continent (Paton et al., 2008).

The reservoirs of the Ibhubesi gas field are located within the Albian interval, Figure 16. The reservoirs are vertically stacked. The base of the sequence, marked by the 14At1 sequence boundary, is overlain by sediments which display an upward fining pattern on the wireline logs. These sequences are separated by thin argillaceous material. The deposition appears to have been cyclic, with the reservoir sequences topped by shales.

This deposition appears to be progradational and aggradational. The prograding sands have been deposited within the delta-front, this is particularly in the A-Y area and it is presented by the upward coarsening wireline log pattern. The aggradation deposits are mainly fluvial sediments, which are presented by the fining upward wireline log pattern.

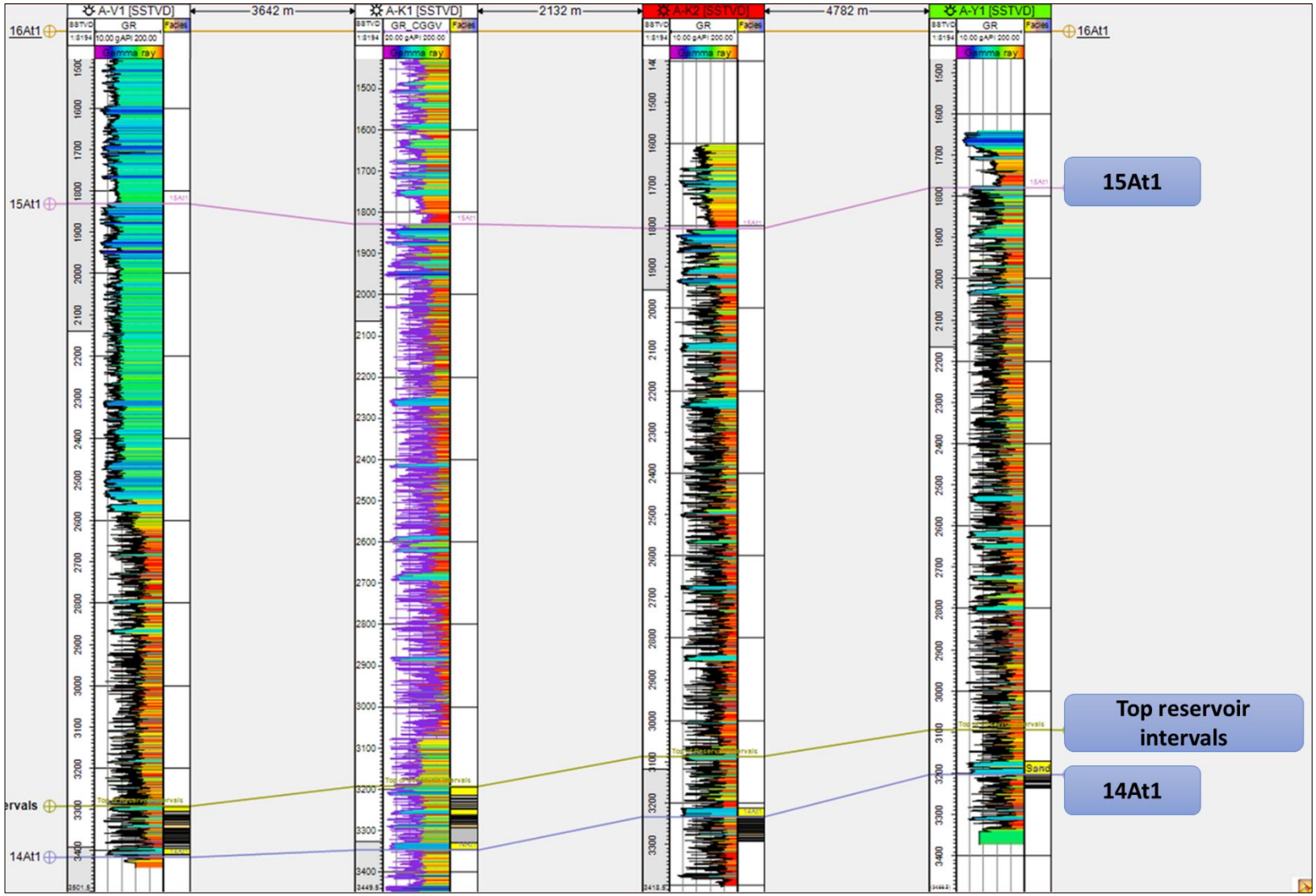


*Figure 14: Regional well marker correlation in the study area*

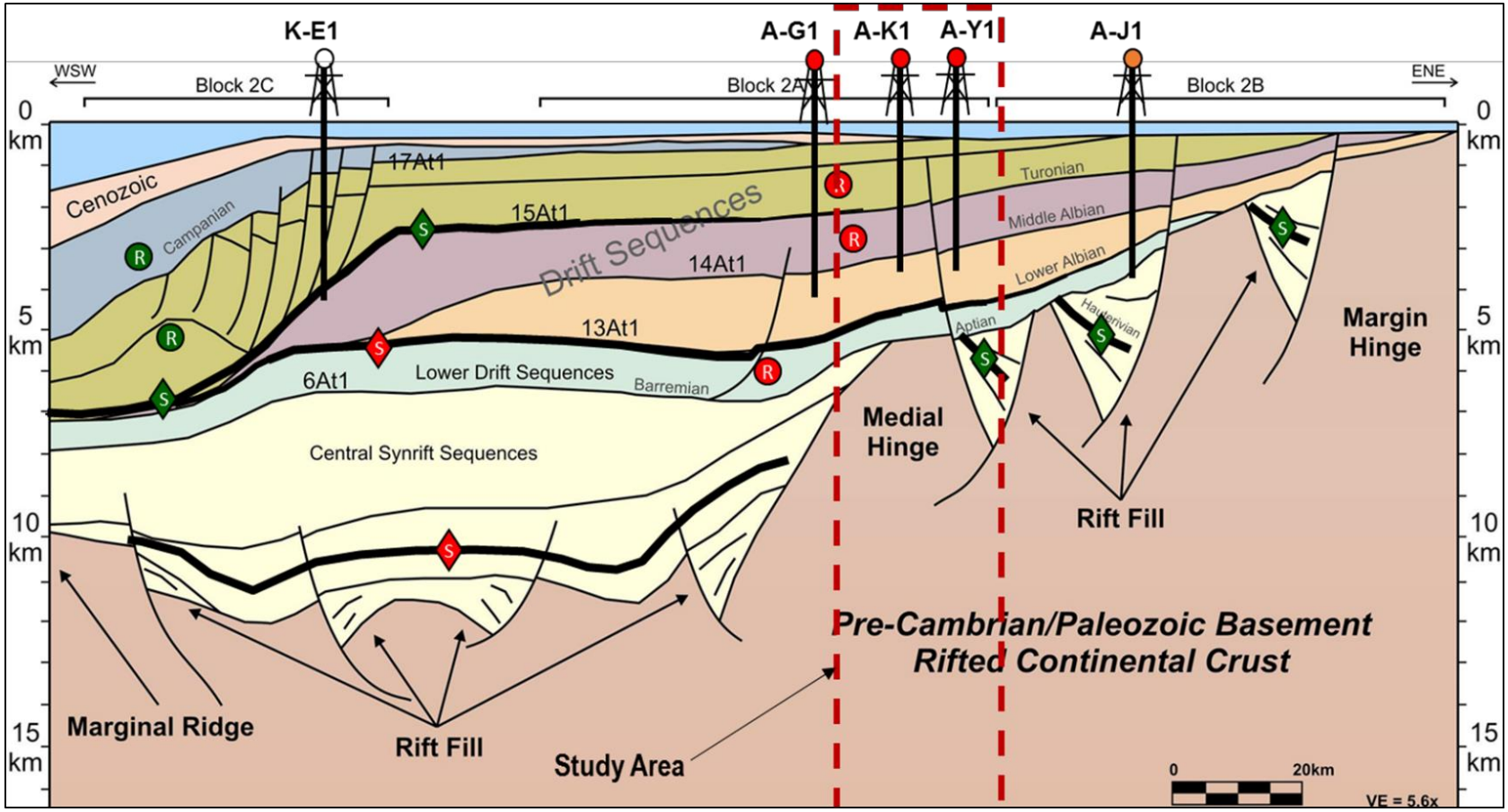


*Figure 15: The cross section through the Orange Basin, indicating the thick sedimentary wedge at the Albian to the Cenomanian. This wedge thins out towards the continent in the ENE side and becomes thicker towards the Basin in WSW.*

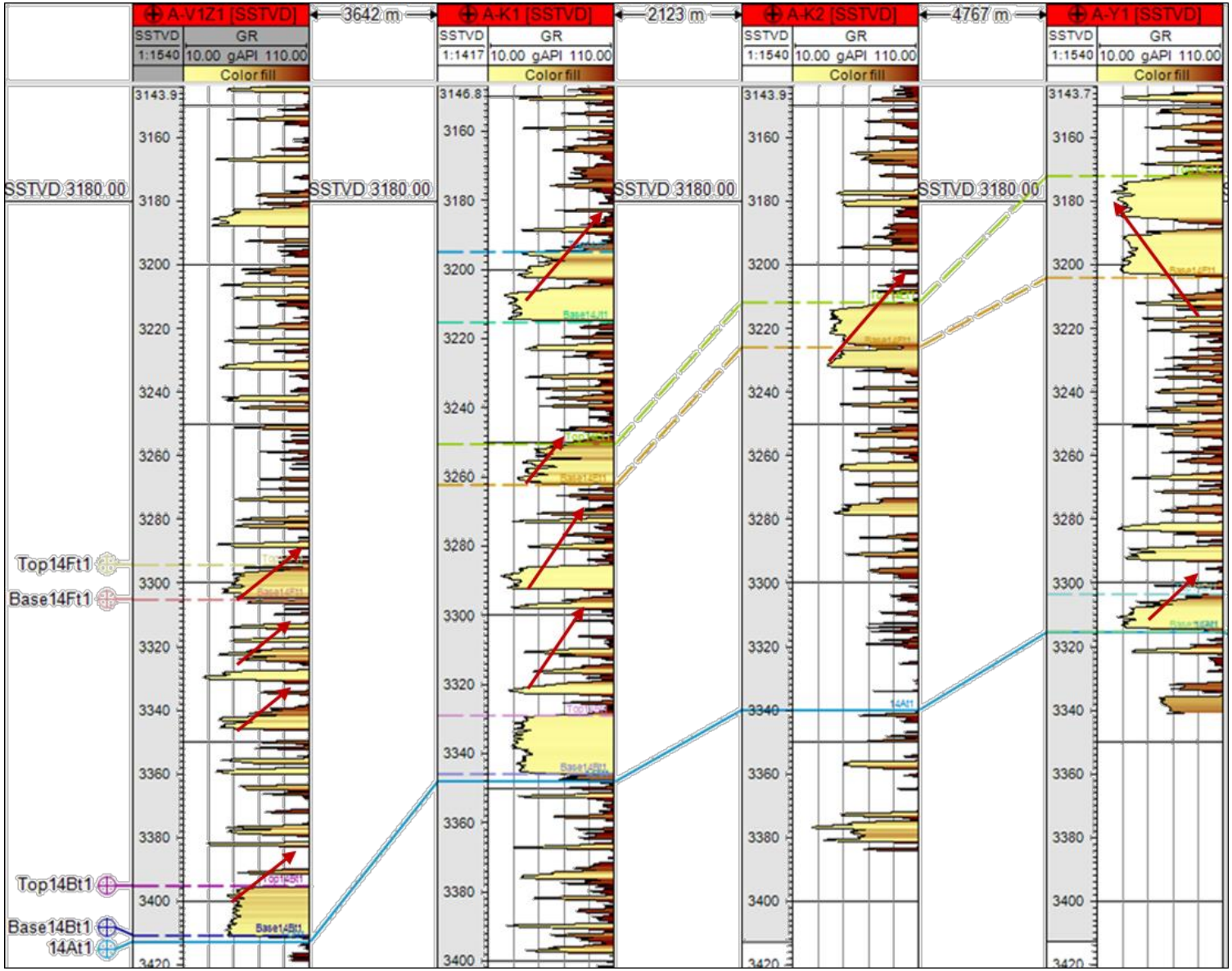


*Figure 16: Reservoirs Well marker correlation in the study area for wells – AV1, A-K1, A-K2 and A-Y1*

### 4.1.2 Seismic to well tie

A fair seismic to well tie was achieved with the minimal shift for all the four wells that are within the study, the results are presented in Figure 17. The achieved correlation factor is 0.38. It can be observed that from the seismic to well tie, the regional horizons are presented as a peak on the seismic data and as a consequence, all the regional horizons were mapped on the peak.

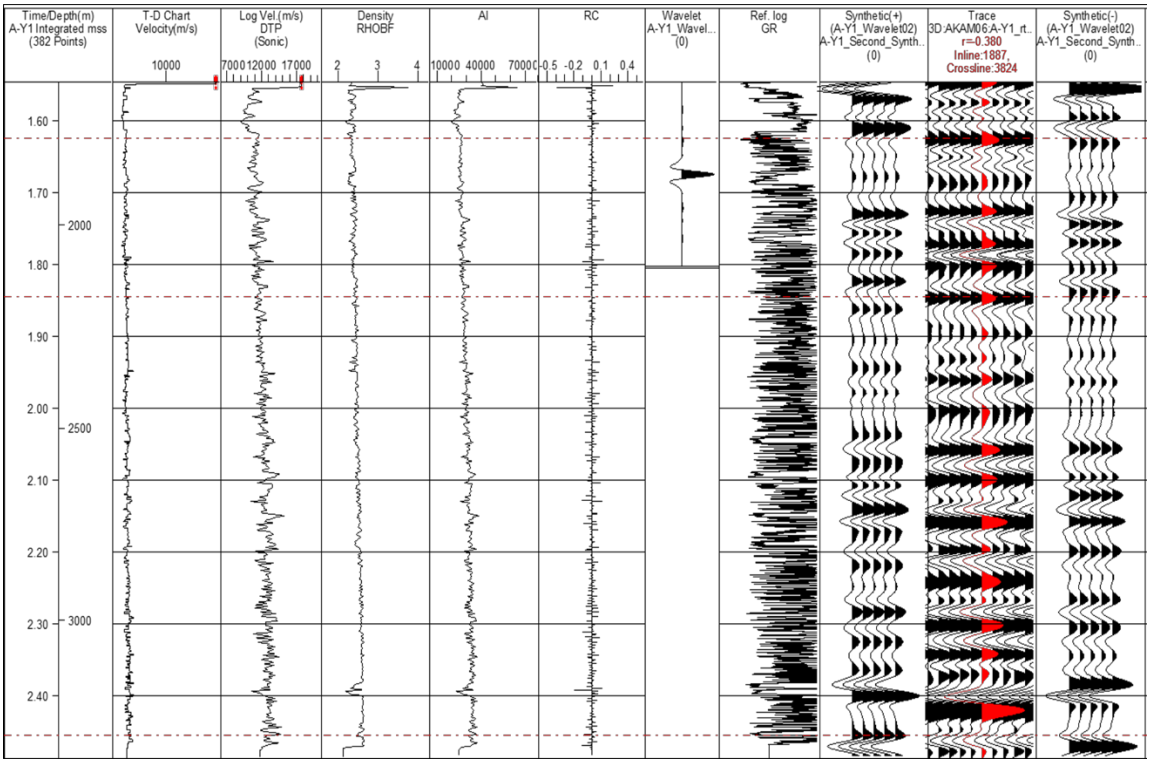


*Figure 17: Seismic to well tie in the study area, the AY-1 well is used in the illustration*

### 4.1.3 Vertical resolution

The vertical resolution refers to the minimum bed thickness that can be resolved by seismic data. The vertical resolution is important in fault mapping. It is important to determine the vertical resolution of the seismic data before fault interpretation is conducted. This is important in fault mapping because, most faults can be determined by the offset between the seismic reflectors. Seismic data can only resolve the faults with a throw that is within seismic resolution. In this study the A-V1 extracted wavelet was used in the estimation of the vertical resolution using the Rayleigh method.

There are two parameters, namely the velocity and the dominant frequency within the interval need to be estimated prior to the computation of vertical resolution. The Rayleigh resolution criterion states that the minimum bed thickness that can be resolved on seismic data is approximately equal to the quarter of the dominant frequency within the interval of interest (Kallweit and Wood, 1982). Mathematically, this is expressed by the equation 4.1.

$$\lambda = \frac{V\,\mathrm{int}}{4(Frequencey)} \qquad (4.1)$$

Where, Vint (m/s) is the interval velocity, λ (Hz) is the wavelength. The interval velocity in A-V1 well was calculated to be 3500m/s and the dominant frequency estimated using the extracted wavelet was found to be 20 Hz. The calculated vertical resolution is 43m. This is presented in Figure 18.

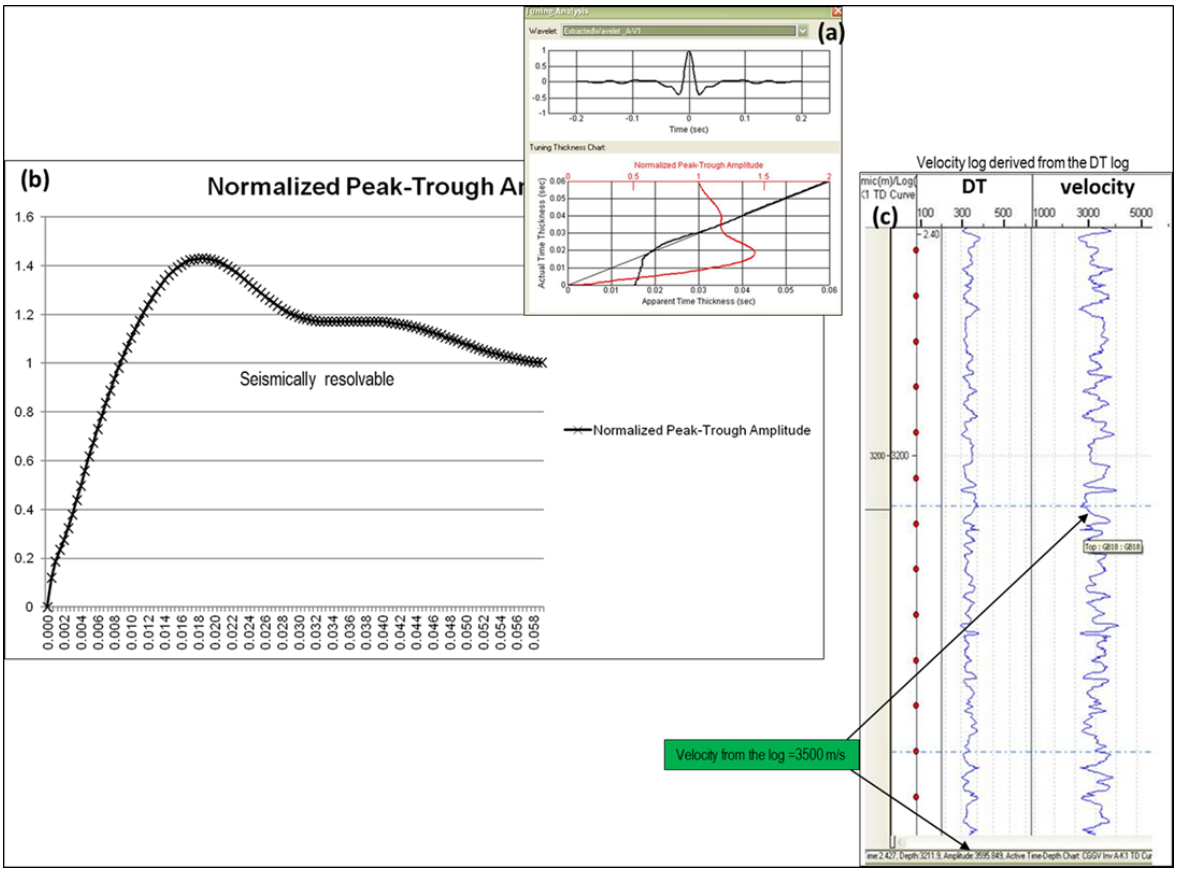


*Figure 18: The calculated seismic vertical resolution. (a) The extracted wavelet that was used (b) the normalized peak-trough amplitude and (c) velocity log that was used to estimate the interval velocity*

### 4.1.4 Structural Interpretation

Four of the regional horizons were mapped in the area: Sea Floor; 15At1; Upper Peak and near 14At1. These were used for depth conversion and for the horizon modelling in the 3D structural grid and these were mapped to estimate the displacement of the fault. The eastern part of the composite line E – W, is the down thrown fault block where there is A-Y1 well, the other 3 wells were drilled on the footwall. From the seismic interpretation it is clearly visible that there is offset in the reflectors which confirms the presence of the A-K fault.

The interpretation is presented in Figure 19 and the resulting structural maps are presented in Figure 20. The maps show that the structure is consistently shallow on the eastern side, closer to the continent and gradually becomes deeper as you go towards the basin in the western side. There are no structural closures observed on the two way time (TWT) structure maps. The hydrocarbons in the Ibhubesi gas field are stratigraphically trapped and the wells were drilled based on high seismic amplitude. This is displayed on Figure 21.

The AK fault cannot be traced on the sea floor structure map and in the successive horizons, the displacement does not appear to be very big. Even though the A-Y1 well is sitting on the hanging wall of the normal fault. On the structural map, it appears to be structurally shallower than the A-K wells which are situated on the foot wall of the AK fault. This can be attributed to two reasons, the A-Y1 well is sitting towards the continent and is on the transitional part from the continent towards the marine side. This is corroborated by the interpreted geological model.

The other reason can be a possibility of inversion. This possibility is ruled out, as it can be seen on the horizon interpretation, that the hanging wall is displaced downward and this can be observed in all the regional horizons.

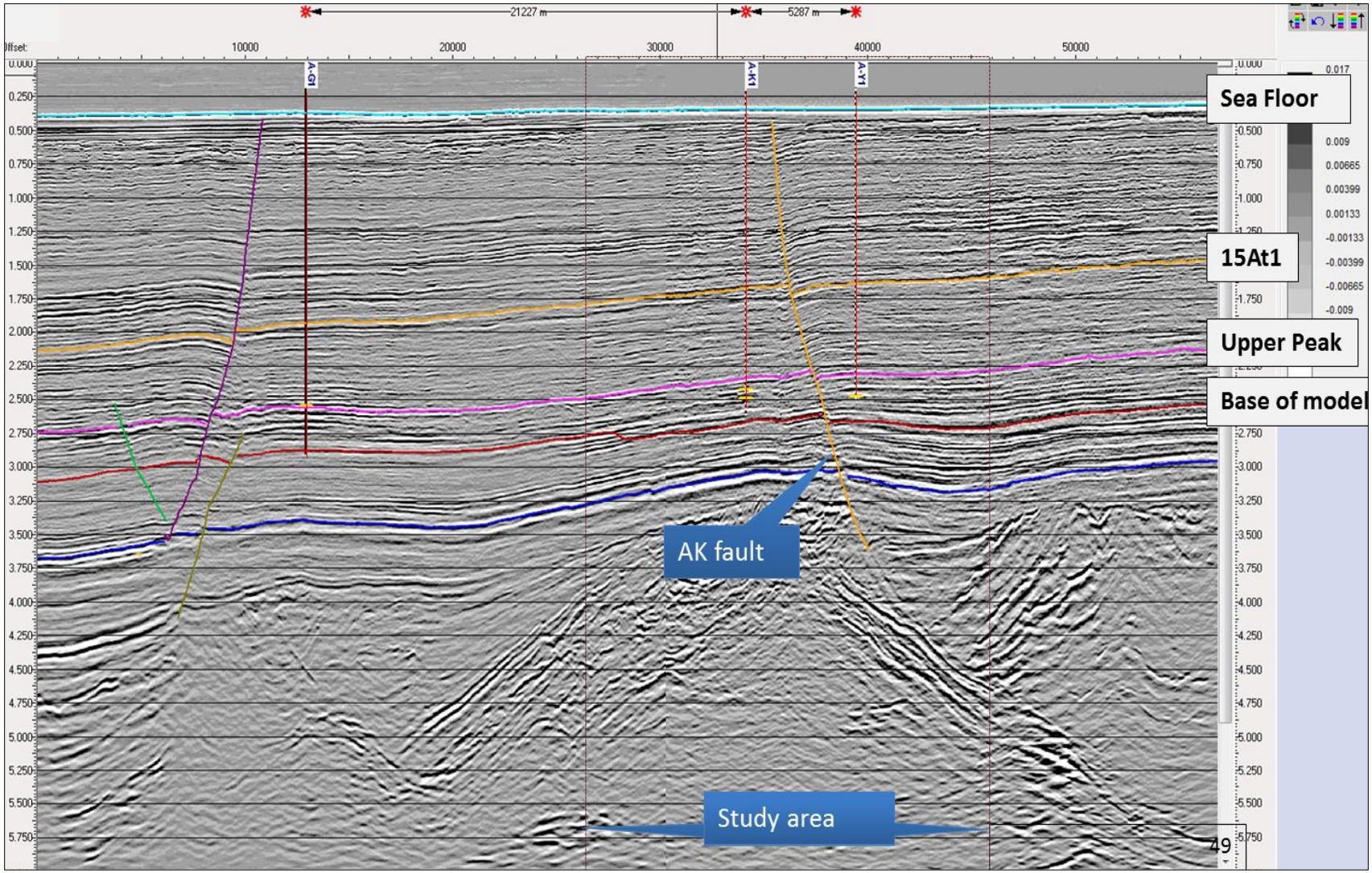


*Figure 19: A composite line, showing the seismic interpretation in the study area. The AK fault is also indicated in the study area.*

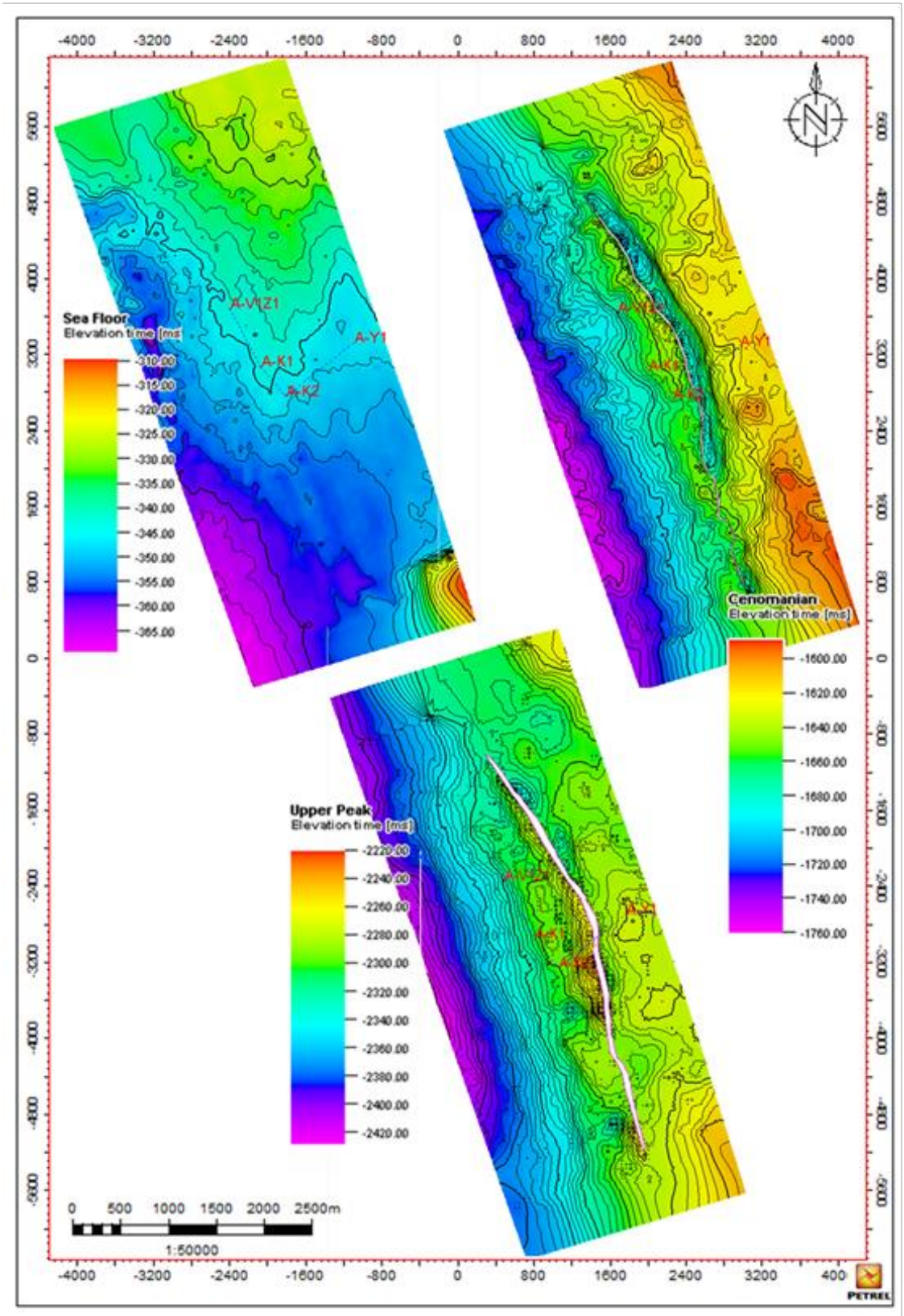


*Figure 20: The structure maps of the regional surfaces mapped in the study area. The structure is shallow on the East towards the continent and gradually deepens towards the Basin (western side)*

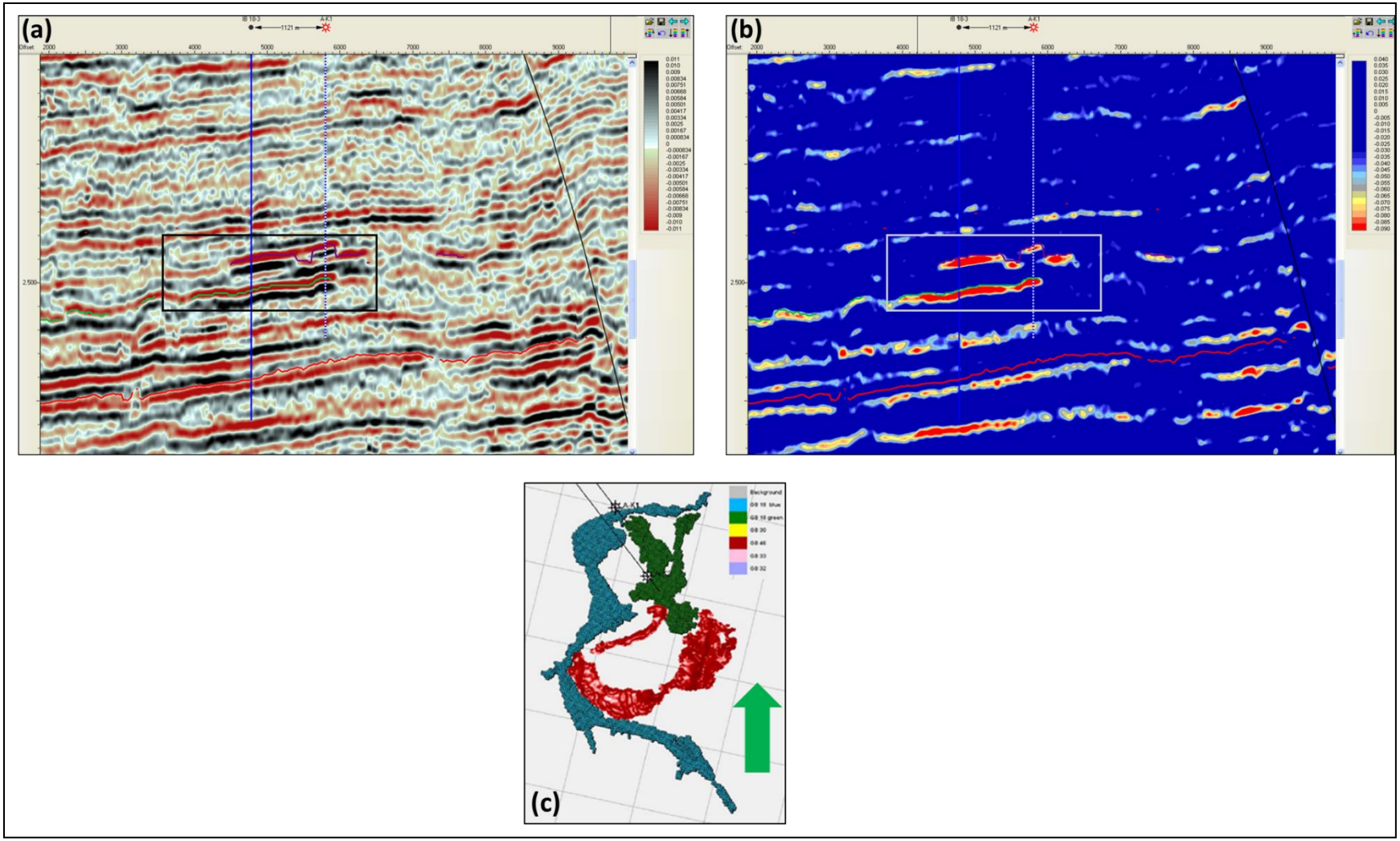


*Figure 21: Seismic section (a) and Relative Acoustic Impedance (RAI) Attribute (b), indicating the amplitude at well A-K1, which motivated the drilling of the well and (c) is the extracted sand body (modified after Msezane, 2015)*

### 4.1.4 Fault Mapping

The fault mapping was guided by the coherency attribute, similarity. A methodology of fault mapping, as outline by Mafurt, (2007) was followed and this methodology was useful during the interpretation and for quality controlling the results. The observations of the fault mapping are discussed below.

#### *4.1.4.1 Conventional seismic data vs. Coherency attribute (similarity)*

The coherency attribute was effective in guiding the fault interpretation. The areas of low coherency are highlighted and presented in dark blue colours. These continuous dark blue colours form a path and they correlate to the offset of the horizons mapped on the seismic data, which is the AK fault. When comparing the similarity attributes and full stack seismic data on vertical seismic profile, Figure 22 (a) and (b) respectively, it can be observed that the similarity attribute highlight the AK fault plane more prominently as compared to the conventional seismic data. In this way it is possible to have confidence in the fault interpretation that was conducted in the study area.

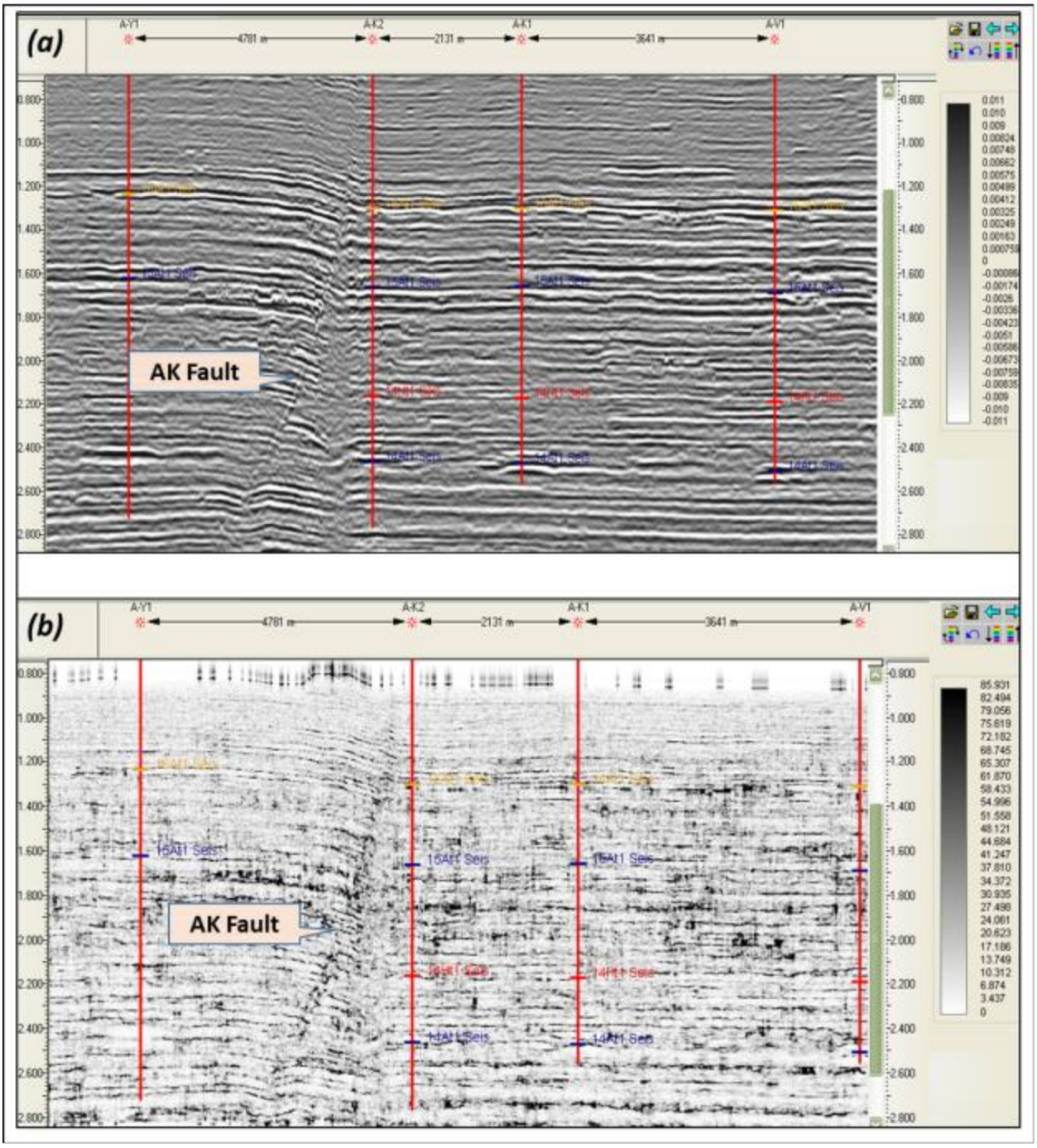


*Figure 22: The comparison between the normal seismic data and the coherency attribute (similarity). The AK fault is observed easier on the similarity attribute (b) as compared to the normal seismic data (a)*

#### *4.1.4.2 Generate seismic time slices*

The seismic time slices show the trend of the AK fault. This trend is generally NNW to SSE. There is no noticeable fault path that could be observed at the sea floor level at seismic time zero seconds. This was interpreted as: either the fault does not extend to the sea floor level or either the fault throw is below seismic resolution at this level. The fault path was first observed at a time slice generated at 0.506 milliseconds (ms), this is just below the sea floor, still at the Tertiary age level. The fault path appears as the dark blue colours which forms a continuous path, Figure 23b.

There are other features that were picked up by the attributes. Towards the left of the AK fault, there appears to be another fault which runs parallel to the AK fault. This fault does not appear to be as prominent as the AK fault. This fault was not easily identified on the conventional seismic data. The coherency attribute enhances the fault visualisation. The other features that were identified look like possible channel edges. These are relatively shallow and would not be prospective for petroleum exploration.

Successive time slices were generated at 1.58 and 2.48 ms, which represent stratigraphic markers, Cenomanian and Albian respectively. These time slices are presented in Figure 23 (c) and (d). At the Cenomanian level, the AK fault path can still be identified, however it was observed that the AK fault path appears to separate to a northern segment and a southern segment. The possible explanation to this could be that the integrity of the stratigraphy is not competent enough to allow brittle deformation. It can be seen from the eastern side, outside the area of study, that the seismic is becoming mottled and minor channel features are resolved.

At the Albian level, the seismic data becomes mottled and it is difficult to pick the faults even on the similarity attribute. On the vertical seismic profile the fault path is difficult to identify. At sections similar to these, the interpretation is guided by interpreter's intuition and there is uncertainty and error that might be inherited. There are other minor faults which appear at 3.104 s. These smaller faults appear to be antithetic to the AK fault. These smaller faults are difficult to map and they were not pursued.

The AK fault appears to be almost vertical at the top and it gently curves out into a shovel shape with depth. It would appear that the fault is a listric fault and therefore syn-depositional. There are certain characteristics that are used to identify a listric fault. These include the thickening of the stratigraphy towards the fault and change in the dip angle with depth (Suppe et al., 1985).

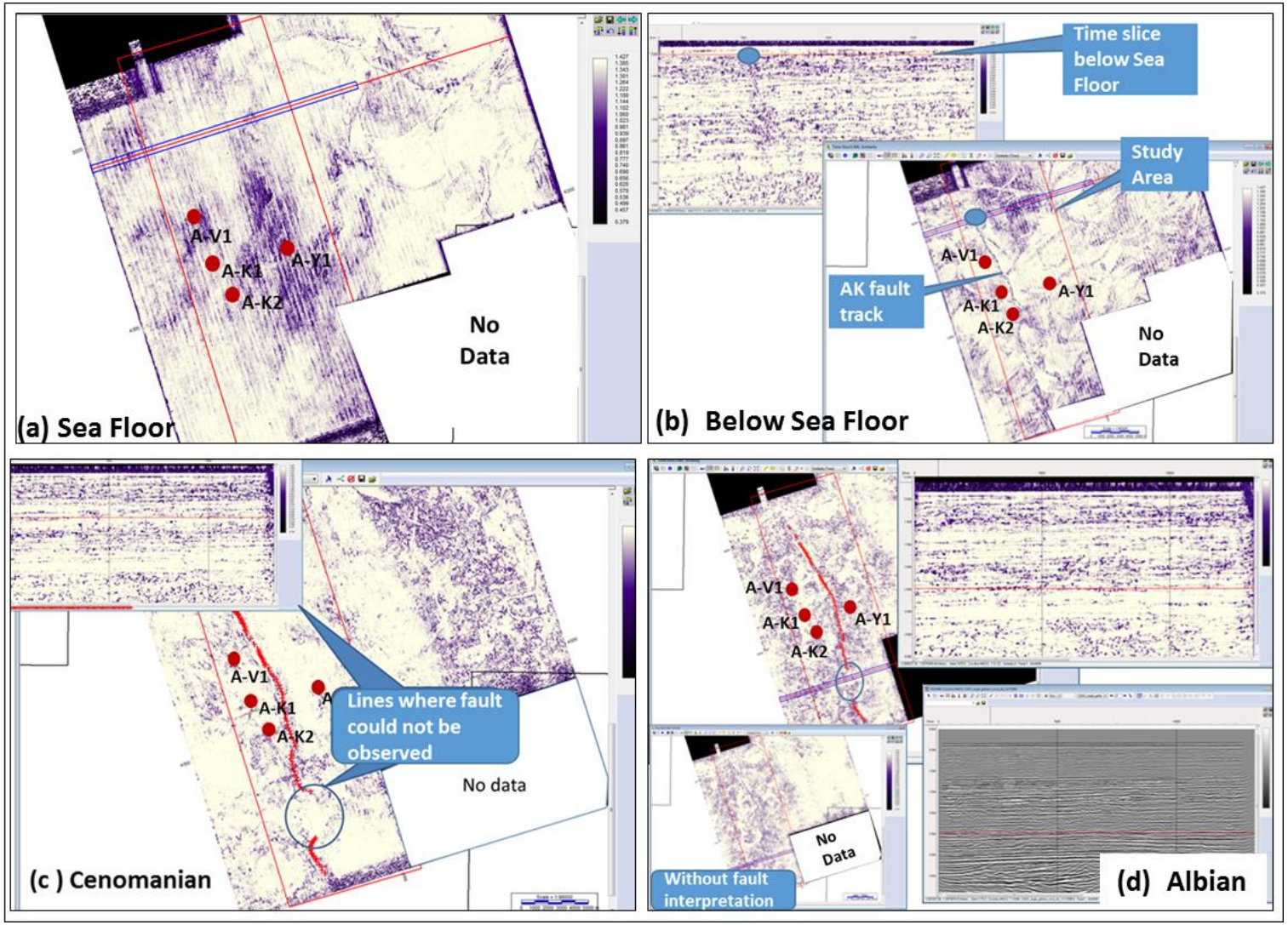


*Figure 23: Generated time slices within the study area. The AK fault cannot be observed at the sea floor (a), at time 0.5s, the first appearance of the AK fault can be seen. This can be traced through the Cenomanian sequence (c), to the Albian sequence, (d) where the amplitude becomes mottled.*

#### *4.1.4.3 3D Visualisation Mapping guided by Coherency Attribute*

The 3D visualization mapping assisted in controlling the fault mapping. This was achieved by tying the vertical seismic profile to the generated time-slice. In Figure 18a, it can be observed that the low coherent areas correspond to the vertical seismic line areas that show discontinuities, in this way the fault mapping control was achieved. The final process was to quality control the interpretation. This was achieved by stacking the different time slices vertically with the vertical seismic profile. A triangle is formed by joining the picks on the time slice with the pics on the vertical seismic profile. This is presented in Figure 18b. The final results give the fault surface, which is presented in Figure 18(c) and (d).

At this stage the AK fault surface is still in the time domain and will be depth converted in the next section. It can be observed from the fault surface colour scale, that the warmer colours (yellow to red ) represent shallow time intervals and the cold colours (green to blue) display the deeper time intervals. It is therefore concluded from this, that the fault is throwing towards the east, where there are deeper colours.

The fault displacement appears to be small and the dip angle appears to decrease with depth (Fig. 18). The fault is almost vertical towards the sea floor, but the angle gradually decreases with depth. The fault displacement and the dip angle will be quantified at the fault analysis stage. Knowing the dip angle of the fault, will help to ascertain whether the fault is a listric fault and the fault displacement is required as input to the fault seal analysis workflow in estimating the fault rock clay and thickness process.

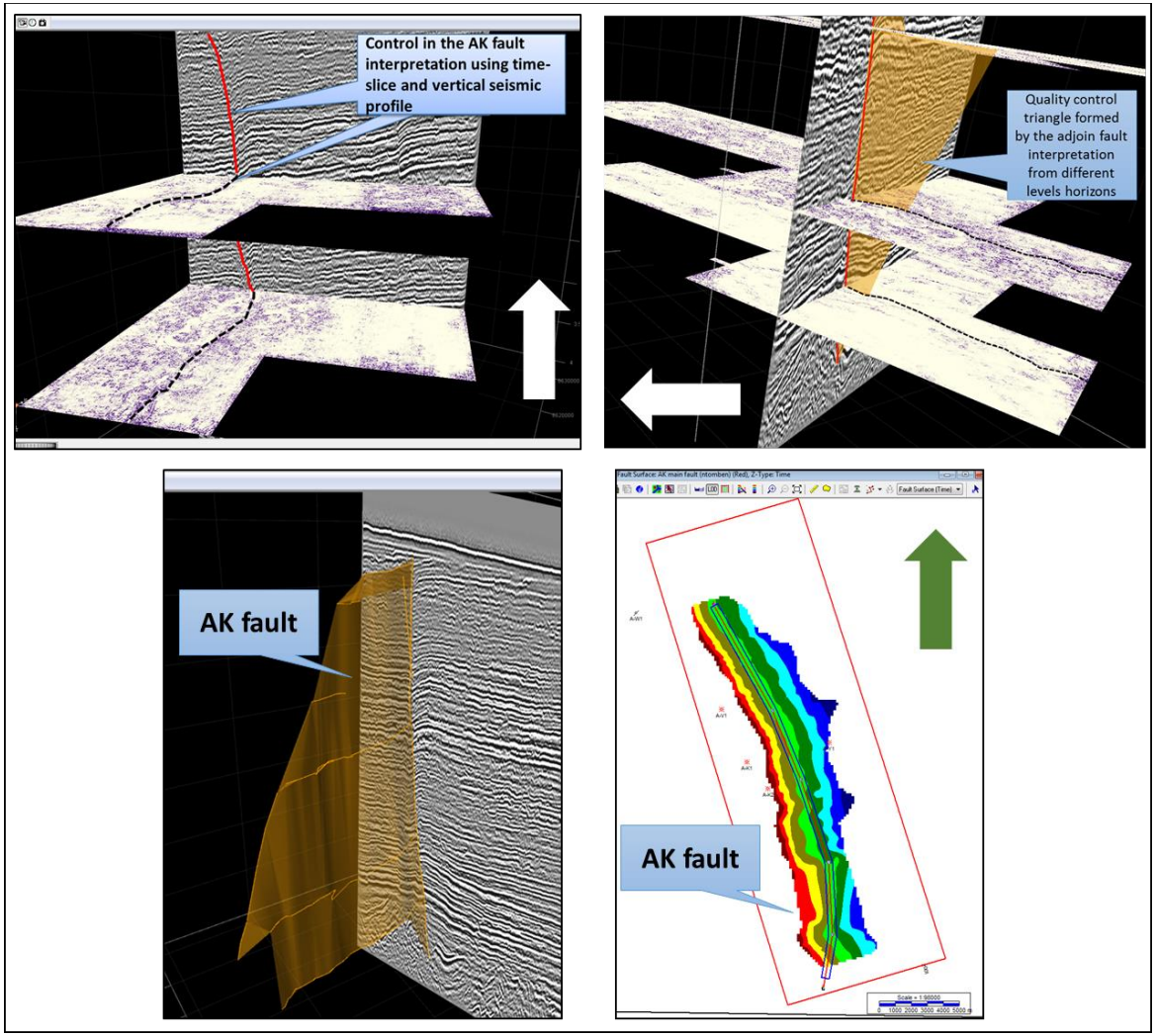


*Figure 24: 3D visualization fault mapping results guided by the Coherency attribute. (a) Fault interpretation on the time slices and vertical seismic profile; (b) quality control the fault interpretation; (c) and (d) AK fault surface*

#### *4.1.4.4 Depth Conversion*

The time domain interpretation of horizons, 15At1 and the Upper Peak were converted into the depth domain. The 15At1 surface varies in depth from 1775m towards the east to 200m towards the west in the study area. The Upper Peak surface is deeper than the 15At1 surface, but it follows the same trend as the 15At1 surface. It is shallow, with depths of 2925m on the eastern side of the study area and becomes deeper towards the western side of the study area, reaching depths of up 3225m within the study area. These are presented in Figure 25 and 26.

The base of the model is a constant surface that was created at a depth where the well logs end instead of making 14At1 the base of the model. This is because the availability of the log data was used at the advantage to evaluate the fault seal ability of the fault.

The results of the depth conversion show that the biggest depth error is inherited in the Upper Peak surface, with the error of up to 110m as compared to the depth error for the 15At1 surface, which is up to 30m, Table 7**.** The higher values associated with the Upper Peak horizon could be attributed to the velocity at the Upper Peak marker depth. The Upper Peak marker is not a regional unconformity. It was identified as one of the reflectors that can be mapped in the study area. It is possible that there is no break in the velocity at the Upper Peak marker and as a result it is giving erroneous values during the depth conversion processes.

The 14At1 horizon cannot be mapped regionally because of the quality of the data. The following regional horizon is the 13At1 horizon. The 13At1 horizon could not be used because the wells in the study area did not intersect the 13At1 sequence and as a consequence there would be additional error that would be inherited on the time depth curve. In the absence of any other horizon that could be mapped the Upper Peak was then selected.

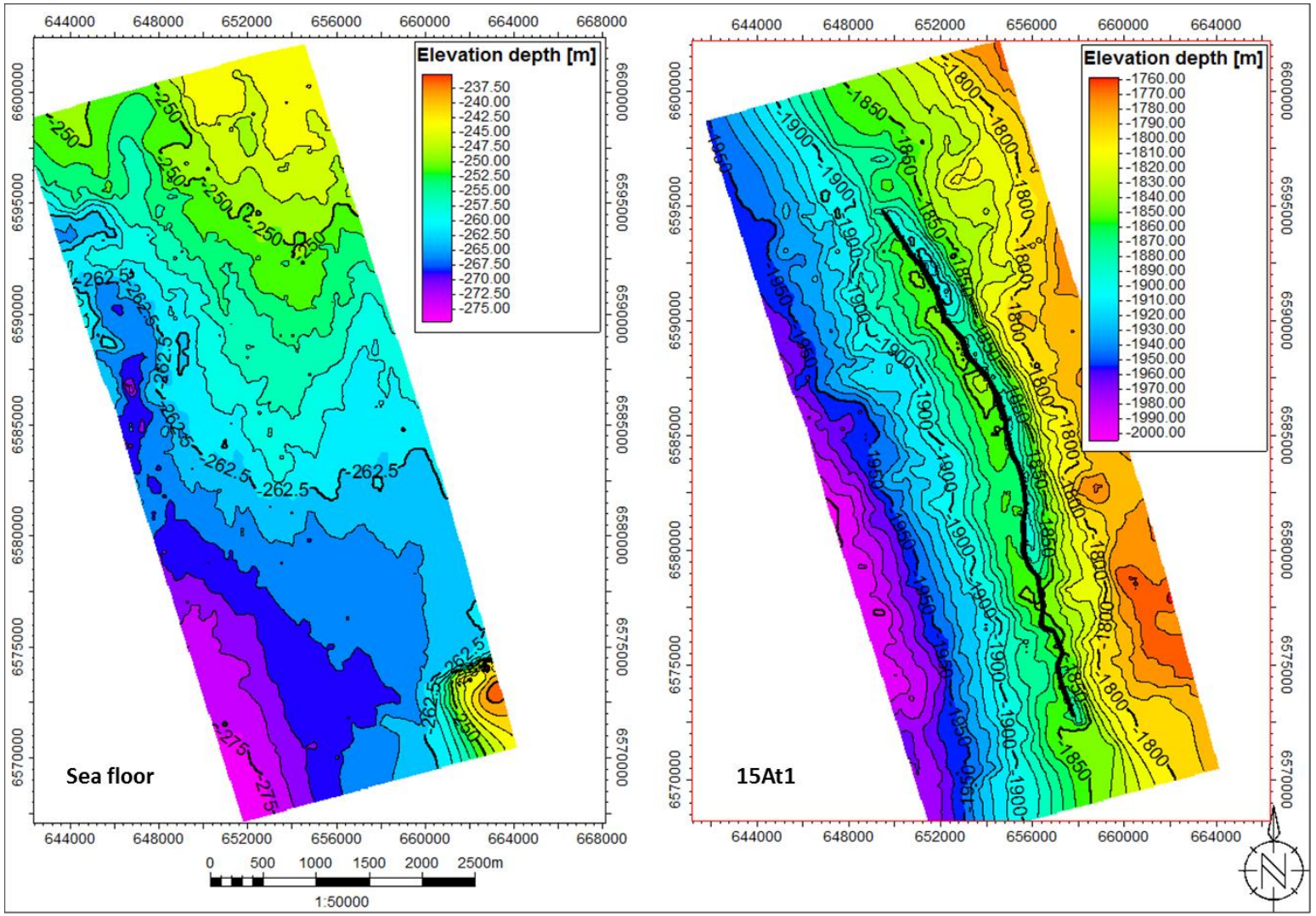


*Figure 25: The depth converted surfaces in the study area: Sea floor and the Cenomanian (15At1)*

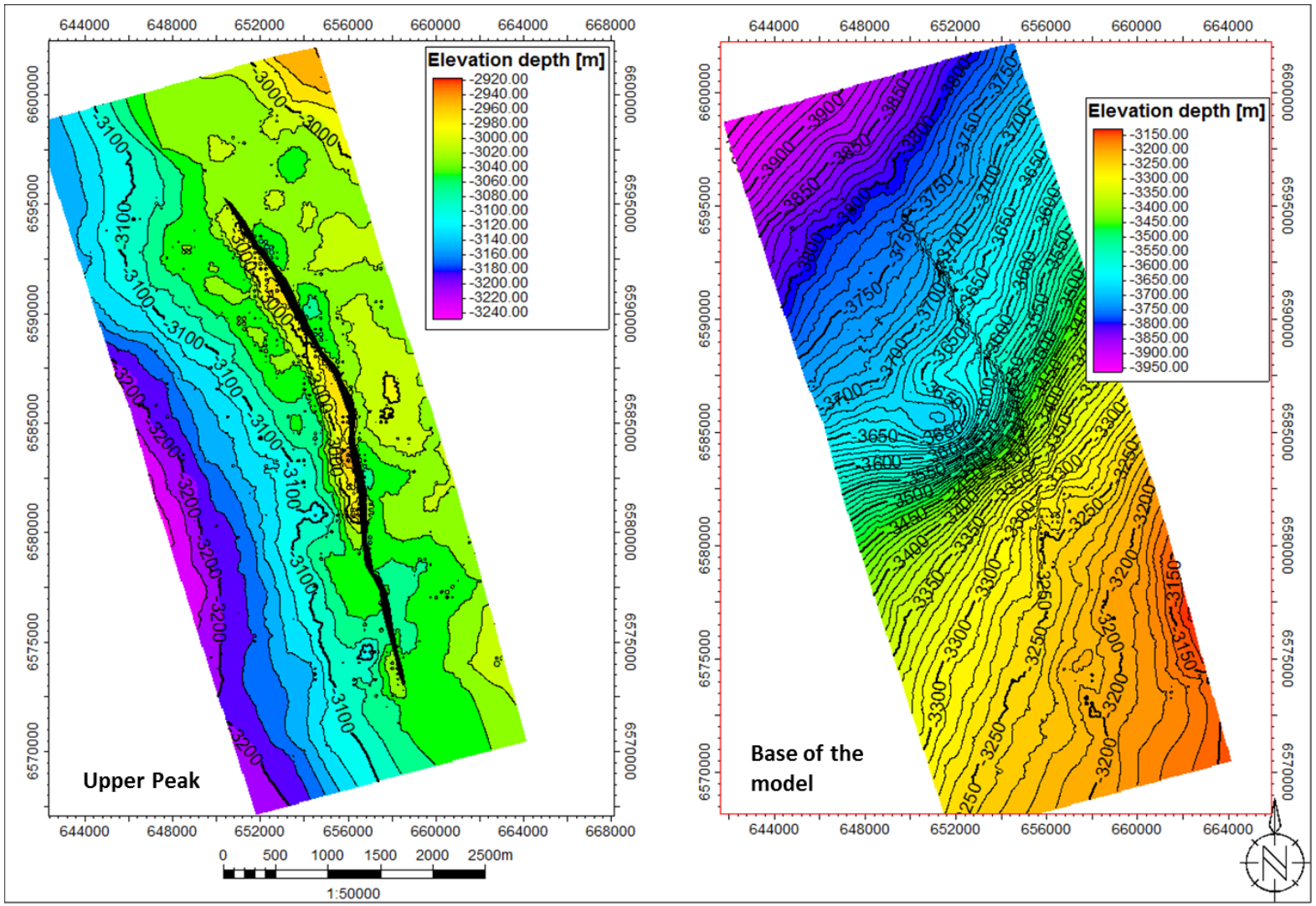


*Figure 26: The depth converted surfaces in the study area: Upper Peak and Base of the model*

*Table 7: Depth conversion error_ between the surface and the well marker*

| Well report for 'Surfaces Depth_SM/15At1 depth (Z)' (In Make surface) | | | | | |
|---|---|---|---|---|---|
| **15At1** | **Well** | **Md** | **Formation marker depth** | **Horizon depth (m)** | **Difference** |
| | A-Y1 | 1800 | -1774.8 | -1790.04 | 15.24 |
| | A-V1 | no well marker, the well logs begin deep than the 15At1 marker | | | |
| | A-K2 | 1865 | -1840 | -1865.04 | 25.04 |
| | A-K1 | 1881 | -1856 | -1877.75 | 21.75 |
| **Well report for 'Surfaces Depth_SM/UP depth (Z)' (In Make surface)** | | | | | |
| **UP** | **Well** | **Md** | **Z-value** | **Horizon before** | **Difference** |
| | A-Y1 | 3024 | -2998.8 | -2946 | -52.8 |
| | A-V1 | 3127 | -3101.8 | -3102.15 | 0.35 |
| | A-K2 | 3121 | -3096 | -2986.7 | -109.3 |
| | A-K1 | 3101 | -3076 | -2996.36 | -79.64 |

## 4.2 Well Data Interpretation

The well data interpretation includes the integration of the petrophysical, sedimentological data results into the determination of the facies and depositional model. The results from the well data interpretation are discussed below and presented in Figure 27 and 28.

### 4.2.1 Petrophysics

The facies, porosity, permeability and porosity logs will be used for petrophysical and facies modeling. The logs that were calculated were compared to the GR logs, whole core, side wall core and petrographic data, where available for quality control.

#### *4.2.1.1 Volume of Clay*

The volume of clay logs were calculated from the GR logs. It can be observed that the Vcl logs follow the signature pattern of the GR logs as a consequence (Fig. 27). The sand rich, reservoir sequences have lower volume of clay with values of up to 17% and the mudstone between the reservoirs have a clay volume which varies from 20% to 60%, (Fig.28).

It is important to ascertain whether these values are within reason and there are no other factors that could be affecting the values of the volume of clay. This is because the volume of clay is an important parameter in the fault seal study. Other fault properties are derived from the volume of clay, e.g. fault permeability is calculated from the fault clay content and the column height, which is the sealing capacity, is also predicted from the fault clay content.

The potential factors which might influence the values of the volume of clay logs are directly inherited from the GR logs. The GR logs respond to the radioactive isotopes, especially potassium, uranium and thorium. It is therefore important to evaluate the occurrence of these radioactive minerals as they would potentially give higher values in the Vcl logs.

The core and petrographic data evaluation does not indicate the presence of radioactive minerals, the minerals which occur in abundance are quartz followed by feldspar and as a result, the reservoirs are mainly arenite sandstones (Fig. 28) indicate the bulk mineralogy that is within the reservoirs.

#### *4.2.1.2 Porosity*

The higher log porosities coincide with the reservoir sequences. The reservoir sequences have log porosities which range between 17 and 26% at the clean sandstone interval and deteriorate to 9% in the interbedded argillaceous sequences. The highest porosities are encountered in the 14Et1 reservoir with 26% porosities at the A-Y1 well location, 23% at the A-K2 location and 21% at the A-K1 location. The 14Et1 reservoir was not intersected at the A-V1 well location.

The other reservoirs are 14Jt1 only intersected by the A-K1 well and the 14Ft1 reservoir, intersected by the A-V1 well only, both had average porosities of 18%. The 14Bt1 reservoirs, intersected by the A-K1 and A-V1 wells had an average log porosity of 20%. The 14Dt1 reservoir was intersected by the A-Y1 well only and it had average log porosity of 15%. To quality control the calculated log porosities, the whole and side wall core, petrography and cuttings data were used.

In the A-K1 well, the core was cut in the 14Et1 reservoir sandstone, from 3236 to 3249m. The core analysis reported a massive sandstone underlain by 10m of predominantly claystone with thin interbedded sandstones. The porosity vary from 5% to 24%. There are a few discrepancies between the calculated porosity logs and the core analysis porosities. The core analysis has higher porosities 24% in the A-K1 well location, as compared to the maximum log porosity of 21%. The difference is minimal and therefore these log porosities were accepted because they are still within the range of the core analysis data.

In the A-V1 well location, the well site cutting descriptions were used to compare with the calculated log porosities. The 14Ft1 reservoir had reported porosity values which range between 18 and 24%. The calculated log porosity values are an average of 18%. In the 14Bt1 reservoir the reported porosity values from the cuttings descriptions range between 14 to 22%. The calculated average log porosity within this reservoir is 20%. The calculated log porosities for both these reservoirs are within the range of the cuttings description report.

In the A-Y1 well locations the well site cuttings description report was used to match the calculated log porosities. The A-Y1 well intersected two reservoirs, 14Et1 and 14Dt1. In the 14Et1 reservoir, the reported cutting porosities from the initial quick look analysis are an average of 20% and in the 14Dt1 reservoir, 12%. The calculated average log porosities in this study for these reservoirs are 20% and 14% respectively.

In the A-K2 well, the acquisition of the side wall core data was not successful, the only available data that was used to compare the log porosities are the cutting descriptions from the wellsite. Here it is reported that the sands are matured, loose and well-rounded with porosities of up to 20% from the quick analysis at the well site using GS software. Even though this was a quick analysis, it however concur with the calculated log porosities in this study for the 14Et1 reservoir in the A-K2 well.

The 10% porosity cut-off was used to differentiate the reservoir sequence from non-reservoir sequences. It can be observed from the results that the cut-off was able to capture the total potential reservoir thickness in the higher quality channel sandstones and the lower quality over bank deposits.

#### *4.2.1.3 Permeability*

It was observed from the logs that there is a variation in the distribution of permeability. The decrease in permeability is presented by the cold colours (blue/green) and the high permeabilities by warmer colours, (yellow). The high permeability occur in the clean, reservoir, channel sandstone interval and the low permeability values occur in the lower quality sandstones representing the over bank deposits.

The calculated log permeabilities were compared to the core analysis and DST data for the different reservoirs. This was done in order to quality control the log permeabilities. This comparison is presented in Table 8.

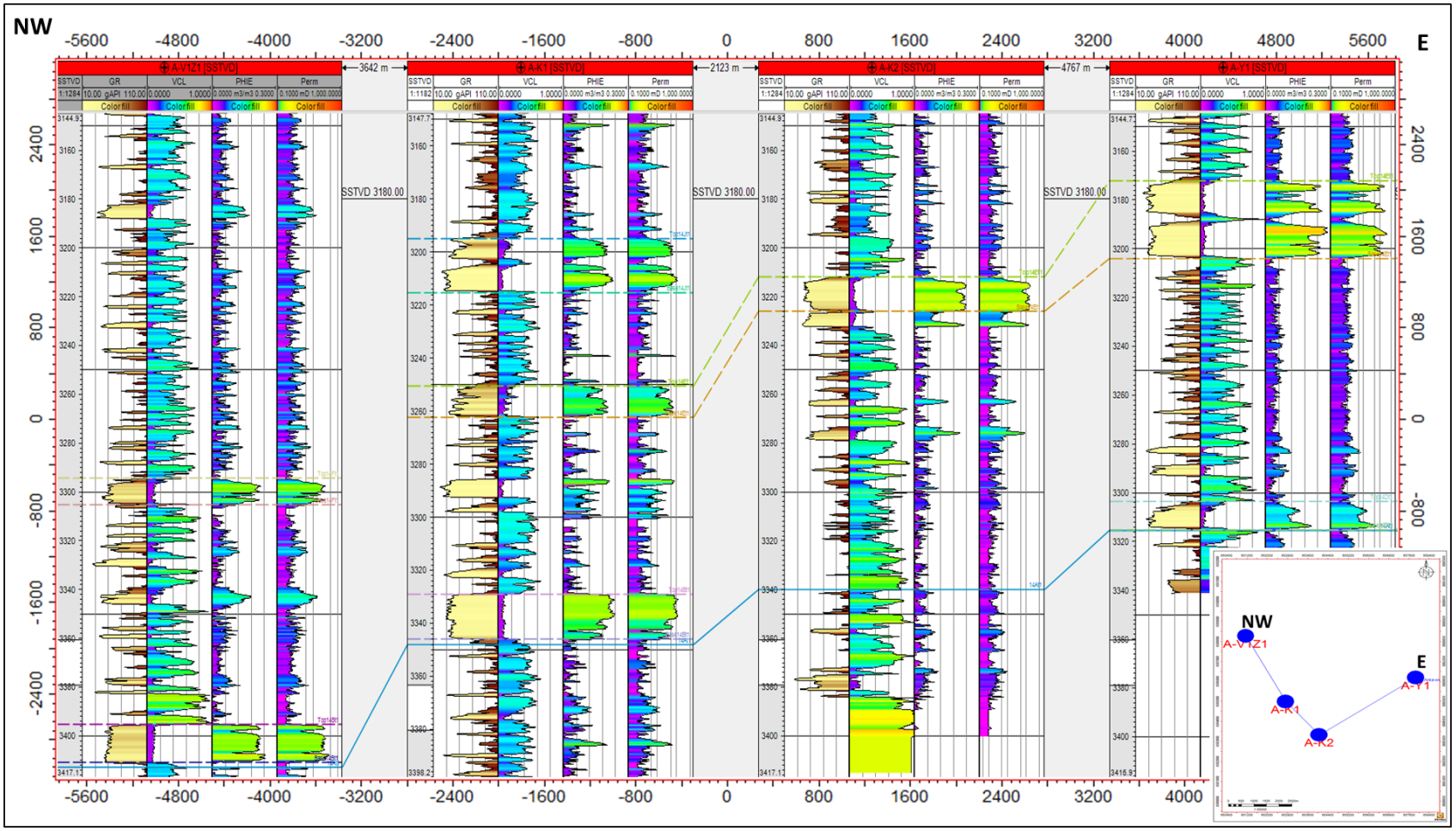


*Figure 27: Calculated petrophysical logs: Vcl; porosity and permeability*

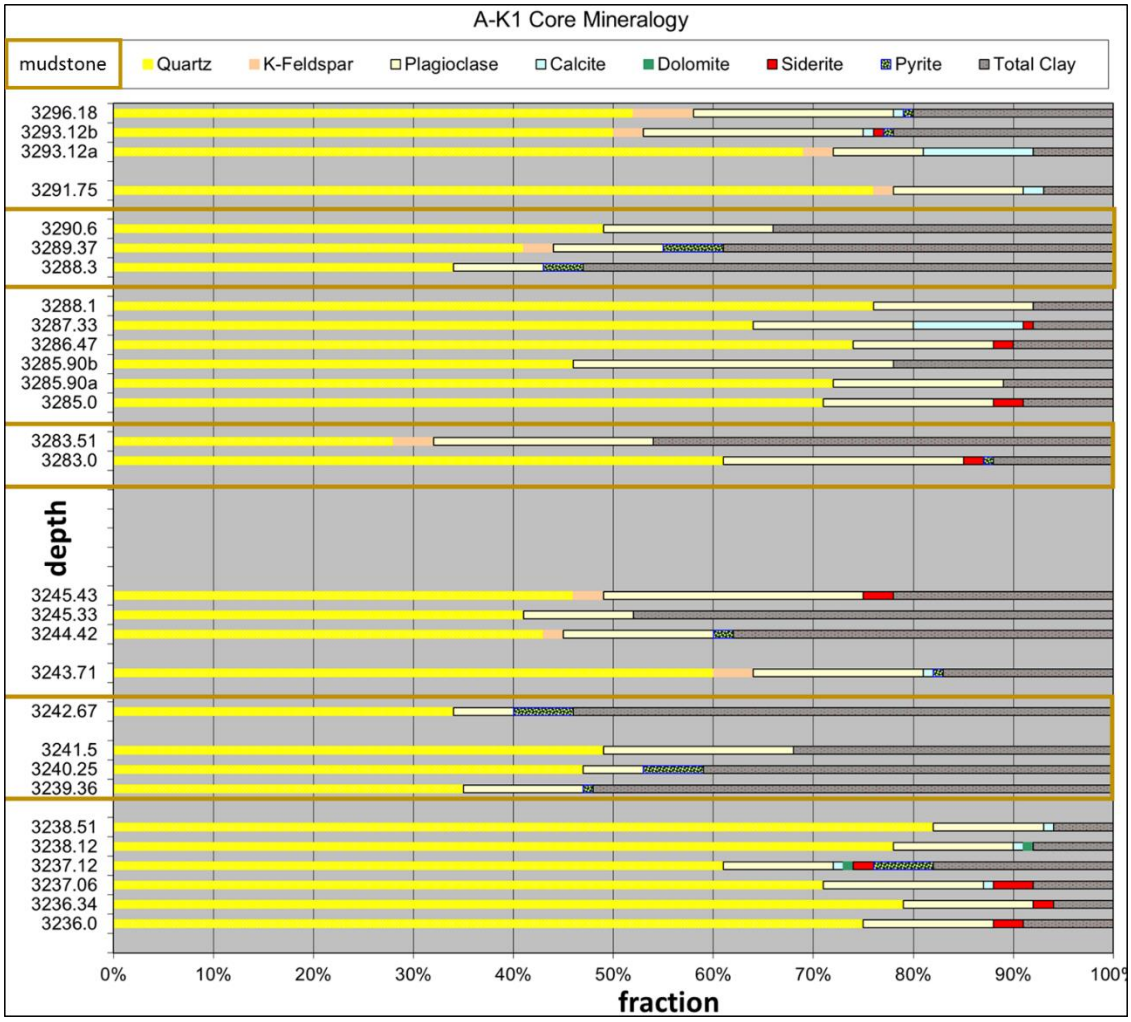


*Figure 28: Core mineralogy from the A-K1 well (Core Lab, 2002*

*Table 8: Log Permeability vs DST and Core analysis*

| Well Name | Zone Name | Top Depth (MD) | Base Depth (MD) | Average Log Permeability (mD) | DST (mD) | Core Analysis (mD) |
|---|---|---|---|---|---|---|
| A-K1 | 14Bt1 | 3353.867 | 3370.936 | 212.7 | 200 | |
| A-K1 | 14Et1 | 3274.314 | 3286.963 | 91.719 | 87 | 79 |
| A-K1 | 14Jt1 | 3217.621 | 3239.567 | 106.837 | 247 | 156 |
| AK-2 | 14Et1 | 3237.281 | 3259.226 | 206.1 | 250 | |
| A-Y1 | 14Et1 | 3197.809 | 3228.137 | 198.045 | 440 | |
| A-Y1 | 14Dt1 | 3330.245 | 3339.541 | 20 | 15 | |
| A-V1 | 14Bt1 | 3419.856 | 3436.01 | 160.127 | Not tested | |
| A-V1 | 14Ft1 | 3320.644 | 3329.178 | 80 | | |

### 4.2.2 Sedimentology

The interpreted depositional environment is based on the integration of the results from the extracted sand bodies, and well data (core, cuttings and wireline logs).

#### *4.2.2.1 Reservoir Sand bodies*

It was observed from the extracted sand bodies that the channel geometries seem to be variable. For the 14Jt1 sand body, the channel has a sinuosity ratio of 1.7; the 14Et1 sand body has a sinuosity ratio of 0.926 in the A-K1 and A-K2 well locations. In the A-Y1 well location, the 14Et1 sand body channel has a sinuosity ratio of 1.2. The channel geometries sinuosity ratios range from 0.926 to 1.7, with 14Jt1 sand body channel being sinuous.

According to Rosgen, 1994 classification (Fig. 29) the channels in the study area fall under the D or DA group. In this group there are multiple channels which is similar to the observed sand body extractions in the study area. The DA classification is preferred since there is high variation in the sinuosity. When comparing the sand bodies' geometries with the Rosgen, 1994 classification, it can be deduced that the channel geometries resemble the geometry of a braided stream.

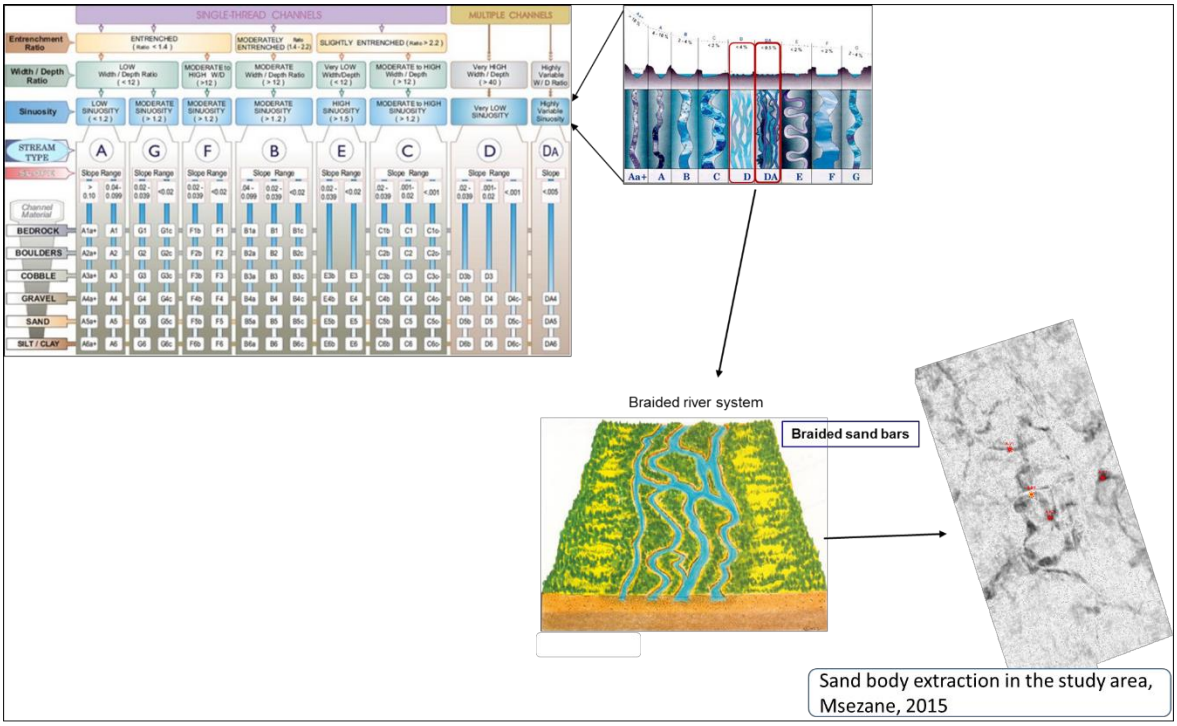


*Figure 29: Rosgen, 1994 channel classification, compared to the extracted sand bodies in the study area*

#### *4.2.2.2. Core and cuttings data*

In the A-K1 core interpretation, two lithofacies that were reported; 1) cross bedded sandstone lithofacies and 2) the thinly interbedded sandstone and claystone lithofacies. The key characteristics observed on the core data are presented in Table 9.

The cross bedded sandstone lithofacies were interpreted to be chemically immature. This is because they contain minerals like feldspar and muscovite, which are chemically unstable and are susceptible to chemical weathering. This indicates that this sandstone has not been transported very far from its source. The coal fragments and the plant material indicate a terrigenous terrain. The sandstone has sub-rounded to well-rounded grains and is well sorted, which indicate maturity of the sediment.

The rip up clasts indicate transport of the sand over the siltstone where it was ripping the finer material at high energy and the finer material got incorporated into the sand forming rip-up clasts of angular to rounded siltstone. Cross bedding indicate that the deposition contained a flowing medium.

The second lithofacies that was identified is the thinly interbedded sandstone, siltstone and claystone facies. This sandstone is grey, fine to argillaceous and dominated by lithics. This would normally point to a terrigenous environment. The mineralogy of this sandstone includes siderite and pyrite.

*Table 9: The key characteristics observed on the A-K1 core data*

| Facies Name | Core Data: A-K1 | | | |
|---|---|---|---|---|
| | **Sample maturity** | **Porosity (%)** | **Diagenetic Cement** | **Mineralogy** |
| Shale | Argillaceous | <10 | Argillaceous matrix | None observed |
| Distributary channel of a delta | Physical and chemical matured | >18 | Chlorite and calcite | Quartz, glauconite, pyrite |
| Fluvial channel fill sands | Chemically matured | >18 | Chlorite, calcite, quartz | Quartz, feldspar, muscovite, pyrite, siderite |

In the A-K2 well, the only intersected reservoir was the 14Et1. In this interval, two lithofacies were interpreted from the cuttings report. The key characteristics of these lithofacies are presented in Table 10. This interval was reported to be interbeds of claystone with siltstone and sandstone.

The sandstones is white to light grey. The colour of a rock tells you more about the mineral composition. Quartz rich sandstones are whitish, feldspar rich sandstones may be pinkish and lithic rich sandstones are generally grey to dark grey. The 14Et1 sand that is observed in the A-K2 location is quartz rich, relating to minor lithic fragments that are incorporated in the matrix. It is well sorted with loose well rounded grains.

This sandstone is interpreted to be chemically mature, it is dominated by quartz and the absence of chemically unstable minerals like feldspar, indicate that it is far from the source of the sediment. This is also supported by the well-rounded and loose grains which show that it has been transported over a long distance, leading to the roundness of the grains and the lithic material has been washed away. The presence of pyrite indicates proximity to marine environment (Berner, 1981) however glauconite is absent.

The interbedded claystone and silt is very fine grained and contains traces of carbonaceous flakes and disseminated pyrite. The very fine grained material points to the energy of the environment of deposition. For finer sediments to settle down, the energy of the transporting agent must be low.

In the A-Y1 well location, the well intersected the 14Et1 and 14Dt1 reservoirs. In the 14Et1 interval, there is only one lithofacies that was interpreted from the cuttings report, a sandstone. The characteristics of this lithofacies are presented in Table 10. The 14Et1 sandstone was described as chemically and physically mature, with mineralogy of the sandstone dominantly quartz rich, relating to minor lithic fragments that are incorporated in the matrix and w well-rounded and lose grains which show that it has been transported for a while leading to the roundness of the grains and the lithic material has been washed away.

There were no fluvial depositional features such as ferruginous staining and carbonaceous material reported, however the glauconite was reported for the first time in the wells within the study area. Geochemical evidence suggests that glauconite form in seawater at low temperatures in an environment that is neither strongly oxidising nor reducing. The 14Dt1 reservoir sandstone

was reported as a light grey fine to medium grained sandstone, chemically and physically matured. It is interbedded with fine silt and has calcareous cement.

*Table 10: Cuttings description of the A-K2 and A-Y1 wells*

| Facies Name | Cuttings Data: A-K2 | | | |
|---|---|---|---|---|
| | Sample maturity | Porosity | Diagenetic Cement | Mineralogy |
| Over-bank deposits | Argillaceous, none observed | <10% | Argillaceous matrix | None observed |
| Distributary channel of delta sands | Matured | >18% | Chlorite, quartz in places, calcite | Quartz, glauconite |
| Fluvial channel fill sands | Chemically immature | > 20% | Chlorite, calcite, quartz | Quartz, pyrite, siderite |
| **Cuttings Data: A-Y1** | | | | |
| Over-bank deposits | Argillaceous, none observed | <10% | Argillaceous matrix | None observed |
| Deltaic sandstone | Matured | >18% | Quartz in places, Chlorite | Quartz, glauconite, pyrite |

#### *4.2.2.3 Wireline logs*

There are three different shapes that were observed from the well log response. These shapes are: bell, funnel and cylinder (Fig. 30). These shapes were identified from the GR log which is an indicator for shale content and are described using the change in the clay content. The funnel shape results when the GR log value decreases regularly upwards from a maximum value. This would mean that the clay content decreases as you go upwards. The bell shape is the opposite of the funnel shape, in this case the GR value increases as you go upwards, indicating the increase in the clay content.

In the study area, the upward coarsening trend or bell shape is observed from the Base of the Albian Sequence in the A-V1 well at depth 3650 to 3480 m and in the A-K1 well at depth 3435 to

3495 m. All the depths quoted in this section are measured depth (MD). The porosity log in A-K1 were it is available, show that these sands are tight. The observed porosities range between 1 to 6 %. This upward coarsening sequence was not observed in the A-K2 and A-Y1 wells. In this interval, one lithofacies could be observed, a tight upward coarsening sandstone.

This sequence is overlain by an upward fining sequence which displays a bell shape. This was observed in the A-V1 well at 3465 to 3448m, in A-K1 at 3489 to 3450m and in A-Y1 at 3340 to 3330m. This interval is absent in the A-K2 well. The porosities of these sands range between 2 to 8 percent in the A-V1 and A-K1 and improves greatly at the A-Y1 well to an average of 15%, in the A-Y1 well, this is the 14Dt1 reservoir sandstone. In this interval, there are two lithofacies that were identified: the tight fining upwards sandstone and porous upward fining sandstone.

This interval is overlain by the 14Bt1 reservoir. The GR log response has a cylinder shape. This can be observed in the A-K1 and A-V1 wells. In this interval, there is one lithofacie that was identified, the cylinder porous sandstone.

In the 14Ft1 interval, only intersected in the A-V1 well, there is an observed upward fining trend, representing a bell shape. One lithofacies identified, a porous upward fining sandstone. In the 14Et1 reservoir interval, intersected in all the wells in the study area, with the exception of A-V1, there are two observed trends. In the A-K1 well, the 14Et1 reservoir sandstone is upward fining and porous, whereas in the A-K2 and A-Y1 wells, the GR log response display a cylindrical shape. Two lithofacies identified in this section. Upward fining porous sandstone and cylindrical shaped sandstone. The GR log response of the 14Jt1 reservoir intersected by A-K1 also displays a bell shape and it is porous. The identified lithofacies based on the GR log shape are presented in Table 11.

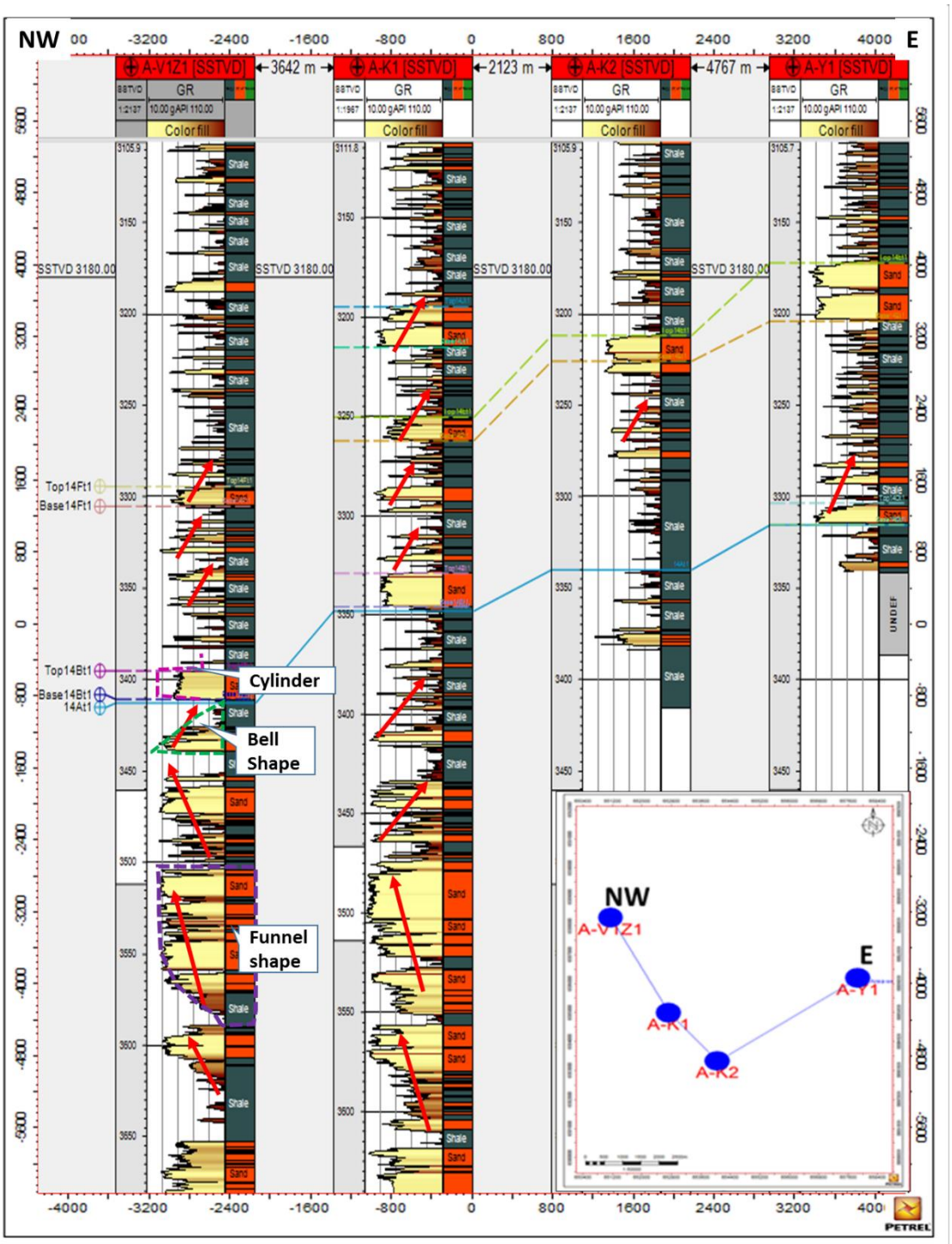


*Figure 30: Facies defined in the study area using core, cuttings and wireline data. The arrows represent the trend of the GR log, which was used in the interpretation of the depositional environment- include the fault and re-capture for better resolution*

*Table 11: Identified lithofacies based on the GR log shape*

| Well Name | Zone Name | Top Depth (MD) | Base Depth (MD) | Lithofacies Identified |
|---|---|---|---|---|
| A-K1 | 14Bt1 | 3353.867 | 3370.936 | Cylinder porous sandstone |
| A-K1 | 14Et1 | 3274.314 | 3286.963 | Fining upward porous sandstone |
| A-K1 | 14Jt1 | 3217.621 | 3239.567 | Cylinder porous sandstone |
| AK-2 | 14Et1 | 3237.281 | 3259.226 | Cylinder porous sandstone |
| A-Y1 | 14Et1 | 3197.809 | 3228.137 | Cylinder porous sandstone |
| A-Y1 | 14Dt1 | 3330.245 | 3339.541 | Fining upward porous sandstone |
| A-V1 | 14Bt1 | 3419.856 | 3436.01 | Cylinder porous sandstone |
| A-V1 | 14Ft1 | 3320.644 | 3329.178 | Fining upward porous sandstone |
| **Other intervals** | | | | |
| A-K1 | | 3330 | 3340 | Upward fining tight sandstone |
| A-K1 | | 3435 | 3495 | Upward coarsening tight sandstone |
| A-V1 | | 3480 | 3650 | Upward coarsening tight sandstone |
| A-V1 | | 3448 | 3465 | Upward fining tight sandstone |

### 4.2.4 Facies definition

There are five lithofacies that were identified in the study area. These are; cross bedded sandstone, thinly interbedded sandstone and claystone facies; sandstone; claystone and siltstone inter-beds. It was observed from these facies that even though they present different log shapes and sedimentary features these facies could further be grouped based on their petrophysical parameters.

The cross bedded sandstone and sandstone facies, whether they have a bell or funnel shape, they still have good porosity and cannot be separated in terms of reservoir quality. The thinly interbedded sandstone still had porosity, which is above the reservoir cut-off of 10% porosity. It is based on this, that these sandstone facies were grouped into one facie referred to porous sandstone.

The upward coarsening and fining upward sandstones located below the 14At1 marker have low porosity and are below the reservoir cut off porosity. These sandstones are the second facies which is the tight sandstone. The last facies is the argillaceous material, shale/claystone. The facies log was created from these facies using a basic calculator in the Petrel software.

In the calculator, a shale facies was defined as the lithology with GR log response greater than 60 API, with a volume of clay greater than 50% and porosity less than 5%. A porous sand facies was defined as the lithology with the GR log response less than 60 API, with volume of clay less than 35% and porosity more than 10%. A tight sand facies was defined as a lithology with GR response less than 60 API, with volume of clay more than 30% but less than 50% and porosity more than 5% but less than 10% (Table 12).

*Table 12: Facies definition in the study area, using core, cuttings and wireline logs*

| Facies Name | Lithology | GR (API) | Porosity (%) | Vclay |
|---|---|---|---|---|
| Porous Sandstone | Sandstone | <60 | Phie >/= 10% | <35% |
| Tight Sandstone | Sandstone | <60 | Phie >5%<10% | >35%<50 % |
| Shale | Argillaceous claystone/shale | >60 | <5% | >50% |

### 4.2.5 Geological Model

The interpreted geological model is based on the integration of the well and seismic data interpretation. The sedimentological data indicate that the deposition in the study area occurred in continental to transitional marine environment. This is evident from the sand bodies' extractions which were interpreted to represent a braided fluvial system according to the Rosgen Channel Scheme (Rosgen, 1994) which display multiple channel system with silt/clay, sand materials.

The A-K1 and A-V1 wells are placed in an upper delta plain (Fig. 31). The complete continental environment is rejected because of the presence of pyrite, which does not form in an oxidising environment as it is oxidised to goethite. A completely marine environment also does not fit because of the presence of siderite, which does not form in marine conditions as they do not allow for the precipitation of siderite. The environment may therefore be transitional.

The combination of the cross- bedded lithofacies and the thinly interbedded siltstone and claystone leads to the proposed interpretation of a distributary channel sandstone which is represented by the cross-bedded lithofacies is cutting into an inter-distributary bay deposit on a transitional environment. The cutting or the cross bedded channel sandstone is supported by the

rip-up clasts which are composed of the siltstone and claystones. The channel erosive nature is supported by the sharp erosional bases.

The A-K2 well is placed in a transitional lower delta plain (Fig. 31). This is because there are no fluvial sedimentary features but there is influence of brackish water which marks the transition from fresh water to sea water. However there are no indicators that strictly point to the sand being deposited in marine water.

The A-Y1 well is placed in a lower delta plain. This is because there are no fluvial depositional features such as ferruginous staining and carbonaceous material. The first appearance of glauconite was reported in this well. Glauconite is indicative of a marine environment. This is the most distal well in the study area, according to the sedimentology data.

The depositional environment of the 3 wells A-K1, A-K2 and A-Y1, show lateral movement towards the basin from A-K1 to A-Y1, West to East. This is however in contrast to what is observed as the paleo coastline is towards the East and as you move westwards, you are approaching the basin. The possible explanation for the reversed sequence is that, there was a rise in sea level during the Albian times, A-K1 and A-K2 were deposited first and then later there was marine regression and the sediments that you would normally find in the distal settings were deposited in a proximal environment and reworked.

This is also evident from the lithofacies that were encountered in the study area. The interpreted geological model is in line with the previous interpretation by Jordan and Pay (2015). These authours described the environment of deposition for the Ibhubesi gas reservoirs to be from upper to lower delta plan. The A-K1 and A-K2 wells were also placed in the meandering distributary channels. Tracs (2007) interpreted the depositional environment as fluvial to deltaic with a strong deltaic influence but no marine component identified.

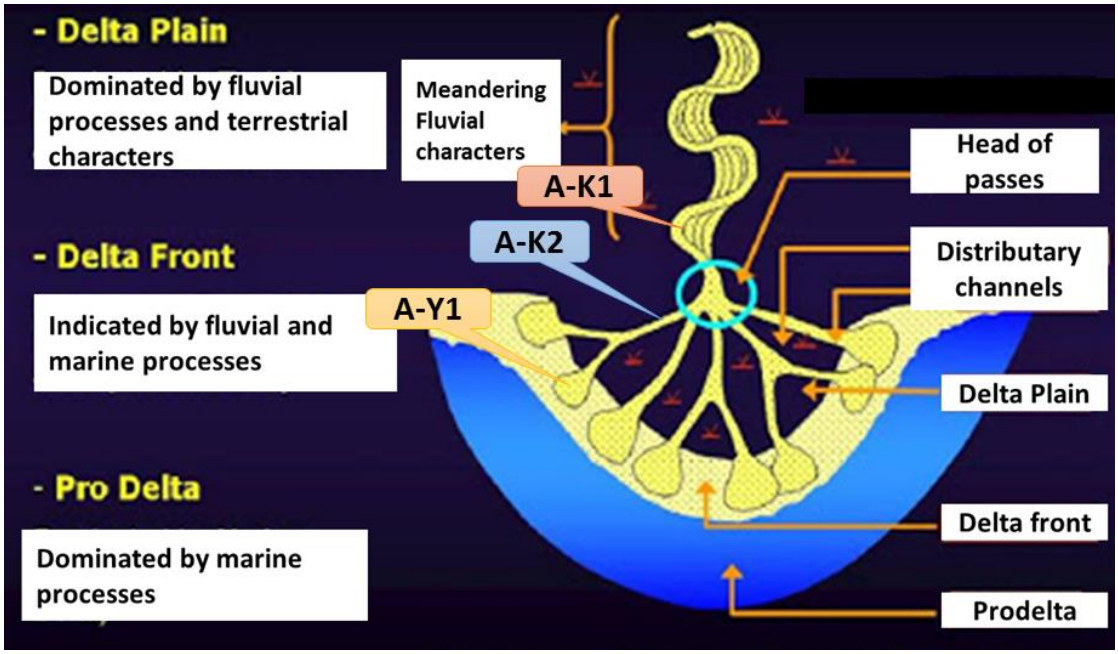


*Figure 31: Interpreted Depositional model of the Ibhubesi Gas Field (modified after Allen, 1998)*

## 4.3 3D Structural model

The results of the structural model that will be discussed are the facies and petrophysical modelling. The input data for facies and petrophysical modelling need to be scaled up prior to populating the grid with the facies and petrophysical data.

### 4.3.1 Well logs up scaling

The up-scaling process is done to account for the difference in the scale of the sampling density of the well logs and the grid cells. In this study, the facies, porosity, permeability and volume of shale logs were up-scaled. The results of the well logs up scaling was acceptable, as presented on the histograms in Figure 32a. The up-scaled logs and the input logs are represented adequately, there is no underestimation from the input well logs.

### 4.3.2 Facies modelling

The histogram in Figure 32a indicates that all the facies were adequately up scaled, when compared to the well logs. The three facies that were defined in the facies log are presented in the final facies grid (Fig. 32b). It was observed that the shale facies dominates followed by the porous sand facies and the tight sandstone facies are the least.

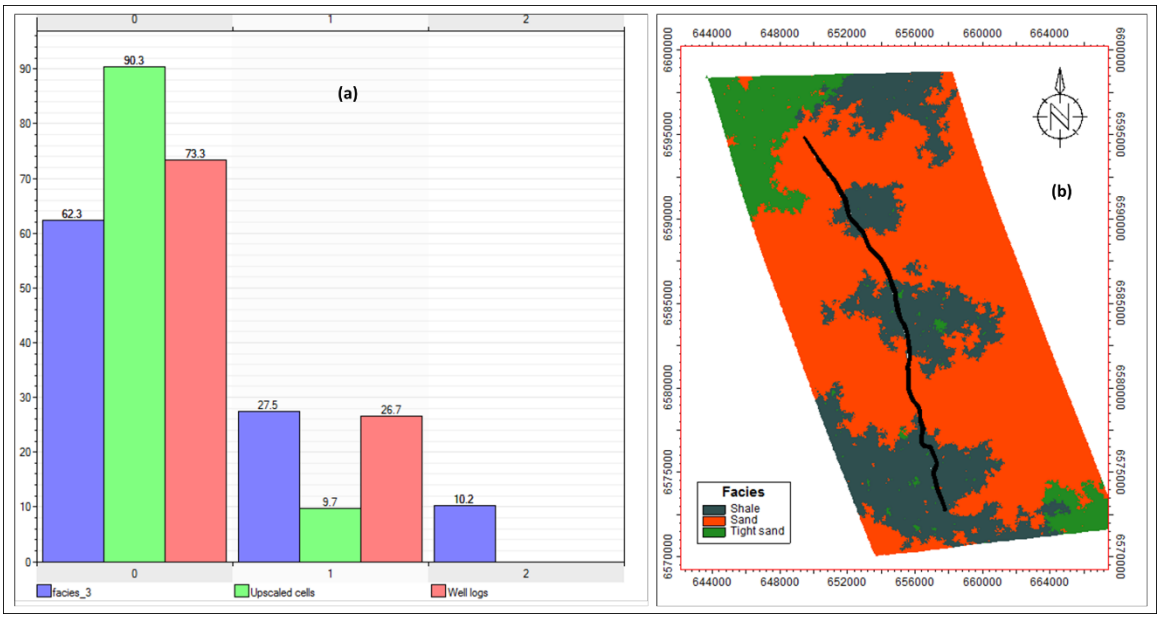


*Figure 32: (a) The histogram showing the up scaled well logs versus the well log data and (b) facies model property showing the different facies defined in the study area- better resolution*

### 4.3.3 Petrophysical modelling

The petrophysical modelling includes the porosity, volume of shale and permeability. The results from the porosity, volume of shale and permeability models were presented on a well section to quality control the results. There is a correlation between the porosity, volume of shale and permeability logs with the respective models. The results of the petrophysical modelling is presented in Figure 26. The facies with the best petrophysical parameters is the porous sandstone.

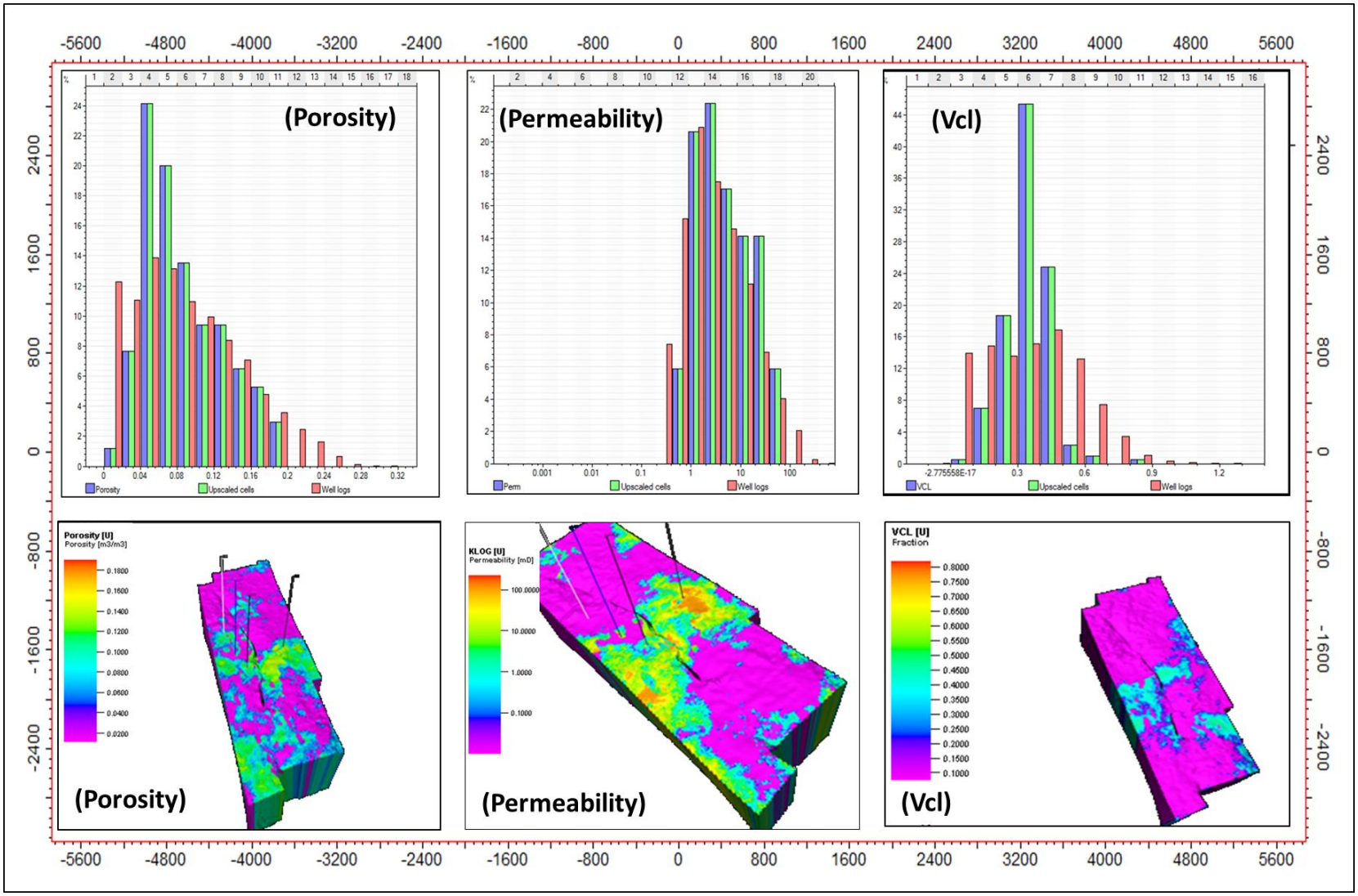


*Figure 33: The histograms of the properties: Porosity; permeability and Vcl with their associated grids*

## 4.4 Fault seal analysis

The fault seal analysis results consist of 2 parts. The juxtaposition analysis and the fault rock properties.

### 4.4.1. Juxtaposition analysis

The 1D well juxtaposition results can be observed from the triangle diagram presented in Figure 34. The reservoir section of the A-Y1 well is shown in the triangle diagram, which is the depth interval from 3200 to 3350. In this interval there are two porous sandstone, the one in the 14Et1 level and the one in the 14Dt1 level. The 14Et1 sandstone is separated by a 5 meters (m) shale and there is a 76m shale interval with minor sandstone stringers as indicated in the facies log which separate the 14Et1 sandstone from the 14Dt1 sandstone.

The juxtapositions that were observed on the triangle diagram, include: sand to sand, shale to sand and very minor tight sand to sand juxtapositions. It can also be observed that where the throw is less than 30m, the sand to sand juxtapositions generally occur. These areas are interpreted to be areas where leaks are most likely to occur. The areas where the sand is either juxtaposed against a shale or a tight sand are interpreted to be areas where the seals are most likely to occur.

The SSF was determined using the equation (1.2). In the 14Et1 reservoir interval (interval 1), the fault throw is about 30m (Fig. 34) and the shale bed that separates the two sands is about 5m. The SSF is about 6. According to Faersh, (2006), if the SSF is large, greater than 5, the smears become discontinuous and are prone to leaks. This is also observed in the triangle diagram. In this instance the throw is six times greater than the shale bed thickness.

The interval 2 is from the Base 14Et1 reservoir to the Top 14Dt1 sandstone (3228 – 3328). This interval is dominated by shale with minor stringers of sandstone. In this interval, the throw is about 100m and the shale interval is about 76m. The calculated SSF is 1.3. This SSF indicate the possibility of continuous smears formation, thus increasing the probability to seal. This is to be expected as the throw is only 1.3 times greater than the shale bed thickness. In this way, the shale veneer is not eroded by the throw.

In interval 3, from the Top of 14Dt1 to just below the base of 14Dt1 (3329 – 3344), the throw is about 15m. The shale bed thickness is about 2m and the calculated SSF is 7.5. The throw is seven times bigger than the shale bed thickness and in this way the shale smear is discontinuous.

In the chosen depth interval (1, 2 and 3), the tight sand rarely occurs and where it occurs, it is interbedded with shales. The tight sandstone interval can be observed in the Vsh log (Fig. 34). The juxtaposition of tight sands with shale will result in the formation of a seal.

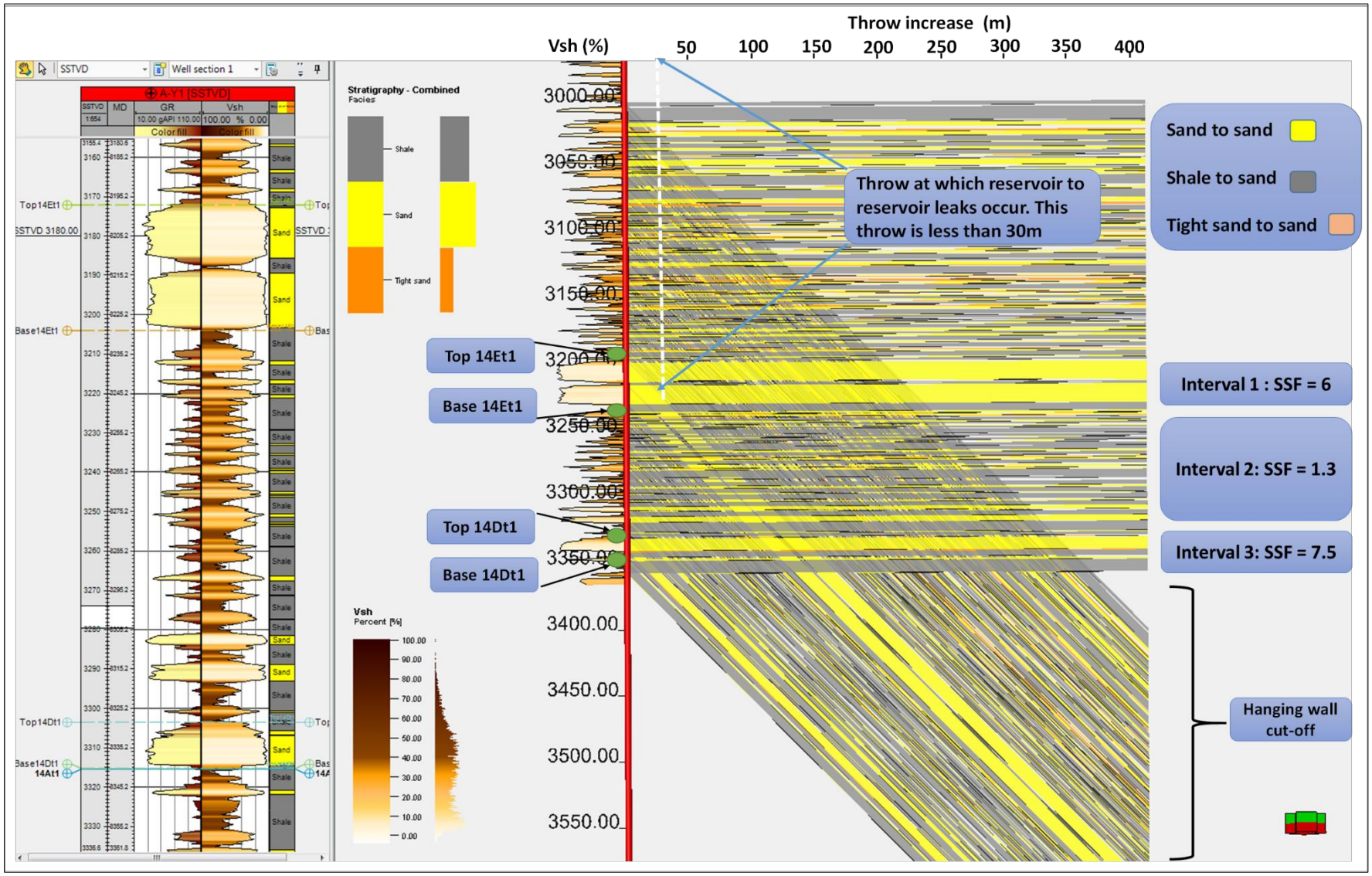


*Figure 34: 1D well juxtaposition diagram for the A-Y1 well, indicating the different lithological juxtapositions of the defined facies (shale, sand and tight sand). The GR and Vsh are used as reference logs*

### 4.4.2 3D facies juxtaposition analysis

The 3D facies juxtaposition is in Figure 35. These juxtaposition types are based on the facies that were defined in the study area and are produced as a new fault property referred to as the juxtaposition mapping property. It was observed from the juxtaposition mapping fault property that there are five juxtaposition types that occur across the AK fault. These are:

1) Shale against a porous sandstone;

2) Porous sandstone against a porous sandstone;

3) Porous sandstone against a tight sandstone

4) Tight sandstone against a tight sandstone

5) Tight sandstone against a shale

#### *4.4.2.1 Shale against a porous sand*

The juxtaposition of a shale against a porous sand may result in the formation of a seal. This is because a low permeability facies (shale) is juxtaposed against a high permeability facies (porous sandstone). This type of seal may form because the pore throats between the shale grains are small and the hydrocarbons will require a higher entry pressure to move through the shale pore throats. In this way, the seal is formed.

#### *4.4.2.2 Porous sandstone against a porous sandstone*

In this juxtaposition type, two facies which have high permeability are juxtaposed against each other across the fault. In this case, there are two possibilities that can occur in the fault zone. Either the fault is leaking and the migration of hydrocarbons can continue across the fault or the fault is sealing by means of cataclasis. Cataclasites occur in porous sandstones by means of mechanical crushing at grain to grain contact (Milliken et al., 2002). During this process the grains are rotated and slide against each other, thereby reducing porosity.

There are other factors that accompany this process. These includes the precipitation and pressure solution of minerals such as quartz, reducing porosity and permeability by cementation. There is a high probability that the resulting fault rock will be sealing.

#### *4.4.2.3 Porous sandstone against a tight sandstone*

In this juxtaposition type, a high permeability facies, porous sandstone is juxtaposed against a low permeability sandstone. There are two scenarios that are proposed for this juxtaposition. A possible fault leak and a fault seal. A fault leak may result because the tight sandstone may have a high capillary entry pressure, but it may not be as competent seal when compared to a shale. Additional work would need to be carried out to validate the competence of a tight sandstone to act as a seal.

The other possibility would be that, a cataclasite will form resulting from the grain crushing of the two sandstones. Even though the tight sandstone is impure, there could be precipitation of quartz leading to the cementation of previously open spaces. In this way a seal would result.

#### *4.4.2.4 Tight sandstone against a tight sandstone*

In this juxtaposition type, a low permeability facies, tight sandstone is juxtaposed against itself. The only foreseeable possibility is a sealing fault rock.

#### *4.4.2.5 Tight sandstone against a shale*

In this juxtaposition type, a low permeability facies, tight sandstone is juxtaposed another low permeability facies, shale. A sealing fault rock is highly possible. There might be a risk of breach of the seal should there geological processes such as reactivation accompanied with the fracturing of the tight sandstone increasing permeability, however, the "fractured sandstone" would still be juxtaposed against a shale and probability of sealing is still anticipated.

The cataclastic seals and shale smears are probably the most likely seal types that will occur in the study area. The 3D fault seal analysis in this study focuses on the probability of fault seals due to shale smears (SGR) at this point in time using the Petrel software 2015. The probability of the formation of cataclasites is based on the composition of the reservoir rocks in the study area and the depth at which these reservoir rocks occur. According to Fisher and Knipe (1998) there are two types of fault rocks that results from the deformation of clean sandstones, these are disaggregation zones and cataclasites.

In this study, the disaggregation zones and cataclasites have been defined according to the definition by Fisher and Knipe (2008). In their definition, the fault rocks that form at shallow depths of less than 500m are disaggregation zones and those that form at depths exceeding this depth are referred to as cataclasites (Fisher and Knipe, 2008).This shallow depth is associated with low stress levels and as a result, the deformation that results is related to the reduction of pore spaces caused by the re-alignment of the grains. In this way, the porosity

and permeability of these disaggregation zones do not vary significantly from that of the host rock.

Cataclasites on the other hand form is depths exceeding 500m (Fisher and Knipe, 2008). These rocks are subjected to higher stress levels leading to the grain fracturing and the collapse of the pores. There is a significant reduction in the permeability and porosity of the cataclasites when compared to that of the host rock. The reduced porosity and permeability is further promoted by the quartz cementation due to the grain to grain contact. The latter has also been observed in the study area.

The A-V1 well was planned to be drilled to a total depth of 4500m. At 3400 m, the well was side tracked due hardness of the formation and associated slow drilling rates. The side track is only 300m as the formation was still too hard to drill and the reported reason to the hardness of the formation was the silicified sandstones. These silicified sandstones had no porosity or permeability. The well was terminated early 800m shallow to the originally planned depth.

In the study area, the timing of the AK fault is between 750m and 3.5km supporting the formation of the cataclasites as compared to the disaggregation zones, according to the Fisher and Knipe definition.

An intersection plane was taken across the 3D facies property model (Fig. 36). In this intersection, it can be observed that the dominant juxtaposition is that of a sandstone against a shale. This was also observed in the reservoir section. There are areas where sand on sand juxtapositions were observed. In these areas the possibility of a leak is high. Even though these areas pose risk to leaking, the shale smear factor is less than 3 and in this way, it is possible that the smears may be continuous and may be able to provide a seal.

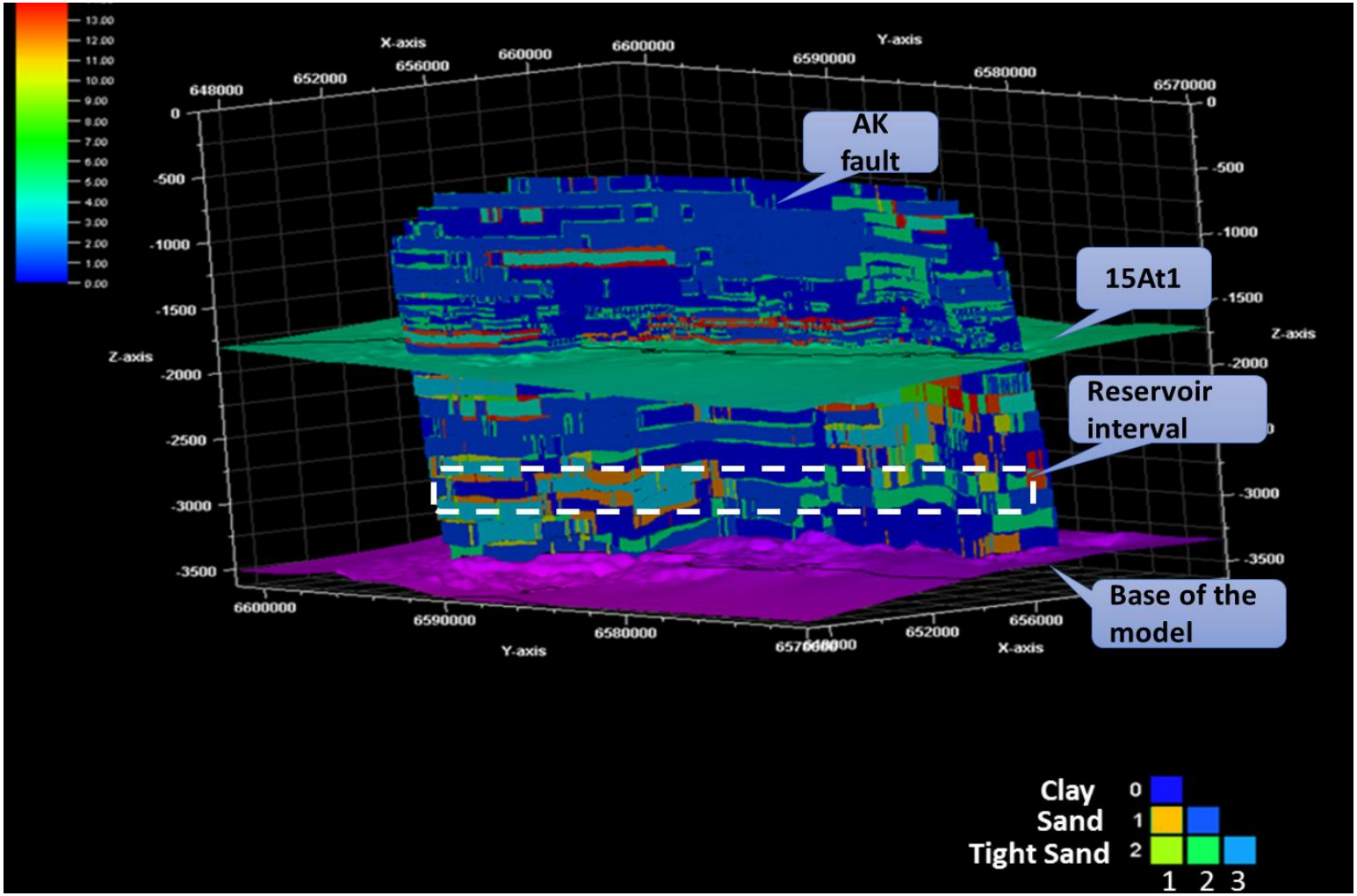


*Figure 35: A strike section of the AK fault plane showing the different facies juxtapositions. In the reservoir interval, the juxtapositions that occur are mainly the sand (orange) against the shale (blue) and the tight sand (green) against the sand (orange and the tight sand against the shale.*

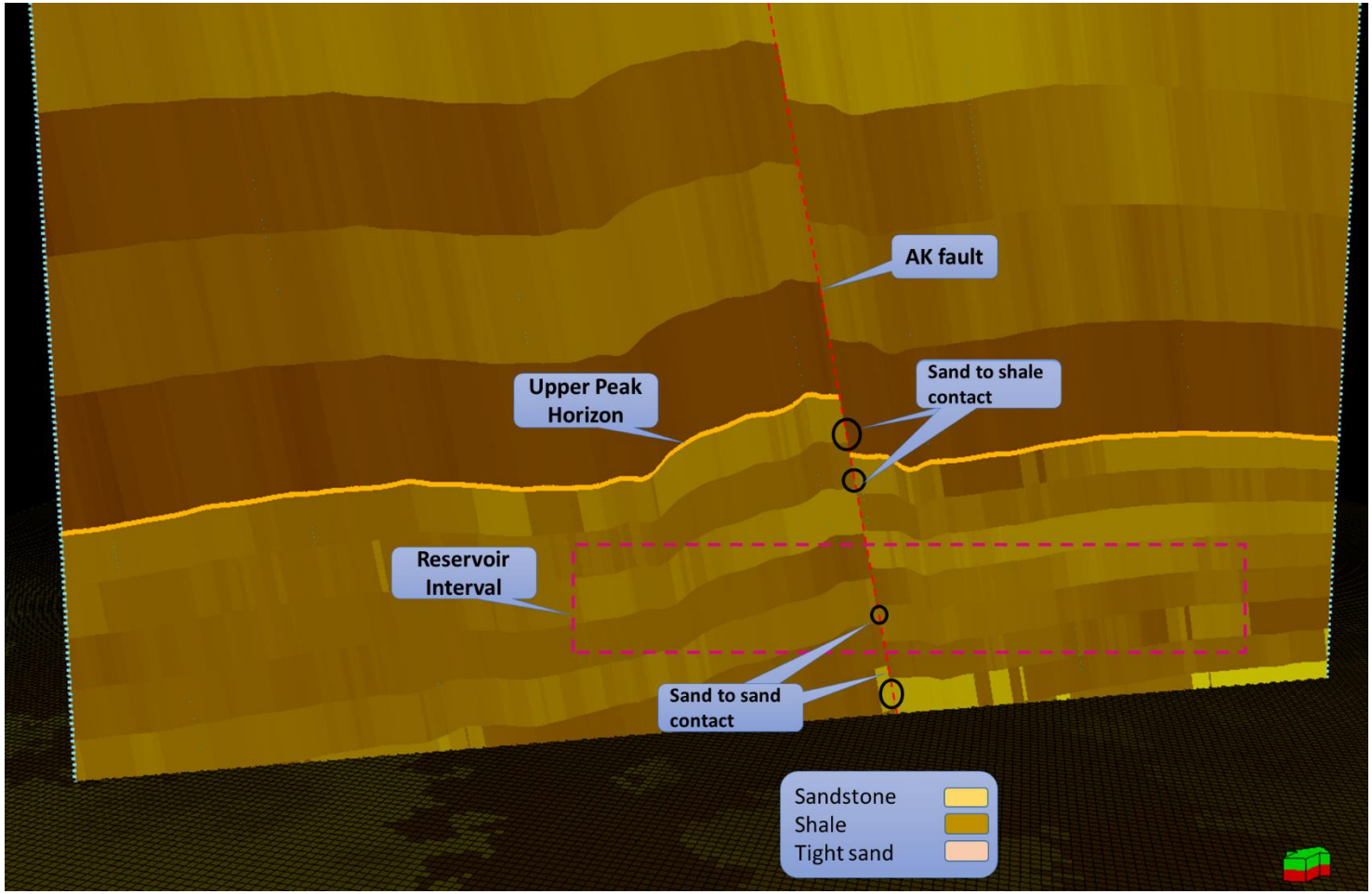


*Figure 36: An intersection plane through a facies property model. In this figure, the AK fault which is currently under study is indicated. The Upper Peak horizon is also shown, which is the closest upper horizon to the reservoirs. The reservoir interval is shown in red. In the reservoir interval, the juxtapositions that occur are mainly shale to sandstones*

### 4.4.2 Fault rock properties

The fault properties that are required to complete a fault seal analysis study are presented in Figure 37 and 38.

#### *4.4.2.1 Fault rock clay / the Shale Gouge Ratio (SGR)*

In Figure 37, the yellow values represent the low fault clay distribution and brownish colours represent high fault clay distribution. It can be observed that the yellow colours juxtaposed against brown colours dominates and the yellow colours juxtaposed against yellow colours association is minimal. The low fault clay distribution is associated with porous sandstone and brownish colours with tight sandstone or shales. The juxtaposition of yellow against yellow then correlates with sand on sand and brown against yellow with sand on shale or tight sand (Fig. 37a).

This is also supported by the juxtaposition analysis results. These results indicated that there is a possibility of porous sandstone against porous sandstone juxtaposition and porous sandstone against a tight sandstone or shale juxtaposition. The fault clay distribution is not a direct measure of the fault seal capacity, however, there is a negative correlation between volume of clay and permeability (Fig. 35 and 36). The permeability deteriorates with increased clay content. In this way, the fault zone with a high clay content will have small permeabilities and increased potential of sealing.

The SGR, relates to the gouge that is present in a fault rock. This gouge is controlled by the fault clay distribution in the fault zone. In this way, the shale gouge can be used to estimate the sealing capacity of a fault. Faults that display a higher fault clay percentage and hence a higher SGR, will consequently have a higher threshold pressure and therefore a high sealing potential.

In the study area, it was observed that the SGR of the AK fault varies between 18% and 55% (Fig. 37b). A compilation of SGR for fault depended traps for sealing and non-sealing faults in the North Sea by Yielding et al (2002), show that the SGR value of approximately 15 – 20% is the cutoff for sealing versus non-sealing faults (Fig. 4c). There is a high probability that the fault will seal if it has an SGR greater than 20%. If the AK fault has a SGR that ranges between 18% and 55%, then it will most likely be sealing.

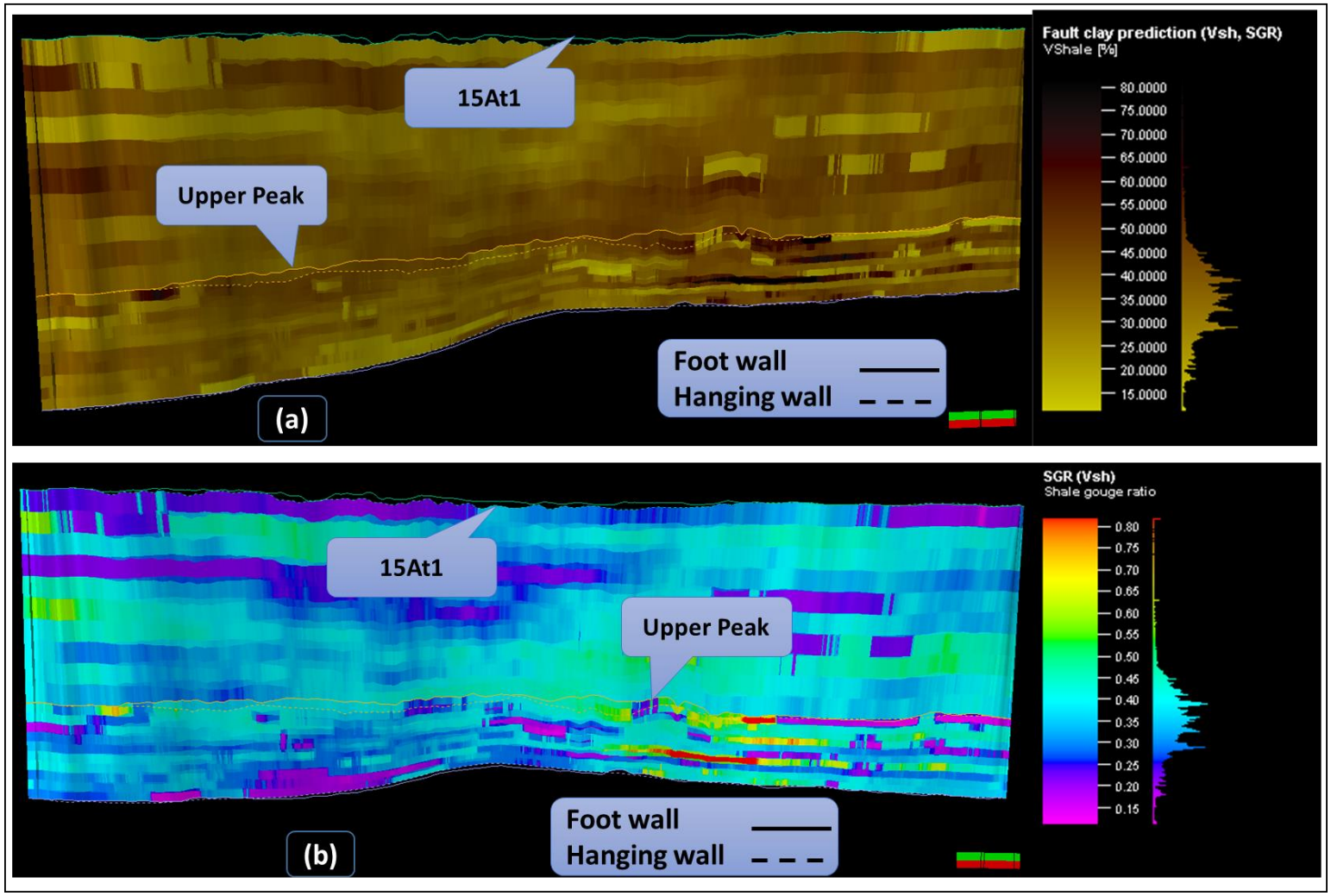


*Figure 37: AK fault rock properties. (a) Fault clay prediction and (b) SGR*

#### *4.4.2.2 Fault rock permeability*

Fault rock permeability is presented in Figure 38(a). The cold colours light blue to purple represent low permeability values and warm colours represent high permeability values. It can be observed from the fault rock permeability property, that the permeability in the study area varies between 0.00 to 0.10mD. The low fault rock permeability values were expected and are attributed to the fault rock clay content. Faults with a high clay content are associated with low permeabilities, (Manzocchi et al., 1999 and Sperrevik et al., 2002). This is also corroborated by the Vcl versus Permeability relationship displayed in Figure 39.

Using the clay content compilation from the fault dependent traps in the North Sea, faults with an SGR greater than 20% are sealing. If this 20% SGR cut-off is used in the correlation of the phyllosilicate content versus fault rock permeability, it can be deduced that the maximum fault rock permeability that can be correlate to percentage phyllosilicate (SGR) of 20%, is just below 1mD, using empirical data (Fig. 40). It can be assumed then that, if a fault has a permeability of less than 1mD, then it is most likely to seal.

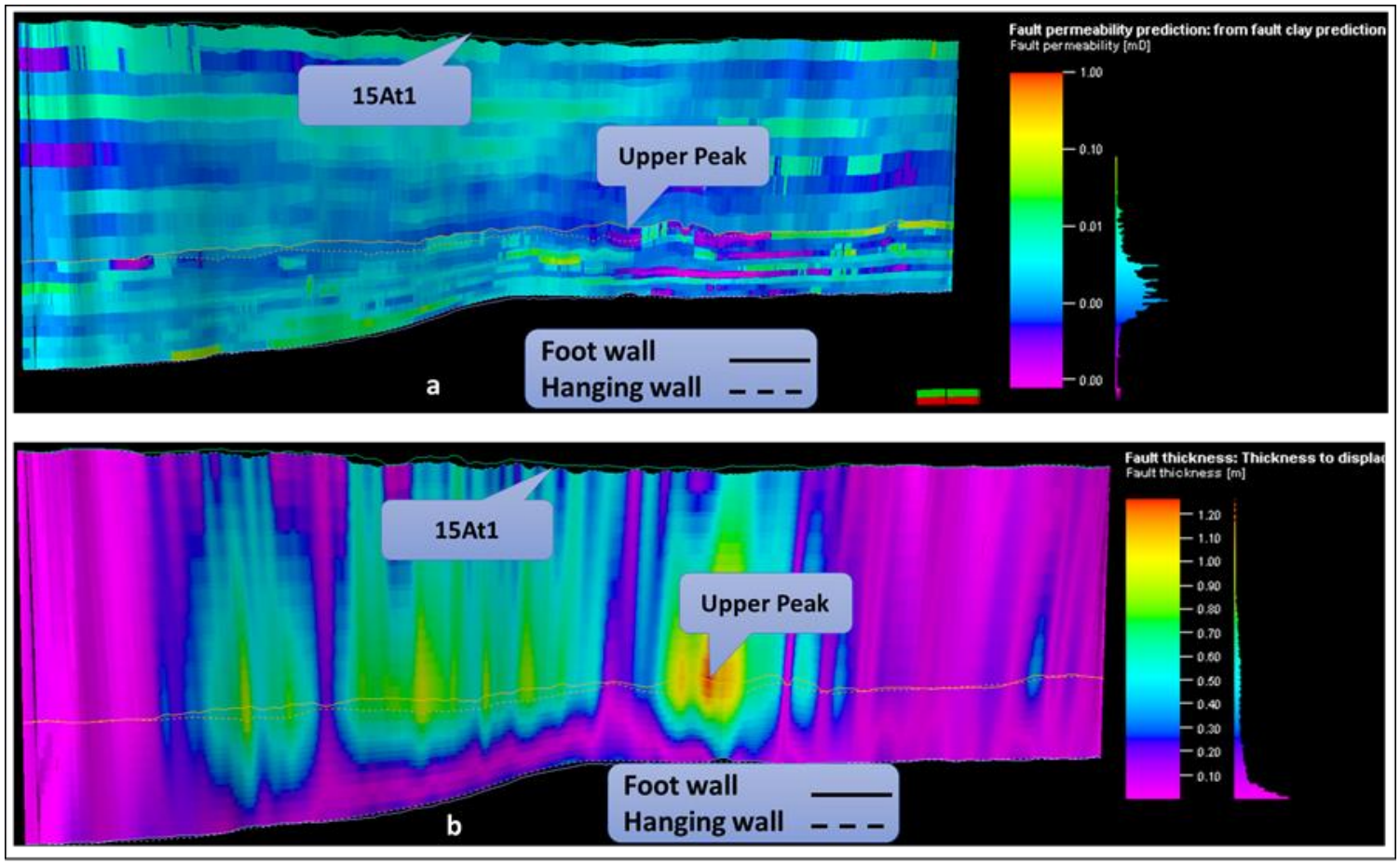


*Figure 38: AK fault rock properties. (a) Fault rock permeability and (b) fault rock thickness*

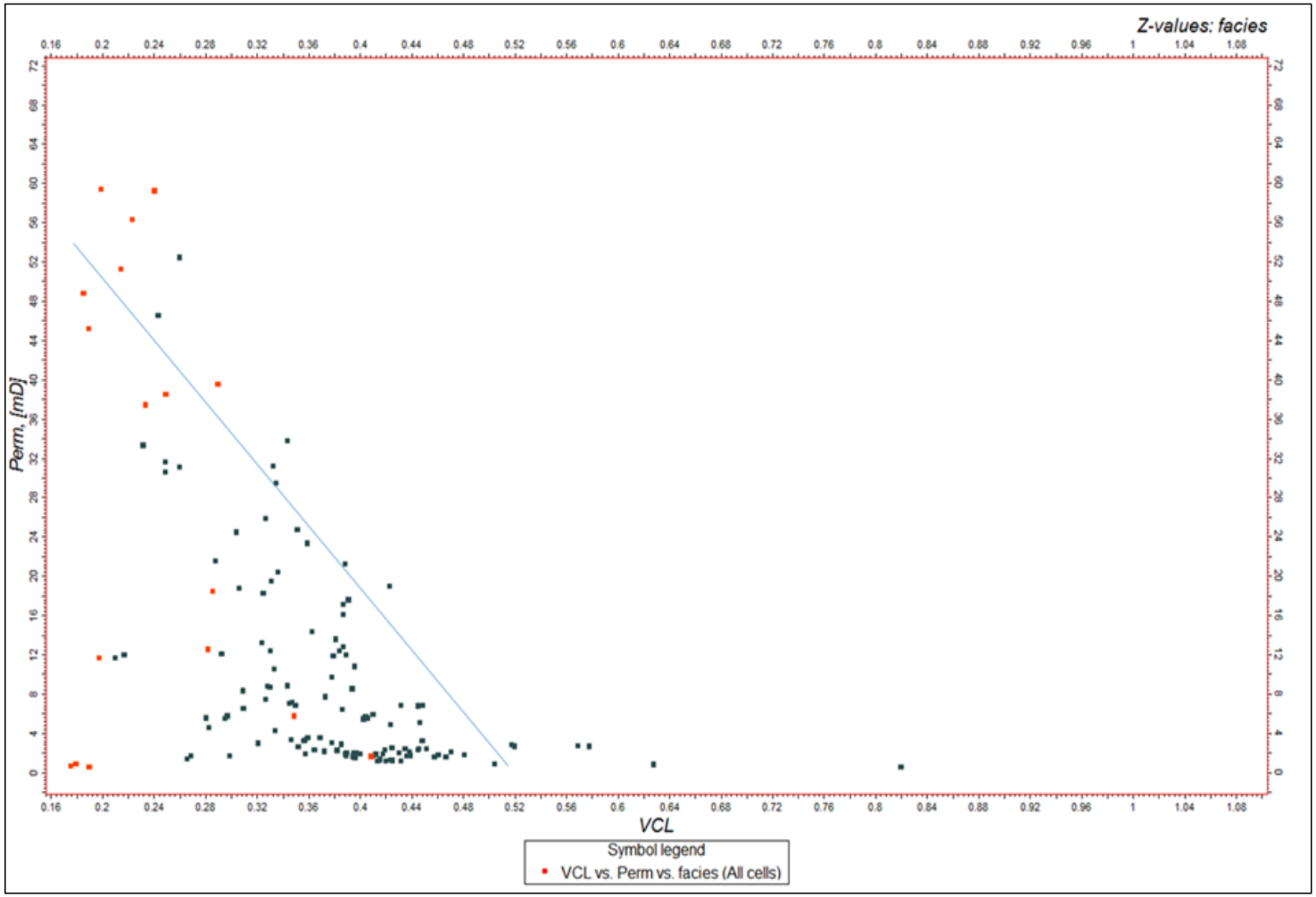


*Figure 39: Graphical presentation of the permeability versus Vcl*

| Area | Dacry |
|---|---|
| $10^{-11}$ m$^2$ | $10^{4}$ mD |
| $10^{-12}$ m$^2$ | $10^{3}$ mD |
| $10^{-13}$ m$^2$ | $10^{2}$ mD |
| $10^{-14}$ m$^2$ | $10^{1}$ mD |
| $10^{-15}$ m$^2$ | 1 |
| $10^{-16}$ m$^2$ | $10^{-1}$ mD |
| $10^{-17}$ m$^2$ | $10^{-2}$ mD |
| $10^{-18}$ m$^2$ | $10^{-3}$ mD |
| $10^{-19}$ m$^2$ | $10^{-4}$ mD |
| $10^{-20}$ m$^2$ | $10^{-5}$ mD |

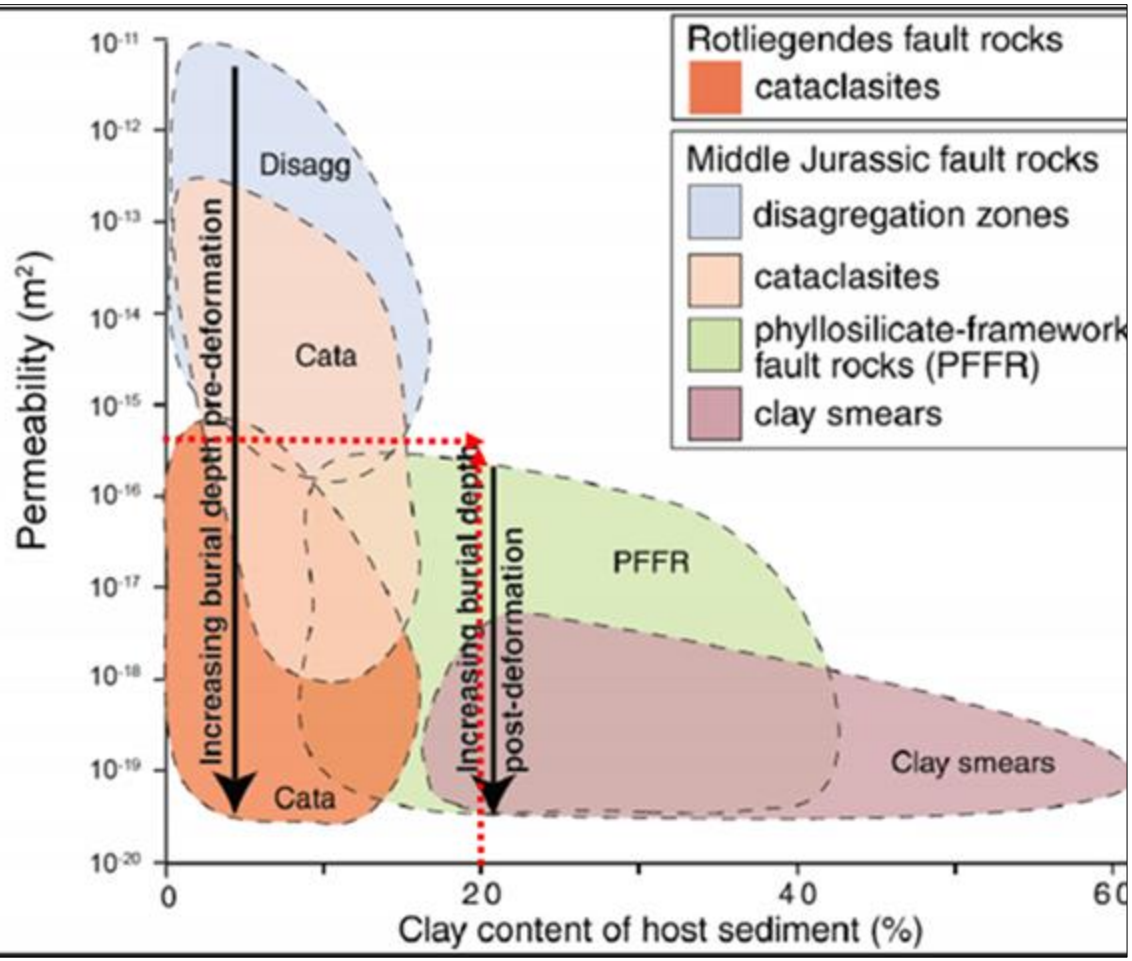


*Figure 40: Fault rock permeability data compilation from North Sea and Norwegian Continental shelf. Permeability plot versus clay content for various fault rock type (figure from Nicol et al., (2016), which has been annotated for comparison)*

#### *4.4.2.3 Fault rock thickness*

The fault rock thickness is presented in Figure 38(b). The fault rock thickness varies from 0.1 to 1.20m. These results were expected and are attributed to the method that was used to determine the fault rock thickness, which was the thickness to displacement ratio. Since the AK fault displacement has an impact on the results of the fault rock thickness, it is worthwhile to review the results of the AK fault displacement.

The AK fault displacement profiles were taken at the 15At1 and Upper Peak levels (Fig. 41). It can be observed from these profiles that the AK fault displacement increases with depth, with an average fault displacement of 35m in the 15At1 level which increases to an average displacement of 54m at the Upper Peak level. The maximum displacement that can be observed on the 15At1 level is 54m and increases up to 120m at the Upper Peak level.

The results from the 1:60 thickness to displacement ratio, indicate that the fault thickness varies between 0.1 to 1.35m. The 1:60 displacement to thickness ratio was preferred because according to Manzocchi et al., (1999) the thickness for major faults is typically 1:66. This thickness ratio was then used to compare with the default of 1:100 ratio.

The lithology also has an impact on the fault rock thickness. The coarser grained material display a large fault rock thickness when compared to the finer grained material at low throws. This is because there is a development of wider deformation bands in the fault zone, than the development of a thin smear in the fault zone when clays are smeared. Even though the faulted coarser material may result in the formation of a thicker fault zone, it is the clay/shale smears that display a significant reduction in permeabilities because of the lower permeabilities associated with shales.

The throw of the fault though must be low or the smeared veneer will get eroded. In the literature, a throw should be at least eight times lower than the source of the shale bed (Childs et al., 2007). In the study area, the minimum throw observed is about 35m. This throw may result in thinner fault rocks and ultimately leaking faults. It is also possible that at these throws the fault may still seal. This is because of the massive nature of the reservoir rocks in the study area. Childs et al., (2007) indicated that when massive rocks deform at low throws they result in a thicker fault zone as compared to shales.

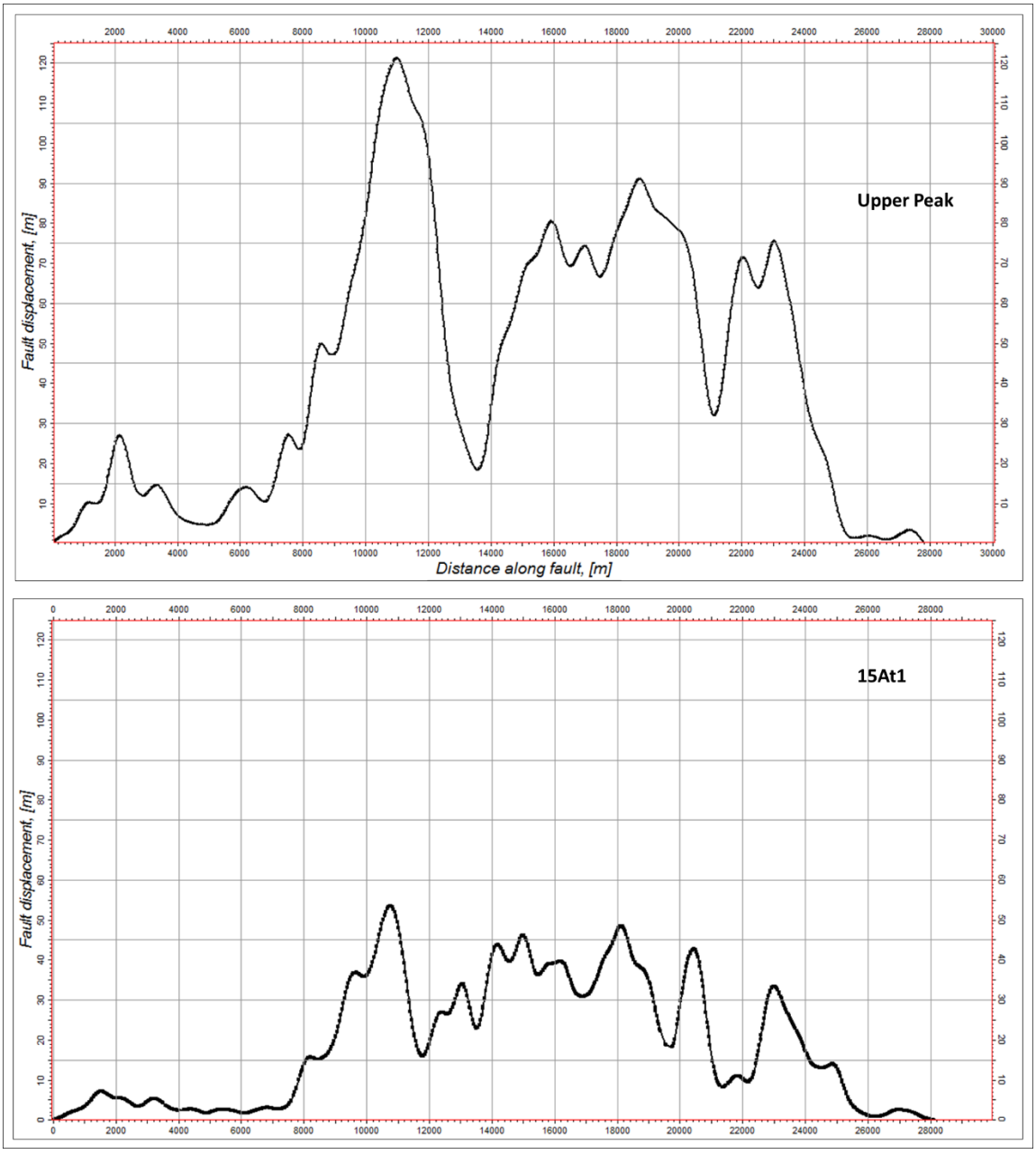


*Figure 41: Fault displacement profiles in the 15At1 and Upper Peak (UP) horizons*

#### *4.4.2.4 Across fault pressure difference (AFPD)*

The depth RFT pressure plot in Figure 42a, indicates that the pressure difference between the footwall reservoir in the A-K2 well and the hanging wall reservoir is up to 290psi, which is about 20Bars. This AFPD pressure difference was plotted on the calibration plot of SGR vs AFPD (Fig. 42b). The calculated SGR of the AK fault range between 18 and 55%. To validate whether the shale gouge ratio calculations will be able to provide a seal, it is important to know the threshold pressure of sealing faults in the field as this provides calibration.

There has not been any fault analysed in the Ibhubesi gas field or in the Orange Basin, where the study area is located. It is because of this that the Oseberg Syd Field, compiled by Fridstad et al., (1996) was used. In this field, an SGR of less than 15% will not seal, between 15 and 18% will support a pressure difference of 0.5bar and that above 18% will support the pressure difference in excess of 8bar.

Given a SGR of up to 55% and AFPD of 20Bars, the AK fault will withstand the buoyancy pressure of the fluids in the reservoir and provide a good seal. This also concurs with the threshold pressure for the AK fault which was computed during the fault seal analysis process (Fig. 42c). The minimum threshold pressure that will support the hydrocarbon column height is 20Bars.

The gas water contact from the A-K2 well is 3225 m, subsea (ss) and from the A-Y1 well is at a depth of 3198 m (ss). There is a difference of about 27m which further alludes to different fluid pressure regimes. In this way it can be concluded that the well are not in hydrostatic communication at the 14Et1 reservoir and as a consequent the AK fault plane is sealing at this reservoir interval.

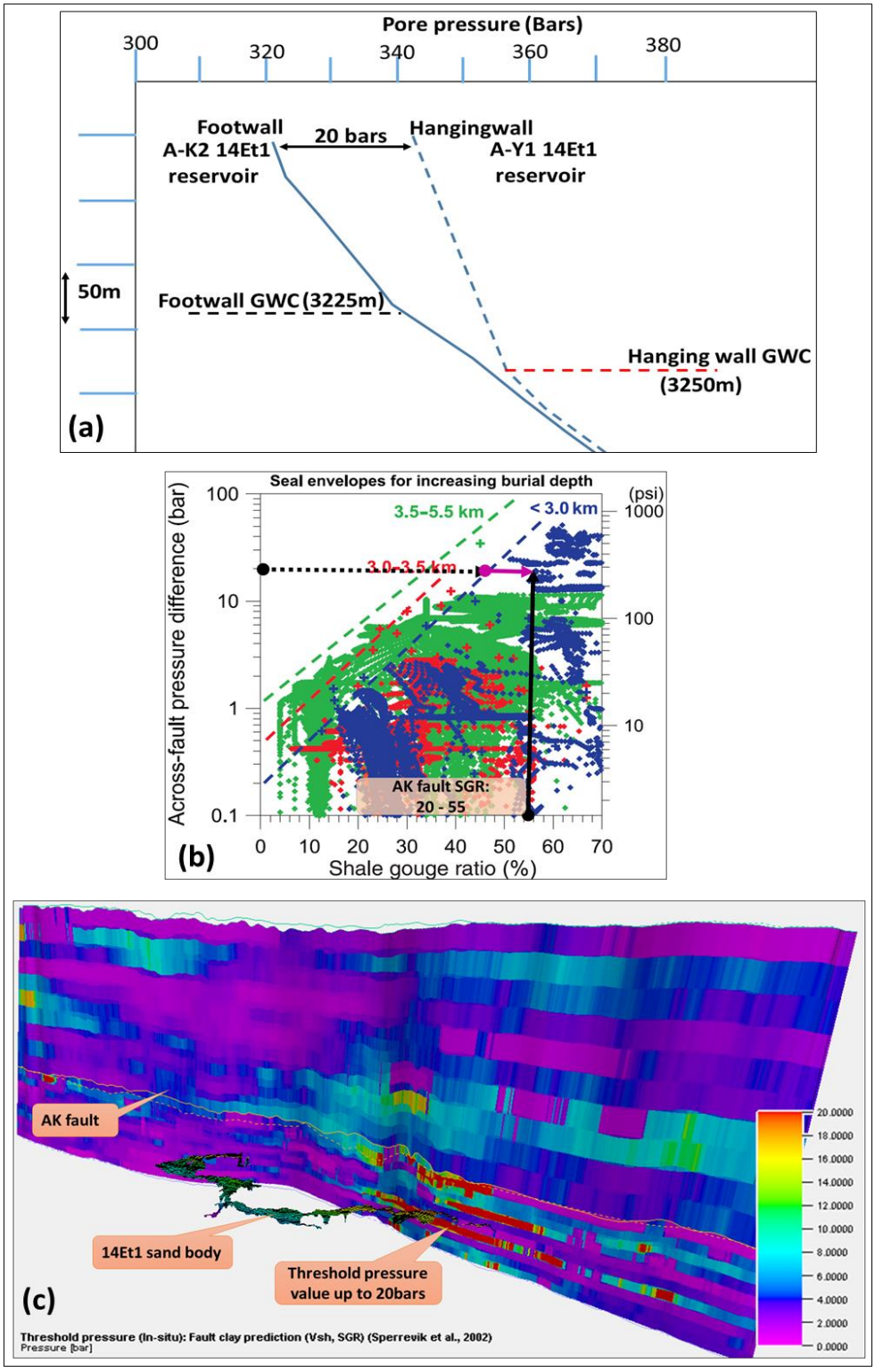


*Figure 42: Across fault pressure difference. (a) The schematic illustration of the across fault pressure difference of the A-K2 and A-Y1 wells for the 14Et1 reservoir and their associated gas water contacts (GWC); (b) Seal envelopes for sealing faults at depths ranging from 3 to 5.5km, illustrating the relationship between across fault pressure difference and the Shale Gouge Ratio; (c) Threshold pressure of the AK fault*

### *4.4.2.5 Column height prediction*

The observed results from the column height prediction are presented in Figure 32a. It can be observed from the column height prediction that the AK fault can support a hydrocarbon column height of up to 120m. The calculated most likely column height ranges between 43m and 127m (Jordan and Pay, 2015) (Fig. 43b and c). The AK fault should be able to support this hydrocarbon column height.

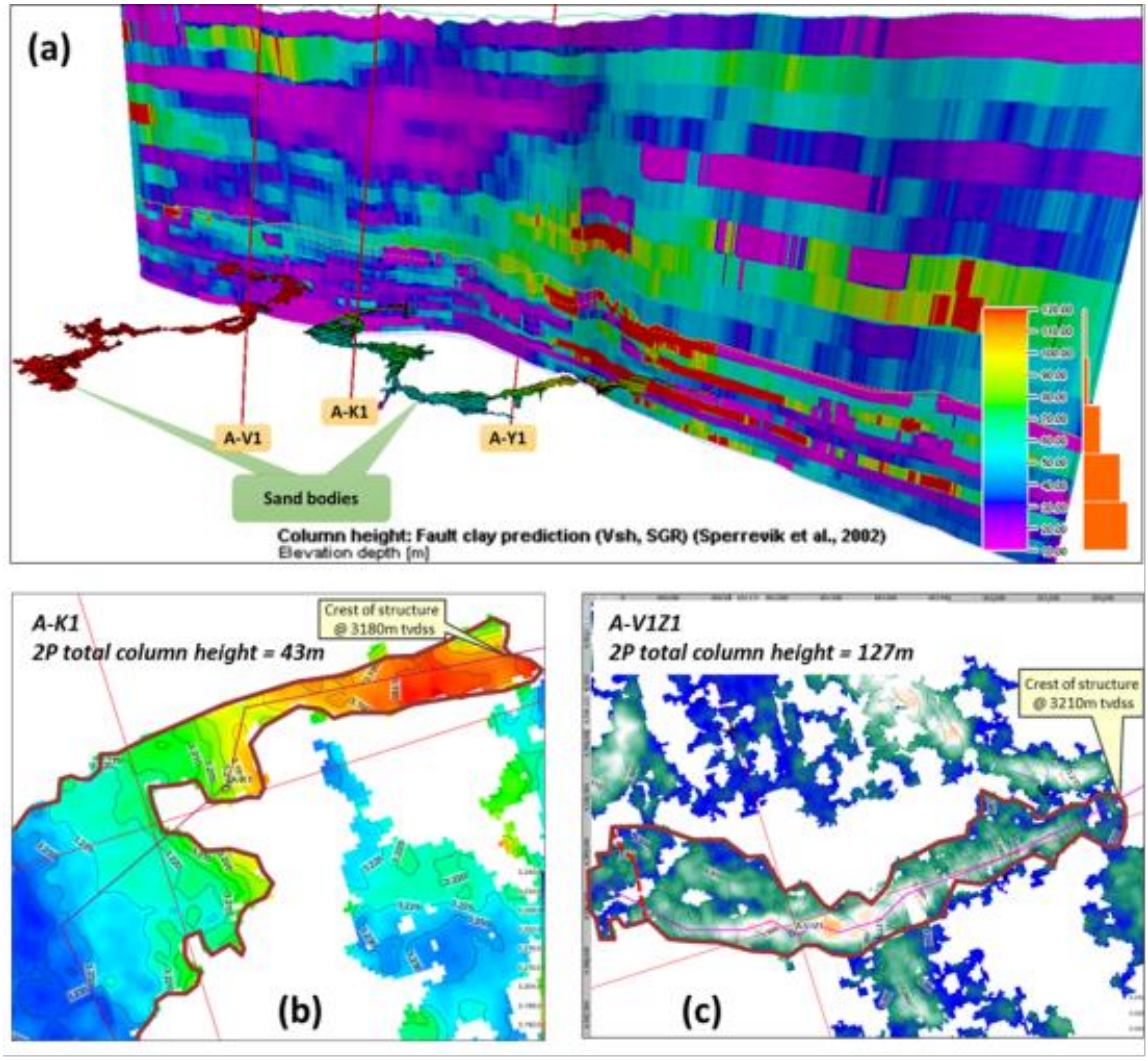


*Figure 43: (a) Hydrocarbon column height on the AK fault. (b) The calculated most likely column height in the study area varies between 43 and 127m (Jordan and Pay, 2015)*

### 4.4.3 Fault transmissibility prediction

The fault transmissibility prediction is the final step in fault seal analysis process in this study. In this step, the fault properties are integrated into the flow model to determine whether the fault has the ability to transmit fluids.

*The measure of transmissibility is between 0 and 1, where:*

- The fault is sealing; the transmissibility multiplier is zero
- The fault is open; the transmissibility multiplier is 1
- The fault is partially sealing and partially open, the transmissibility multiplier is between 0 and 1

The results from this study show that the AK fault transmissibility multiplier is zero, for the low and mid sealing scenarios (Fig. 44a and b). In this way, there is a high probability that the AK fault is sealing. The AK fault transmissibility histogram (Fig. 44c) indicates that the transmissibility values only go up to 0.1.

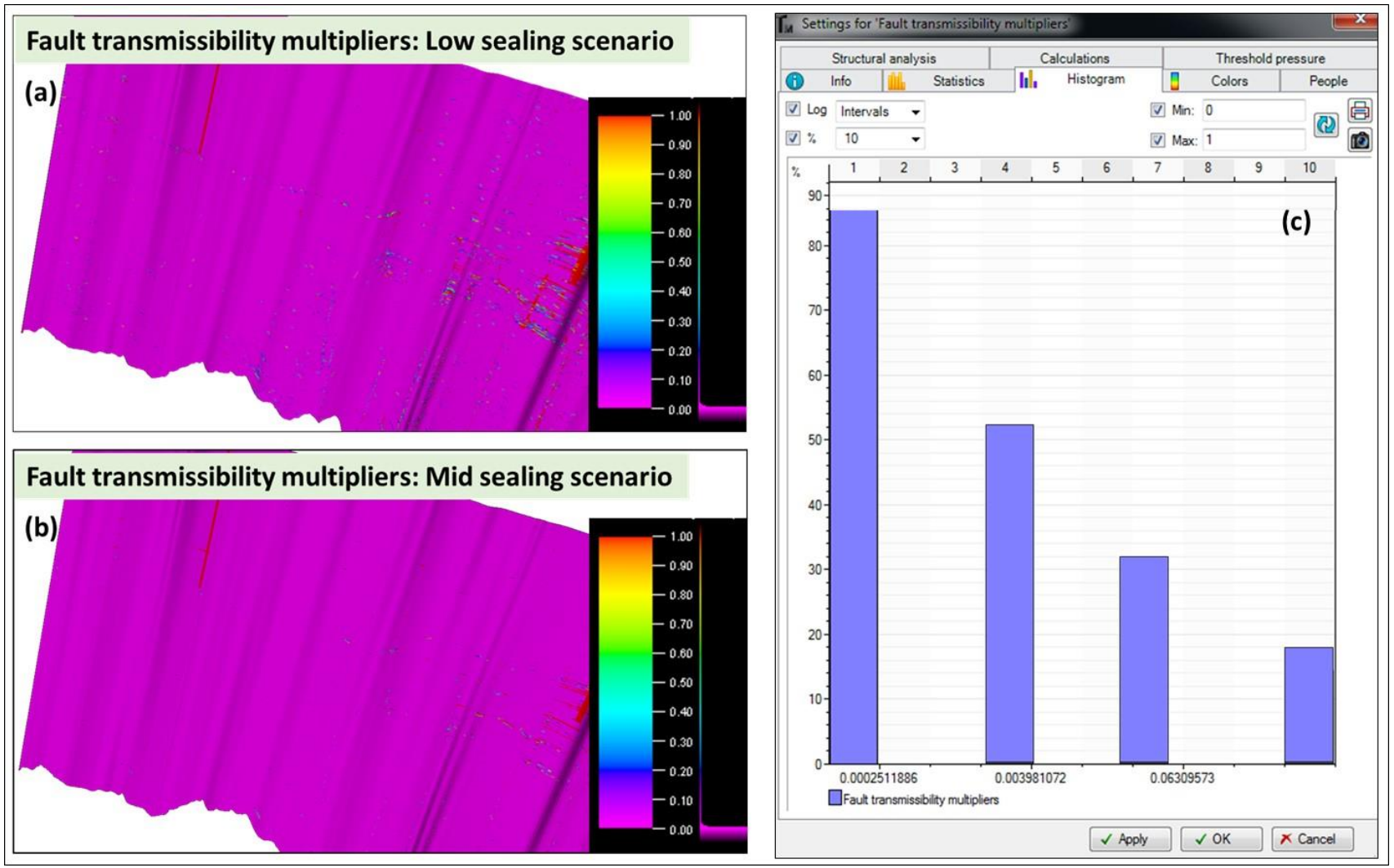


*Figure 44: Fault transmissibility multipliers for the AK fault. (a) Low sealing scenario, (b) Mid sealing scenario and (c) AK fault transmissibility histogram*

# 5. DISCUSSION

The aim of the study was to determine whether the AK fault acts as a barrier or conduit to fluid flow in the Ibhubesi Gas Field. This was achieved through the process of conducting a 3D fault seal analysis study and the results show that there is a high probability that the AK fault is sealing. These results are important in the understanding of the reservoirs in the Ibhubesi gas field in terms of trapping mechanism and compartmentalisation. This has a significant impact on the field development plan, as there will have to be additional wells that will have to drain areas, which were previously thought to be in hydraulic communication.

Even though the results indicate a high possibility of the AK fault to be sealing, it is important to keep in mind that for the fault seal analysis study to be successful, substantial amount of data interpretation is integrated. This data interpretation comes with its own errors and limitations. In an attempt to minimize the final amount of error that will be inherited in the final results, an approach to quality control all the results was effected.

There are however other factors which could not be excluded even with the quality control of the results. These factors include the limitations of the software, the availability of data and the uncertainties associated with the fault seal analysis study.

## 5.1 Uncertainties associated with fault seal analysis input parameters

### 5.1.1 Volume of clay

The key input for the evaluation of the fault rock properties is the Vcl. The Vcl parameter was derived from gamma-ray log and it is used as a parameter that describes the actual volumetric clay content (Vclay or % phyllosilicates) of the rock. A detailed analysis of thin sections by x-ray diffraction analysis (Core Lab report) was conducted to validate volume of clay content where data was available. The well that had the most complete data set in the study area, is the A-K1 well. The well which had the least amount of geological data available is the A-Y1 well. As a consequence, the Vcl that was derived from the GR log at the A-Y1 well location could not be calibrated as in the A-K1 well.

Since the Vcl parameter is a derived product, there are some errors that could be inherited in the calculation of the Vcl. These inherited errors will be incorporated in the whole workflow of the fault rock properties evaluation, since the primary input in the calculation of these fault properties is the Vcl, e.g. the fault clay is derived from the mapping of the volume of clay from the 3D grid and the fault displacement. The resulting fault clay (SGR) will be used to derive a

transform relationship between the fault clay and the fault permeability of the fault rock. This transform will be used to convert the fault clay to fault permeability.

In the prediction of the hydrocarbon column height on the AK fault, the SGR of the fault is calibrated to estimate the maximum pressure that can be supported by the fault, using equations that relate the SGR to the threshold pressure. This maximum pressure is taken to be equivalent to capillary entry pressure along the fault plane (Brentan et al., 2003). As it has been alluded to, the Vcl play an important role in the fault analysis study. There are probably inherited errors in the calculation, which will affect the final results of the study.

### 5.1.2 Seismic resolution

The major uncertainty that is associated with fault interpretation is the seismic resolution. The seismic resolution refers to the minimum thickness of the top and the base of a bed that can be resolved by seismic data. The seismic data has a minimum resolution of about 30m. This has an impact in a number of elements in the fault analysis study and these are namely: Fault displacement and in turn fault clay prediction, fault thickness, fault permeability and hydrocarbon column height on the AK fault.

The fault displacement that is observed on seismic data along a vertical profile is assumed to be resulting from one fault. Outcrops in the field have shown that, there is a possibility that the observed displacement from one fault is actually a collective displacement from more than one fault. The other faults may be below seismic resolution and as a result not resolved by seismic data.

The fault zone consists of deformation bands. It has been observed from the outcrops, that faulting is accompanied by the formation of deformation bands (Hesthammer et al, 2000). According to this author, the occurrence of these deformation bands is not dependent on any deformation style or the type of the host rock and the geometry of the deformation bands has an impact on the fluid flow and they can reduce permeability. The availability of the core data acquired at the fault zone is important as it provides more information about the deformation bands.

Even with the core data from the fault zone, there is still an amount of uncertainty. This is because the core data samples the vertical part of the borehole and it has its limitation when it comes to documenting the lateral variation of the deformation bands, which may extend beyond the area of the core acquisition.

Relay structures are also associated with fault zones (Hesthammer et al, 2000). The relay zones are commonly below seismic resolution. These also then introduce uncertainty. This is

because these relay structures can create areas that may allow fluid flow even though fault is considered to be sealing. This uncertainty is increased in the study area because there is no core data available that was acquired in the fault zone.

The fault thickness is impacted by the seismic resolution because it is estimated from the fault displacement. The inherited error in the interpretation of the fault will be inherited in the estimation of the fault displacement. Similarly, the errors in the fault displacement will have an impact in the prediction of the fault clay and in turn the prediction of the permeability and the hydrocarbon column height on the AK fault.

The wireline logs took precedence over the seismic data when the reservoir layering process was conducted. This is because the well scale is different than the seismic scale. As a result, the minimum reservoir layer that was used to capture the heterogeneity adequately was 2m. This is below the seismic resolution of about 3m at which the minimum throw of the AK fault be captured by seismic data. It is important that the heterogeneity of the reservoir was captured correctly because the facies defined form basis of the fault seal analysis process.

## 5.2 Limitations of the software

The limitation of the software was identified in the prediction of fault rock permeability and thickness. The studies conducted by Manzocchi et al. (1999) and Sperrevik et al (2002) both indicated that there is a negative correlation between the phyllosilicate percentage and the permeability of the fault rock. Both authors also agreed that the permeability of the fault rock from deeper levels is lower than the permeability that is encountered from the shallower levels. Based on this the depth of the fault should be included in the prediction of the fault rock permeability.

These are the only two equations that can be used in the prediction of permeability from the SGR, using the Petrel software. The Manzocchi et al (1999) equation, which takes into consideration the throw of the fault, but neglects the depth of the fault and Sperrevick et al (2002) equation which does not take into consideration the throw of the fault but considers the depth of the fault. Antonellini and Aydin (1994, 1995) studies indicated that there is a relationship between the deformation bands and the permeability of the fault zone. Faults with high displacements have a high density of deformation bands and as a result low permeability, while faults with lower displacements result in the formation of small amount of deformation bands and therefore, minor reduction in permeability.

It is based on this that, in addition to the fault clay, both the fault displacement and the depth of the fault should be incorporated in the prediction of the fault permeability. This was

identified as a software limitation as it is not possible to include all these parameters to estimate the fault rock permeability.

In the case of the fault thickness, lithology also plays an important role in the prediction of the fault thickness, especially at low throws (Childs et al., 2007), however using the Petrel software the fault thickness can be predicted either from the fault displacement or from the lithology and there is no option to include both in the calculation. At this point in time this is seen as the limitation of the software and the results of the fault rock thickness will be used as input in the fault transmissibility calculation.

# 6. Conclusion

The fault seal analysis study was conducted in the Ibhubesi gas field offshore west coast of South Africa to determine the role of the AK fault in the reservoirs of the Ibhubesi gas field. The study was carried out using a Petrel™ software. The bulk of the work that was carried out contributes to achieving the required inputs to the 3D fault seal analysis. The work that was carried out included, seismic interpretation, well data interpretation and 3D structural grid which feed in to the fault seal analysis.

The results from 3D fault seal analysis indicate that there is a high probability that the AK fault could be sealing. This is based on the following results from the AK fault rock properties evaluation:

## 6.1 Fault rock clay

This fault property indicated high percentages of fault rock clay, ~ 50%. The fault rock clay property was calibrated by the AFPD to get the SGR, which is a fault seal indicator. Based on the SGR vs AFPD plot from other sealing faults, it shows that based on the SGR of 20 to 60%, there is a high potential of the AK fault to be sealing. Given the SGR of up to 55%, the AFPD or the threshold pressure will withstand the buoyancy of the fluids in the reservoir and provide a seal.

## 6.2 Fault rock permeability

It was observed that the AK fault permeability vary between 0 to 0.1mD. This correlates with a fault rock thickness of up to 1.2meters. Faults with such low permeabilities form seals.

6.3 Across Fault Pressure Difference

The across fault pressure data indicates that the slopes of the gas gradients from the 14Et1 reservoir intersected in the A-K2 and AY1 wells are different. There is about 200psi in the AFPD. This AFPD and the SGR of the AK fault was plotted in the SGR vs AFPD plot of other sealing faults and it lies in the area of sealing faults. Furthermore, the fluid gradients from the footwall reservoir vs. that in the hanging wall indicate that they are separate fluid gradients and the gas water contact depths for the same reservoir on opposite sides of the fault are also different.

This indicates that these reservoirs are not in hydraulic communication and there could be a potential barrier between the reservoirs. This barrier between the two reservoirs was interpreted to be the AK fault.

Even though there are inherited uncertainties in the fault seal analysis studies generally. In this study, the uncertainty was reduced as follows:

## 6.4 Quality control the input data

### 6.4.1 Volume of Clay logs (Vcl)

The main input to the fault seal analysis, with the exception of the fault is the Vcl. The Vcl was quality controlled using petrography reports, to evaluate whether the resulting Vcl values are not GR effects from radioactive minerals. It was further quality controlled using the facies, where particular facies would correspond to a particular value of the Vcl, e.g. channel reservoir sandstone, referred to this study as a porous sandstone, would not be expected to have values that are greater than 35% Vcl.

### 6.4.2 3D grid property models

The same approach was applied in quality controlling the petrophysical modelled parameters. In this instance the quality control was done by reviewing whether the petrophysical parameter, e.g. porosity would correspond to the facies type (shale) that was defined. In this way, good petrophysical parameters would correspond with a certain facies type, e.g. channel sand would have good porosity and permeability when compared to a shale, which has poor porosity and permeability.

This study is viewed to have contributed insight towards the geological understanding of the trap. This is because the reservoirs are sand bodies, which are derived using seismic attribute extraction. The extent of the reservoirs especially the thinning edges of the channels are not adequately captured in these extractions. This study therefore provides understanding of the connectivity of the sand bodies located in the foot wall as compared to those in the hanging wall. The reservoir channels do not extend beyond the fault and therefore the reserves estimation should not be calculated beyond the fault and that the reservoirs are compartmentalized by the fault and will not be drained by one well.

This risk can be further reduced by updating this study will the actual fault zone data if or when drilling were to occur in the Ibhubesi gas field. In this way it will be possible to calibrate the inputs to the fault analysis study with data from the fault zone.

# 7. REFERENCES


Alberty, M. W., 1992. Introduction – Wireline Methods. In: Morton – Thompson, D. and Woods, A. M., ed., Development Geology Reference Manual. AAPG Methods in Exploration series, 10, pp 142 – 194.

Allen, G.P., Chambers, J.L.C., 1998. Sedimentation in the Modern and Miocene Mahakam delta. Jakarta, Indonesian Petroleum Association, Field Trip Guidebook, pp. 236.

Alger, R.P 1980. Geological use of wireline logs. In: Hobson, G.D., ed., Developments in petroleum – 2: London, Applied Science Publishers, Ltd., pp.345.

Antonellini, M., and A. Aydin, 1994. Effect of faulting on fluid flow on porous sandstone: petrophysical properties: AAPG Bulletin, v.78, pp. 355-377

Brown, L.F. et al., 1995. Sequence Stratigraphy. In: Offshore South African Divergent Basins. American Association of Petroleum Geologist Bulletin, 41, pp.184.

Berg, R.R. & Avery, A.H 1995. Sealing properties of Tertiary growth faults, Texas Gulf coast. American Association of Petroleum Geologist Bulletin, 79, pp. 375-393.

Berner, R.A., 1981. A new geochemical classification of sedimentary environments. Journal of sedimentary petrology, 51, pp 359 – 365.

Bretan, P., Yielding, G., and Jones, H., 2003. Using calibrated shale gouge ratio to estimate hydrocarbon column heights. American Association of Petroleum Geologist Bulletin, 87, pp 397-413.

Broad, D.S., Jungslager, E.H.A., MacLachlan, I.R., Roux, J., 2006. Offshore Mesozoic Basins. In: M.R. Johnson, C.R. Anhaeusser, R.J. Thomas ed., The Geology of South Africa. Geological Society of South Africa/Council for GeoScience, Pretoria, pp. 553–571.

Brown, L.F., Jr., Benson, J.M., Brink, G.J., Doherty, S., Jollands, A., Jungslager, E.H.A., Keenan, J.H.G., Muntingh, A., and van Wyk, N.J.S., 1995. Sequence stratigraphy in offshore South African divergent basins. In: An atlas on exploration for Cretaceous lowstand traps by SOEKOR (Pty) Ltd. American Association of Petroleum Geologists, 41, pp. 184.

Cerveny, K., Davies, R., Dudley, R. F., Kaufman, P., Knipe, R., and Krants, B., 2004. Reducing uncertainty with Fault-Seal Analysis.

Chopra, S., and K. J. Marfurt, 2007. Volumetric curvature attributes for fault/fracture characterization: First Break, 25, 19-30.

Childs, C., Manzochhi, T., Nell, P.A.R., Walsh, J.J., Strand, J.A., Heath, A.E and Lygren, T.H., 2002. Geological implications of a large pressure difference across a small fault in the Viking Graben.

Childs, C., Walsh, J., Manzochhi, T., Strand, J.A., Nicol, M., Tomasso, M., Schopfer, M.P., Aplin, A.C., 2007. Definition of a fault permeability predictor from outcrop studies of a faulted sequence, Taranaki, New Zealand.

Clemson, J., Cartwright, J. and Booth, J., 1997. Structural segmentation and the influence of basement structure on the Namibian passive margin. Journal of the Geological Society of London, 154: pp. 477-482.

Clemson, J., Cartwright, J. and Zwart, R., 1999. The Namib Rift: a rift system of possible Karoo age, offshore Namibia. In: N.R. Cameron, R.H. Bate and V.S. Clure, ed., The Oil and Gas Habitats of the South Atlantic. The Geological Society, London, pp. 381-402.

COLIN P. NORTH AND GAIL L. WARWICK, 2007 Fluvial Fans: Myths, Misconceptions, and the End of the Terminal Fan Model. Department of Geology & Petroleum Geology, University of Aberdeen, Aberdeen AB24 3UE, Scotland, U.K. e-mail: c.p.north@abdn.ac.uk

Coogan, S., Nice, R., Gboyega, A., Cater-Walford, K., (n.d). Faults as Fluid Barriers and Their Role in Trapping Hydrocarbons.

Davies, K., An, L., Jones, P., Mathis, A. and Cornette, C., 2003. Fault seal analysis South Marsh Island 36 field, Gulf of Mexico. The American Association of Petroleum Geologists. AAPG Bulleting, 87, pp 479-491.

Dingle, R.V. and Robson, S.H., 1992. Southwestern Africa continental rise: structural and sedimentary evolution. In: C.W. Poag and P.C.d. Graciansky, ed., Geologic evolution of Atlantic continental rises. Van Nostrand Reinhold, New York, pp. 62-76.

Faerseth, R., 2006. Shale smear along large faults: continuity of smear and the fault seal capacity. Journal of Geological Society, 163, pp 741- 751.

Fisher, Q.J. and Knipe, R. J., 1998. Fault sealing processes in siliciclastic sediments. Geological Society, London, Special publication, 147, pp 117 – 134.

Fisher, Q.J. and Knipe, R. J., 2001. The permeability of faults within siliciclastic petroleum reservoirs of the North Sea and Norwegian Continental Shelf. Marine and Petroleum Geology, 18 (10), pp 1063 – 1081.

Freeman, B., G. Yielding, D. T. Needham, and M. E Bradley, 1997. Fault seal prediction: the gouge ratio method in H.D. Johnson and M.P. Cowards, eds., Structural geology in reservoir characterisation and field development: Geological Society Special Publication, London

Freeman, S.R., Harris, S.D. and Knipe, R.J., 2010. Cross fault sealing, baffling and fluid flow in 3D geological models: tools for analysis, visualisation and interpretation. ed., Jolley, S.J., Fisher, Q.J., Ainsworth, R. B., Vrolijk, P.J. and Delisle, S.J., 2010. Reservoir compartmentalisation. The Geological Society, London, Special Publications, 347, pp 257 – 282.

Fristad, T., Groth, A., Yielding, G & Freeman, B., 1996. Quantitative fault seal prediction – a case study from the Osenberg Syd area.

Gerrard, I. and Smith, G.C., 1982. Post-Paleozoic succession and structure of the Southwestern African continental margin. In: J.S. Watkins and C.L. Drake, ed.,Studies in continental margin geology. American Association of Petroleum Geologists, pp. 49-76.

Hesthammer, J. and Fossen H., 2000. Uncertainties associated with fault sealing analysis. Statoil, N-5020 Bergen, Norway, Department of Geology, University of Bergen, Allegt. 41, N5007 Bergen, Norway.

Holdsworth, R.E., van Diggeln, E.W.E., Spiers, C.J., de Bresser, J.H.P., Walker, R.J., and Bowen, L., 2011, Fault rocks from the SAFOD core samples: Implications for weakening at shallow depths along the San Andreas fault, California: Journal of Structural Geology, v. 33, pp. 132–144, doi:10.1016/j.jsg.2010.11.010.

Hull, J., 1988. Thickness – displacement relationships for deformation zones. Journal of Geology, 10, pp. 431-435.

Jolley, S.J., Dijk, H., Lamens, J.H., Fisher, Q.J., Manzocchi, T., Eikmans, H. and Huang, Y., 2007. Faulting and fault sealing in production simulation models: Brent Province, northern North Sea, In, Freeman, S.R., Harris, S.D. and Knipe, R.J., 2010. Cross fault sealing, baffling and fluid flow in 3D geological models: tools for analysis, visualisation and interpretation. ed., Jolley, S.J., Fisher, Q.J., Ainsworth, R. B., Vrolijk, P.J. and Delisle, S.J., 2010. Reservoir compartmentalisation. The Geological Society, London, Special Publications, 347, pp 257 – 282.

Jordan and Pay Exploration Consultants, 2015. Exploration Potential of Block 2A, Orange Basin, South Africa. Final Report.

Jungslager, E.H.A., 1999. Petroleum habitats of the Atlantic margin of South Africa. In: N.R. Cameron, R.H. Bate and V.S. Clure, ed., The Oil and Gas Habitats of the South Atlantic. Geological Society of London, London, pp. 153-168.

Kallweit, R. S., Wood, L.S., 1982. The limits of resolution of zero phase wavelets: Geophysics, 47(7), pp. 1035 – 1046.

Knipe, R. J., 1992, Faulting processes and fault seal in R. M Larsen, H. Brekke, B. T. Larsen and E. Talleras, eds., Structural and tectonic modelling and its application to petroleum geology: pp. 325 - 342

Knipe, R.J., Fisher, Q.J., Jones, G., Clenell, M.R., Farmer, A.B., Harrison, A., Kidd, B., McAllister, E., Porter, J.R and White, E.A., 1997. Fault Seal Analysis: successful methodologies, application and future directions. In: Rivenaes, J.C. and Dart, C., 2002. Reservoir compartmentalization by water saturated faults – Is evaluation possible using today's tools.

Knott, S.D., Beach, A., Brockbank, P.J., Brown, J.l., McCallum, J.E., and Welbon, A.I., 1996. Spatial and mechanical controls on normal fault populations. Journal of Structural Geology, 18, pp 359 - 372.

Leopold, L.B., Woman, M.G and Miller, J.P, 1964. Fluvial processes in geomorphology, San Francisco: W.H. Freeman

Light, M.P.R., Maslanyj, M.P., Greenwood, R.J. and Banks, N.L., 1993. Seismic sequence stratigraphy and tectonics offshore Namibia. In: G.D. Williams and A. Dobb, ed., Tectonic and seismic sequence stratigraphy. Geol. Soc. London, pp. 163-191.

Lindsay, N. G., F.C. Murphy, J.J. Walsh, and J. Watterson, 1993, Outcrop studies of shale smear on fault surfaces: International Association of Sedimentologist Special Publication 15, pp. 113 - 123

Manzocchi, T., Walsh, J.J., Nell, P., and Yielding, G., 1999. Fault transmissibility multipliers for flow simulation models. Petroleum Geoscience, 5, pp. 53-63.

McMillan, I.K. 2003 Foraminiferally defined biostratigraphic episodes and sedimentation pattern of the Cretaceous drift succession ( Early Barremian to Late Maastrichtian) in seven basins on the

South African and southern Namibian continental margin. South African Journal of Science, 99, pp. 537 – 576.

Milliken, K.L., Reed, R.M., 2002. Internal Structure of Deformation Bands as Revealed by Cathoduminescence Imaging, Hickory Sandstone (Cambrian), Central Texas. Gulf Coast Association of Geological Societies Transactions, 52, pp725 – 736.

Muntingh, A. and Brown, L.F.J., 1993. Sequence stratigraphy of petroleum plays, post-rift Cretaceous rocks (lower Aptian to upper Maastrichtian), Orange Basin, South Africa. In: P. Weimer and H.Posamentier, ed., Siliciclastic sequence stratigraphy - Recent developments and applications. South Atlantic margins of Africa. American Association of Petroleum Geologists, Tulsa, Oklahoma, pp. 71-98.

Nicol, N., Seeback, H., MacNamara, D., Field, B., 2016. IEAGHG, "Fault Permeability".

Paton, D.A., Van Der Spuy, D., Di Primio, R., Field, B. 2008. Tectonically inducted adjustment of passive-margin accommodation space: Influence on the hydrocarbon potential of the Orange Basin, South Africa, AAPG Bulletin, 92, pp. 589 -609.

Rosgen, D.L., 1994. A classification of natural rivers. Catena, 22, pp. 169 – 199

Rivenaes, J.C., and Dart, C., 2002. Reservoir compartmentalisation by water-saturated faults – Is evaluation possible with today's tools? In Koestler, A.G., and Hunsdale, R., ed., Hydrocarbon Seal Quantification. Elsevier Science B. V., Amsterdam. Norwegian Petroleum Society (NPF), pp 173 – 186.

Rust, D.J. and Summerfield, M.A., 1990. Isopach and borehole data as indicators of rifted marine evolution in southwestern Africa. Marine and Petroleum Geology, 7(3): pp. 277-287

Sallomo, J., 2012. Seismic Stratigraphy of the Deep Water Area in the Northern Orang Basin Offshore South Africa. In Search and Discovery Article 10389

Skerlec, G.M., 1999. Evaluating top and fault seal. In Beaumont E. A: Exploration for Oil and Gas Traps. AAPG Treatise of Petroleum Geology, Handbook of Petroleum Geology, 10-1-10-94.

Sperrevik, S. et al. 2002: Emperical estimation of fault rock properties, in: Hydrocarbon Seal Quantification (edited by Koestler, A.G and Hunsdale, R, NPF Special Publication 11, pp. 109-125.

Supper, J., 1985. Priniciples of structural geology. New Jersey, Prentice Hall, 537p.

Timur, A. 1968. An Investigation of Permeability, Porosity and Residual Water Saturation Relationships for Sandstone Reservoirs. The Log Analyst 9 (4).

Tracs International, 2007. Reserve Assessment – Ibhubesi Field (A-G, A-K, A-V, A-Y and A-X areas) Block 2A.

API RP 40, Recommended Practices for Core Analysis, second edition. 1998. Washington, DC: API.

Walsh, J.J., Watterson, J., Heath, A.E and Childs, C., 1998. Representation and scaling of faults in fluid flow models. Petroleum Geoscience, 4, 241-251.

Watts, N., 1987, Theoretical aspects of cap-rock and fault seals for sing and two phase hydrocarbon columns: Marine and Petroleum Geology, v.7, p. 274 -30

Yielding, G., Freeman, B., and Needham, D.T., 1997. Quantitative fault seal prediction. American Association of Petroleum Geologist Bulletin, 81, pp 897 – 917.

Yielding, G., Bretan, P., and Freeman, B., 2010. Fault seal calibration: a brief review. In, Jolley, S.J., Fisher, Q.J., Ainsworth, B.R., Vrolik, P.J., and Delisle, S., ed., Reservoir Compartmentalisation. Geological Society of London, Special Publication 347. Pp 243 – 255.